Link between medium and long-range order to macroscopics properties of silicate glasses and melts

Daniel R. Neuville, Charles Le Losq

Link between medium and long-range order to macroscopics properties of silicate glasses and melts

Daniel R. Neuville and Charles Le Losq

Géomatériaux, Institut de physique du globe de Paris, CNRS, Université de Paris

neuville@ipgp.fr - lelosq@ipgp.fr

Abstract: Understanding the cationic network and the medium range order of glasses and melts allows rationalization of each elements role in terms of the network former, charge compensator or network modifier concepts. Such knowledge can be combined with further details, e.g. regarding the role of highly coordinated network former elements, to model the macroscopic properties of glasses and melts, like their molar volume, density, configurational entropy and viscosity. In this chapter, we present recent advances on such work, which open new avenues for the production of useful and precise models of geologic and industrial glasses and melts.

1. Introduction

The two first chapters of this volume focus on the structure of magmas at different scales: short and medium range order. A quick review of the glass literature, from the 90's or older, reveals that most published papers focused on the structure of glasses, or on properties of glasses or melts. Depending on their original discipline, the work of the scientific community in those areas are different. Physicists published papers on glass structure, including the structure of SiO_2, GeO_2, B_2O_3 as seen by X-Ray or neutron diffraction and Raman spectroscopy for example (Wright 1990, Gaskell et al., 1991, Galeener et al., 1983). Chemists worked on more complex glass compositions, like chalcogenide (Poulain and Lucas, 1970, Poulain 1983), or focused their work on specific properties of glasses like refractive index, density or the oxidation state of multivalent elements (Schreiber, 1986). Earth scientists worked on properties of

34 melts involved in geologic phenomena, like diffusivity, heat capacity, density or viscosity (Ryan and
35 Blevins, 1987, Carmichael et al. 1977, Bacon 1977; Robie et al., 1979, Bottinga and Weill 1970, 1972).
36 This has changed over time. Since the 2000's, it is easier to simultaneously investigate the structure and
37 properties of glasses. Industrial and technological needs evolved, and the interest of the Earth sciences
38 community became more and more focused on the acquisition and interpretation of *in situ* data to address
39 problems requiring insights about silicate melts at high temperature and high pressure. As a result, the
40 scientific community became more unified, performing more and more studies that simultaneously
41 investigated the structure and properties of glasses and melts. Presently, we have reached a point where
42 it is possible to link together experimental and structural/thermodynamic data to build models for solving
43 industrial or Earth sciences problems. The aim of this chapter is to show how this is possible.
44
45 *1.1 Glass structure versus macroscopic properties*
46 Among the most important questions about glasses and melts, one is critical for many applications
47 and studies: how the melt/glass structure affects macroscopic properties? For Doremus (1973), a glass is
48 an amorphous solid. The term solid implies a high viscosity, usually greater than 10^{10} Pa.s. This viscosity
49 therefore limits the flow of the body. The amorphous term implies the absence of long-range order (see
50 Figure 5A in the previous chapter, Drewitt et al., 2021), which reveals an analogy with the liquid state.
51 So, a glass is a solid whose properties are similar to those of liquids. Parks and Huffman (1926) even talk
52 about "a fourth state of matter". However, no consensus exists regarding glass, and the nature of glass
53 and the glass transition are two fundamental questions that remain open in condensed matter physics
54 (e.g., see the different definitions in and debate between Zanotto and Mauro, (2017), Popov (2018),
55 Schmelzer and Tropin, (2018)).
56
57 An important point is that glasses can exhibit very different chemical compositions and can be
58 prepared by different means. Mineral (i.e. silicate), oxide, non-oxide, metal and organic glasses exist (see
59 for an exhaustive description in Musgraves et al. (2019)). In fact, glasses are found regardless of the type
60 of chemical bonds that link the atoms they contain: covalent, ionic, metallic, Van der Waals or hydrogen
61 bonding. The glassy state is a characteristic of condensed matter. Glasses can be obtained by the rapid
62 quench of liquids, or of a gas by solid condensation, by amorphization of a crystalline phase or by sol-
63 gel methods (Descamps 2017). The most common method for obtaining a glass is by the rapid quench of
64 a liquid[1]. During the quench, viscosity continuously increases up to a value so high that the final state
65 can be considered as solid. One can therefore imagine the structure of the glass as being similar to that

[1] rapid cooling rate means 15°/min, the term classic cooling rate is also used.

of a liquid whose movements are hindered. Glasses, like undercooled liquids, have a disordered structure that was frozen in at the glass transition temperature.

A fundamental question is *what happens when a liquid crosses the glass transition temperature?* The latter is the temperature (often abbreviated T_g, and more realistically it is a small temperature interval) at which second order thermodynamic properties like heat capacity show a transition, revealing the locking-in of the atoms in fixed (but undetermined) positions. In essence, T_g is the temperature at which a number of thermodynamic properties go from liquid-like to solid-like values.

Unlike a crystallized solid, it is not possible to introduce the term of melting temperature for the glassy state. The solidification of a liquid into glass is accompanied, in fact, by a continuous and gradual increase in viscosity upon cooling, without the appearance of a crystalline structure (Figure 1). This behavior remains true regardless of the glass/melt chemical composition (silicate, aluminosilicate, borate, borosilicate, germanate, chalcogenate, tellurate, metallic, organic... see for details regarding each glass family the Musgraves et al., 2019). This shows the continuous transition from glass to liquid for a property such as viscosity (Tamman, 1925; see Figure 1). The glass transition is a dynamic phenomenon that characterizes the loss of internal thermodynamic equilibrium. Indeed, the properties of a glass no longer depend solely on pressure and temperature, but also on the temperature at which the glass transition occurs. Finally, Tamman (1925) sums the concept as "*The viscosity of a liquid increases with increasing undercooling, and in a rather narrow temperature interval it increases very rapidly to values characteristic of solid crystals. A brittle glass is thus formed from an easily mobile liquid. This change in viscosity does not correspond to the behavior of the other properties, which in this temperature interval change relatively only slightly. The change in viscosity is a continuous one and no temperature can be chosen as the freezing-point, the point at which the liquid becomes solid. Glasses are undercooled liquids*."

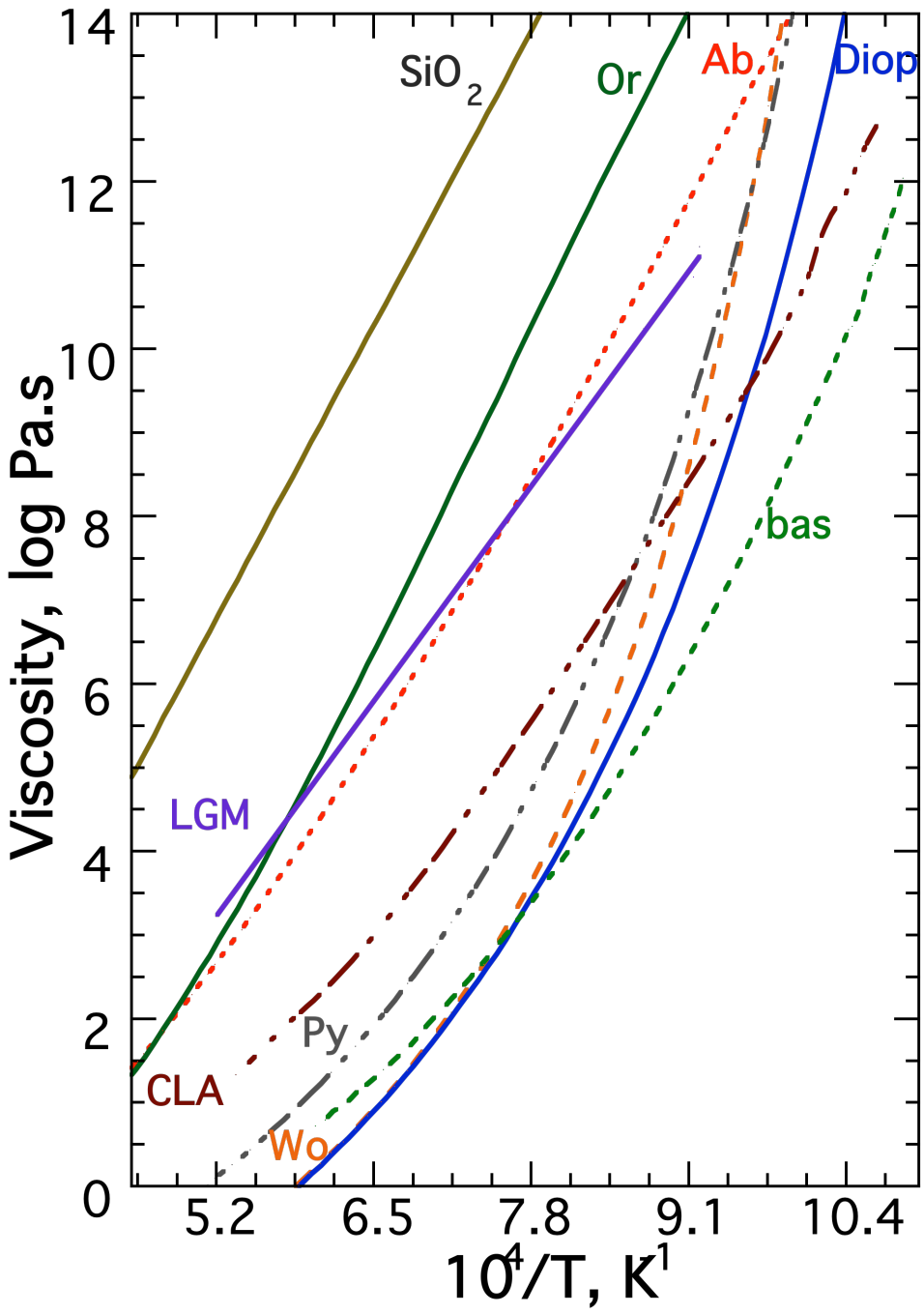

Figure 1: Viscosity versus 1/T curves for different melt compositions. LGM and CLA are rhyolite and andesite melts from Neuville et al. (1993), bas is a basalt melt from Villeneuve et al. (2008), SiO_2 is silica melt from Heterington et al. (1964) and Urbain et al., (1982), Ab and Or are albite, $NaAlSi_3O_8$, and orthoclase, $KAlSi_3O_8$ melts from (Le Losq and Neuville, 2013; Le Losq et al., 2017); Py, Wo, Diop, are Pyrope, $Mg_3Al_2Si_3O_{12}$, Wollastonite, $CaSiO_3$, and Diopside, $(CaMg)SiO_3$, melt compositions (Neuville and Richet, 1991).

The simplest and earliest characterization of the glass transition is due to Parks and Huffmann (1927), who investigated organic liquids. They note Nernst (1911), has stated that heating a glass *"externally it has the properties of a solid, owing to great viscosity and considerable rigidity, produced by strong mutual action of the molecules. An amorphous body differs from a crystal, however, in its complete isotropy and absence of a melting point; on heating, it passes continuously from the amorphous to the usual liquid state, as its properties show steady change with rise of temperature, and no breaks anywhere."*

In fact, Parks and Huffmann (1927) stated *"While there is no definite temperature, comparable to the melting point of a crystal, at which all properties undergo a sharp change, there is nevertheless a temperature interval, definite and reproducible, in which a number of properties change with a rapidity approaching that observed in the case of the melting process of a crystal. In brief, there is a softening region instead of a melting point. The glass as it exists below this softening region differs so markedly from the liquid existing above that it might well be considered as a different state of the substance."*

From an energetic point of view, Moyniham et al. (1974) showed that the variations in relative enthalpy and heat capacity with temperature for two different cooling or heating speeds exhibit a sudden change in temperature and corresponds to a dampened variation of these two properties. They showed that for the same liquid, the glass transition temperature varies with the cooling or heating rate. The higher the cooling rate, the higher relative enthalpy or heat capacity (Figure 2). The glass transition thus corresponds to a small temperature and pressure interval upon which properties such as heat capacity undergo a second order transition (Moyniham et al., 1974). This interval is at higher temperatures at high cooling rates (situation A in Figure 2), and moves to lower temperatures at slower cooling rates (situation B in Figure 2).

It is theoretically possible to obtain identical variations for all properties as a function of time at the same temperature (thermal expansion, viscosity for example) but it is not necessary (Moyniham, et al., 1974). With sudden changes in temperature, variations of the liquid properties linked to atomic mobility require some time to reach a new equilibrium. This time is called the relaxation time, τ. A liquid has a large number of different configurational states (Goldstein 1969; 1976). Each state corresponds to a minimum in potential energy and when temperature decreases, the number of possible configurations decreases as the domains for structural rearrangement become larger and larger. As a result, the time for structural relaxation, τ, of the liquid increases. Crossing the glass transition leads to the atoms trapped in given but disorganised positions. This results in quenching the liquid into a glass. The configuration state of the glass does not change from T_g to 0 K, as shown by the fact that the residual entropy of glass remains constant below T_g (e.g., see Tequi et al., 1993; Richet et al., 1991; Richet and Neuville, 1992; Richet et al., 1986; Goldstein, 2011; Schmelzer et al. 2018 and references cited therein). It should be

noted that Raman and infrared vibrational spectroscopy data suggest that the structure of a glass is an image of the instantaneous configuration of the liquid at T_g (Kashio et al, 1980; Kusabiraki and Shiraishi, 1981; Kusabiraki 1986; Sharma et al., 1978; Shevyakov et al., 1978, Neuville and Mysen, 1996).

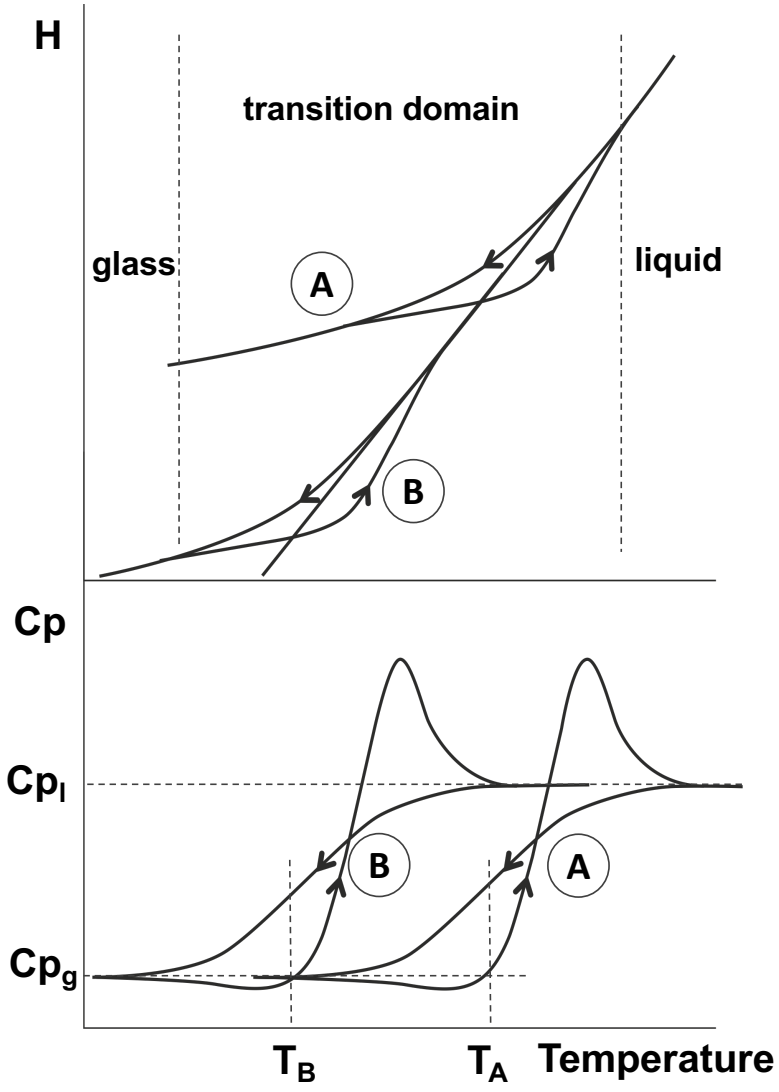

Figure 2: relative enthalpy and heat capacity versus temperature for 2 different cooling rates, A and B correspond respectively to fast and low temperature change (redrafted from Moyniham et al., 1974). Cp_l and Cp_g correspond to the heat capacities of the liquid and the glass, respectively. T_B and T_A correspond to the glass transition at the two different rates A and B, respectively.

The uniform cooling of a liquid at a rate $q=dT/dt$ can be likened to a series of instant temperature jumps $\Delta T = T_{fi} - T_i$, where T_{fi} and T_i are the final and initial temperatures, each jump being followed by a Δt period during which the temperature remains constant and equal to T_{fi}. Just after each jump, the viscosity of the liquid, η_l, is still worth η_{Ti} and differs from $\eta_{Tfi} - \eta_{Ti}$ from the new balance value, η_{Tfi}. This is called relaxation, the process by which the liquid tends to reach the state of equilibrium associated with the final temperature T_{fi}. To characterize the kinetics of this evolution, we can define a viscous relaxation time τ_η as equal to:

$$\tau_\eta = \eta_l - \eta_{Tfi} / (\delta\eta/\tau_\eta). \qquad (1)$$

Experimentally, τ_η increases when T decreases. Three cases can be distinguished:

$\Delta\tau >> \tau_\eta$, the substance has a relatively long time to equilibrate its structure at the new temperature. We are in the liquid state or in a glass state at the thermodynamic equilibrium for which the equilibrium viscosity is reached almost instantaneously. During cooling, the viscosity increases to its equilibrium value.

$\Delta\tau \sim \tau_\eta$, this corresponds to the glass transition domain. Viscosity depends on both the time and temperature to which the glass was previously subjected.

$\Delta\tau << \tau_\eta$, the relaxation time is much higher than the measurement time. No configurational rearrangement is then possible. The liquid freezes. Only the vibrational part of the heat capacity remains, which is close to the heat capacity of the crystal.

Relaxation times depend heavily on temperature (Rekhson, 1975; 1989, Simmons et al., 1970; 1974, Dingwell and Webb, 1990), as well as on the structure and therefore glass composition; e.g. borosilicate glasses have higher relaxation times than silicate or aluminosilicate glass compositions (Sipp et al., 1997). Figure 3 shows, for a soda-lime silicate glass, that relaxation time increases with decreasing temperature: e.g. equilibrium is reached after 500, 1200, 1600 min respectively at 795, 788 and 777 K.

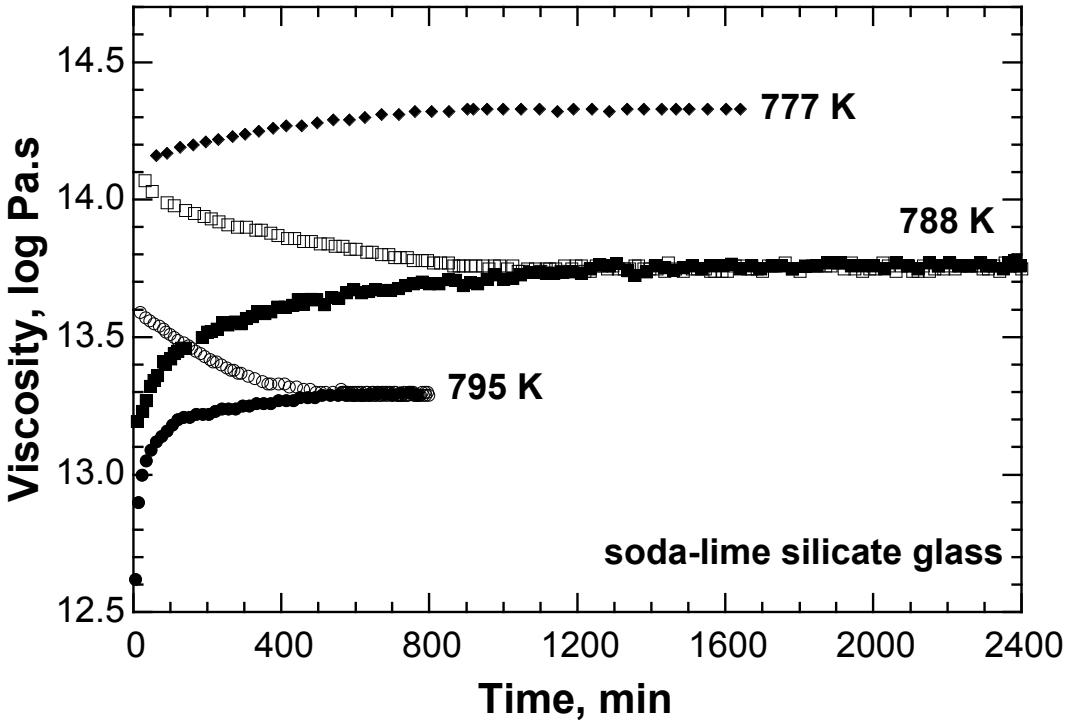

Figure 3: Viscosity versus time for a soda-lime silicate glass at different temperatures (redrafted from Sipp et al., 1997). We can note that increasing viscosities represent relaxation after previous measurements performed at higher temperatures, whereas decreasing viscosities indicate relaxation after annealing at lower temperatures.

However, it is important to note that there is no reason why the relaxation times of the various properties should be identical at equal cooling speeds. Moynihan et al. (1976a) indicate that *"for example, the enthalpy changes occurring during the approach to equilibrium of a network glass following a change in temperature could be considered to arise from the breaking of some of the network bonds, while the volume changes are due to rearrangement of the structure into less densely packed configurations. One cannot say a priori, however, which of these two processes should on the average occur earlier in time. That is, bond breaking might be a necessary precursor to volume-changing rearrangements of the structure, so that one would expect H to relax faster than V. On the other hand, configurational rearrangements leading to large volume changes might occur early in time, stressing the network and leading to subsequent bond breaking, so that one would expect V to relax faster than H."* In practice, it appears that the differences in relaxation time between volumetric and calorimetric relaxation times are relatively small, if not almost non-existent, and are essentially due to differences in cooling or heating

rates (Sasabe et al., 1977; Moynihan and Gupta, 1978; Dingwell and Webb, 1990). Differences between relaxation times for the same material but determined with methods sensitive to different properties are clearly visible when comparing data from dilatometry, calorimetry and viscosimetry. For example, in the case of alkaline-earth aluminosilicate glass compositions, drop calorimetry T_g are generally found at temperatures at which viscosities are of 10.7 ± 0.5 log Pa.s, a value lower than that of ~12 log Pa.s that is known to be the reference for the determination of the viscous T_g (Neuville and Richet 1991; Tequi et al., 1991).

1.2 Thermodynamic approach to glass transition

We have seen that temperature and pressure are not sufficient parameters to characterize the state of glass. Tool and Eichlin (1931) introduced the concept of fictive temperature, T_{fic}, to characterize a glass at constant pressure. It can be defined as the temperature at which the glass would be in an equilibrium state (as a melt) if it could be heated and measured instantly. The fictive temperature can be defined during cooling in dilatometry or calorimetry, as the glassy transition temperature.

It is possible to give a formal thermodynamic definition of the fictive temperature, considering it as an order parameter. Moynihan et al. (1974, 1976a,b) discussed fictive temperatures, their influence on enthalpy properties and order parameters. It can be recalled, that the glass transition looks like a second-order transition for which volume, enthalpy and viscosity are continuous functions of T but not heat capacity, dilatation and compressibility coefficients. For the latter parameters, a steep transition is observed when temperature crosses the glass transition.

In reality, fictive temperature is a critical parameter as it reflects how viscosity, hence relaxation time, can show non-equilibrium behavior and can depend on time in the supercooled domain. In Figure 3, the effect of fictive temperature is clearly visible. The downward curve is obtained from a sample that has a fictive temperature below the measurement temperature. Similar behaviors are visible for density, or refractive index (Winter, 1943, Ritland, 1954). When the fictive temperature of the glass is higher than the measurement temperature, the glass has a more disordered configurational state than the state it should have if the glass were in thermodynamic equilibrium, i.e. its "fictive" configuration entropy is too high. It has a lower viscosity than its equilibrium viscosity, so its viscosity increases over time until the fictive temperature equals the measurement temperature. For a fictive temperature lower than that of measurement, the viscosity decreases until the establishment of the thermal equilibrium characterized by the equality of the two temperatures. In Figure 2, the relaxation curves over time for the cases of cooling

or heating are asymmetrical. This is because a liquid increases its entropy faster with an increase in temperature (Rekhson, 1980, Dingwell and Webb, 1990; Sipp et al., 1997)[2].

1.3 Viscosity and glass transition

The glass transition is closely related to transport phenomena and more specifically to viscosity (Adam and Gibbs 1965; Gibbs and Dimarzio, 1958; Goldstein, 1969; Grest and Cohen, 1980; Scherer 1984, Richet, 1984), one of the fundamental properties of liquids that intervenes in transport processes. For the experimentalist, liquid viscosity also can be considered as a structural probe. Many models attempt to describe the variation of viscosity with temperature. Among them, we can cite the empirical Arrhenius and Tamman-Vogel-Flucher (TVF) equations, or the thermodynamic Adam-Gibbs (AG) model (see also section 2) allows linking melt mobility to its thermodynamic properties such as heat capacity and configurational entropy, and can be used for viscosity predictions and extrapolations (Neuville and Richet, 1990). Le Losq and Neuville (2017) further showed that the AG model allows linking melt structural knowledge to thermodynamic properties and viscosity, in order to build complete, extensive models for property predictions.

1.4 Configurational properties and glass structure

Configuration properties are the key to understand the difference between liquids and glasses. To illustrate the importance of such configurational aspects, consider the second order thermodynamic properties of crystal, glass and liquid pyrope ($Mg_3Al_2Si_3O_{12}$).

TABLE 1: Heat capacity of pyrope and $Mg_3Al_2Si_3O_{12}$, glass and liquid in J mol^{-1} K^{-1}. Data are from Tequi et al. (1991).

T(K)	Crystal	Glass	Liquid
298	325,6	327,8	
1020	492,2	504,4	665,7
1700	522,6		689,5

Above room temperature, the glass and crystalline phase have similar heat capacities, *Cp*. On the contrary, the *Cp* of the liquid is 25% higher than that of solids (crystal or glass). Moreover, it should also be noted that the *Cp* of the liquid usually increases with temperature of the liquid and cannot be considered as a constant. These differences can have a significant impact when you integrate with

[2] A fictive pressure, P_{fic}, can be defined as the pressure at which the glass would be in an equilibrium state if it were subjected instantly to pressure equal to P_{fic}, at constant temperature.

temperature or pressure, as shown by the example of pyrope and $Mg_3Al_2Si_3O_{12}$ liquid. For instance, a simple extrapolation of the heat capacity of the $Mg_3Al_2Si_3O_{12}$ liquid to low temperatures would produce a liquid with a lower entropy than that of its crystalline form below 694 K (Figure 4A). This temperature actually corresponds to the Kauzmann temperature, a temperature below which the liquid entropy would become lower than that of a crystal with the same composition. Such a system does not exist because a property of a liquid like the entropy should always remain higher than that of its crystalline form at a given temperature. The violation of this idea is known as the Kauzmann paradox (Kauzmann, 1948)[3]. The pyrope example shows that configuration terms play an important role on the properties of liquids. It is therefore necessary to understand how configurational properties vary, and their link to melt and glass structure. Figure 4A shows the variation of the entropy of a crystal, glass and liquid for the $Mg_3Al_2Si_3O_{12}$ composition as a function of temperature. It is clear that the residual entropy corresponds to the difference between the entropy of the glass and that of the crystal at 0 K. This residual entropy is very small compared to the entropy of glass, crystal and liquid. This residual entropy is called configurational entropy, S^{conf}, and it is the key to understanding glasses and liquids. To determine S^{conf}, it is necessary to solve the entropic cycle represented in Figure 4A. However, this is only possible for minerals that melt congruently, and with a composition that can exist in a stable form as crystal, liquid and glass. Measuring the heat capacity of the crystal, Cp_c, from 0 K to the melting temperature, T_m, allows determining its absolute entropy S_c at T_m:

$$Sc = \int_0^{Tm} \frac{Cpc}{T} dt. \qquad (2)$$

By adding the entropy of fusion of the crystal, ΔS_f, to S_c, the entropy of the liquid S_l is then obtained at T_m. Measuring the heat capacity between the melting temperature, T_m, and the glass transition temperature, T_g, allows determining the heat capacity of the liquid and the supercooled liquid, Cp_l. The measurement of the heat capacity of the glass between T_g and 0 K provides Cp_g. Finally, the residual entropy, also known as the so-called configurational entropy S^{conf}, is obtained at 0 K via:

$$S^{conf}(0\ K) = \int_0^{Tm} \frac{Cpc}{T} dt + \Delta Sf + \int_{Tm}^{Tg} \frac{Cpl}{T} dt + \int_{Tg}^{0} \frac{Cpg}{T} dt. \qquad (3)$$

This calculation is illustrated in Figure 4A for a composition of $Mg_3Al_2Si_3O_{12}$ (Tequi et al., 1991). As this Figure shows, S^{conf} represents a small difference between large numbers, and its value will be affected by a very large error if calorimetric measurements are not made with the highest possible accuracy. For this purpose, the studies focused on determining S^{conf} from calorimetry measurements require high-precision measurements of thermal capacity: heat capacities need to be determined better

[3] this well-known paradox in temperature is recently proposed via pressure, but without any experimental basis see papers of Schmelzer et al., (2016) and Mauro (2011).

than 0.2 % by adiabatic calorimetry between 0 K and ambient, and better than 0.5 % by high-temperature drop calorimetry (e.g. Tequi et al., 1991). Aside from the time and the difficulty of performing such high precision heat capacity measurements, one of the main drawbacks of the calculation of the configurational entropy through the thermodynamic cycle is the necessity to study minerals that melt congruently, with compositions existing as glass, liquid and crystal as stated previously. Only a few chemical compositions can be studied in this way. Fortunately, as we shall see later, S^{conf} can be determined through the use of the Adam and Gibbs model combined with viscosity measurements.

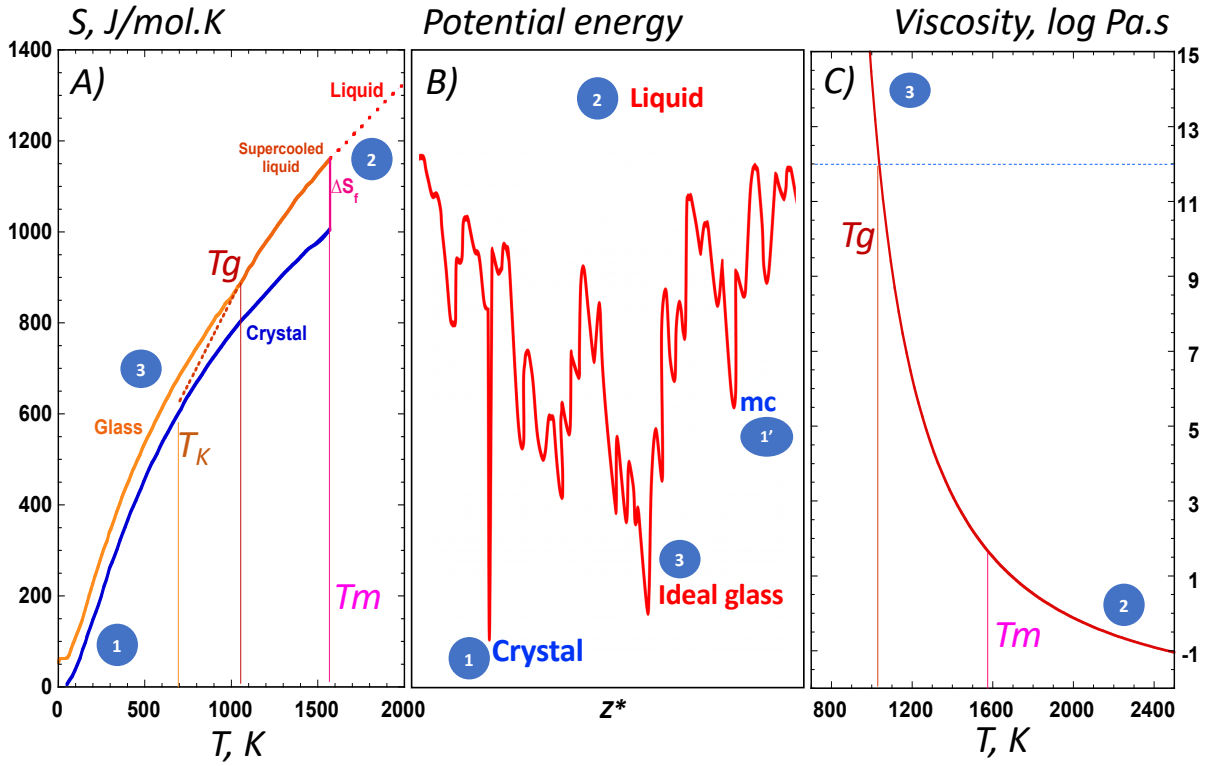

Figure 4: A) entropy versus temperature (Tequi et al., 1991), B) schematic representation of the complex higher dimensional potential energy hypersurface of an N-particle system in terms of a two-dimensional diagram of chemical potential versus some collective configuration coordinate Z, which defies precise definition, but the width of the funnel represents entropy (Angell, 1991; Mossa et al . 2002), and C) viscosity versus temperature for the $Mg_3Al_2Si_3O_{12}$ composition (Neuville and Richet, 1991). The same numbers are all connected together in the three figures. 1 is the Pyrope crystal that presents the minimum potential energy. 1' is a metastable crystal, mc, that can have a potential energy higher than that observed for the glass. 2 is the liquid with a low viscosity, high entropy and high potential energy, in which atoms can move rapidly from one position to one other. 3 is the glass, in which atoms can move very slowly, there is a relaxation time, viscosity increase and entropy decrease, and the atom can fall in different potential energy minima and stay inside or jump to another with a lower potential energy. T_m is melting temperature, T_g, glass transition temperature, T_K Kauzmann temperature, ΔS_f entropy of melting at the melting temperature. Supercooled liquids are liquids between melting temperature and glass transition temperature.*

Figure 4B schematically illustrates the positions of atoms in a crystal as a function of the collective configuration coordinate, as determined by local minima of interatomic potentials that are at specific positions, allowing the building of a repetitive pattern characterized by long range order. In a glass, the bond angles and interatomic distances are not constant but extend over a range of relatively close values. Long-range order does not exist, and one can represent the interatomic potentials as a plane showing minima separated by barriers with varying shapes and heights. As a result, glass entropy is higher than that of crystal at given temperature (point 3, Figure 4). The ideal glass with the minimum potential exists, but also other minima can exist with higher potential for the glass state or even the metastable crystal (point 1'). Now suppose that a certain amount of heat is brought instantly to the glass. Below the glass transition, the thermal energy brought upon increasing temperature is accommodated as vibrations, via an increase in average vibration amplitudes. The specific heat is vibrational in nature and the material behaves like a solid. At and above T_g, the thermal energy becomes important enough to allow the atoms to cross the energy barriers that separate the different configurational states (Richet and Neuville, 1992). This configurational contribution is necessarily positive, and the liquid or glass states can be defined by the existence or absence of this contribution (Davis and Jones, 1953). In a way, the glass transition can be seen as the beginning of the exploration by atoms of positions corresponding to the highest values of interatomic potential (Goldstein, 1969). This distribution of configurations over increasingly high potential energy states is the main characteristic of atomic mobility and low viscosity or relaxation time (point 2, Figure 4).

If we now look at the changes in volume in an amorphous material, we notice that a general characteristic of interatomic potentials is their anharmonic nature, i.e. that the forces applied to the vibrational atoms are not exactly proportional to the movements in relation to the equilibrium positions of these atoms (Richet and Neuville, 1992). An increase in vibration amplitudes therefore leads to an increase in interatomic distances. Like solids, liquids also have such anharmonic vibrational expansion, but higher-energy patterns that begin to be explored over the glass transition are generally associated with increased interatomic distances. This is why the thermal expansion coefficient generally increases significantly at the glass transition (Richet and Neuville 1992).

1.5 pressure-temperature space

As we have mentioned before, there is a glassy transition pressure (Rosenhauer et al., 1979), which allows one to place the glass transition in a pressure-temperature plane for a given cooling or heating

rate. However, the effects of pressure and temperature on the properties of glasses are actually different. High pressure can produce irreversible configurational changes. So, for given experimental quench rates or measurement time scales, the kinetics of configurational changes are markedly different depending on whether they are caused by pressure or temperature. The main reason for this difference is that the shape of potential energy wells varies little with temperature but significantly with pressure. If high kinetic energy is required to cross the potential barriers at constant pressure, changes in these barriers with pressure can lead to new configurational states at lower temperatures, if the pressure is high enough. The processes occurring at high pressure in glasses are likely similar to those that occur in liquids. Since the 2000's, many papers have shown significant changes in the glass structure with increasing pressure, more or less linked to changes in their properties (e.g. Poe et al., 2001, Suzuki et al., 2002, Wang et al., 2014). In this volume, an exhaustive chapter can be found on the effect of pressure on the structure and properties of melts and glasses by Sakamaki and Ohtani (2021).

2. Silicate glasses and melts

2.1 Alkali or earth alkaline silicate glasses and melts

As depicted in the previous two chapters, silica glass is a material well-connected at the molecular scale, built from a three-dimensional network of tetrahedral units composed of covalently bonded central Si and apical O atoms (a.k.a. Bridging Oxygens or BO). However, contrary to α-quartz that forms perfect trigonal crystals, SiO_2 glass is built by SiO_4 tetrahedra distributed disorderly yet not totally randomly (e.g. see Figure 5A in chapter 3, this volume). The relative density d of silica glass equals 2.20 (molar volume $V_m = 27.311$ cm^3), a value lower than that observed for α-quartz ($d = 2.65$, $V_m = 22.673$ cm^3) that presents a compact and well-ordered structure. This implies that silica glass presents a rather porous structure, with possibly a minor amount of Non-Bridging Oxygen (NBO, see Chapter 2, this volume) atoms not connected to 2 Si atoms (Brückner 1970; Fanderlik, 1990). The fraction of NBO in silica is usually considered as negligible, making the silica structure a very strong one.

As an alkali oxide is added, Na_2O for example, more and more NBO are created until reaching the possibility to create isolated SiO_4 tetrahedra linked together by only ionic Na-O bonds. For alkali silicates, this corresponds to a theoretical view because Na_4SiO_4 glasses do not exist. However, in the Ba-silicate system, it is possible to obtain glasses with 33% and 37% silica with classic cooling rate (Bender et al., 2002), while in the Mg-silicate system it is possible to obtain glasses up to 62 MgO in mole percent (38%SiO_2) but below 50 percent of silica, it is necessary to use a fast cooling rate as shown in Raman spectra (Neuville et al., 2014). Glass formation in the SiO_2-Na_2O system is actually not possible for amounts of Na_2O lower than that of the metasilicate composition Na_2SiO_3 (Schairer and Bowen, 1956). At higher Na_2O contents, up to 58 mole percent, it is possible to obtain Na silicate glasses only

via high-speed quenching of a small quantity of melt (a few grams; Imaoka and Yamazaki, 1963). Stable, large pieces of glass cannot be formed below 60 mol% of SiO_2 in this system (Neuville, 2006). For other alkali-silicate glasses, it is possible to make glasses up to 35 and 55 mole % of Li_2O and K_2O, respectively (Imaoka and Yamazaki, 1963, Levin et al., 1964).

To summarize, alkali silicate glasses can be easily obtained at normal cooling rates in the 60 to 99 mole % SiO_2 range (see Raman spectra of silicate glasses in Neuville et al., (2014)), and alkaline-earth silicate glasses between 33 and 75 mol% SiO_2, particularly with heavy alkaline-earth elements like Ba. For Mg, the glass forming domain is smaller, and ranges between 37 and 55 mole % SiO_2 (Imaoka and Yamazaki, 1963, Richet et al., 2009). In the CaO-SiO_2 system between 1 and 62 mole % SiO_2, the melts at temperatures just above the liquidus consists of two immiscible phases (Imaoka and Yamazaki, 1963, Levin et al., 1964, Hudon and Baker 2002ab; Neuville 2006).

Alkali or alkaline-earth silicate glasses show almost linear variations in molar volume with addition of M_2O or $M^{2+}O$ in silica glasses (Figure 5). Molar volumes obtained from density measurements for CaO-Al_2O_3-SiO_2 and Na_2O-Al_2O_3-SiO_2 are also available in the literature (Seifert et al., 1982, Doweidar 1998, 1999) but we have chosen not to report them on the figures for two reasons: -i) they show similar trends to ours, - ii) they are made with different cooling rate than ours (not mentioned in the articles). The molar volume (V_m) of silicate glasses increases or decreases as a function of the cation size[4]. In the case of cations presenting an ionic radius larger than O^{2-} (132 pm), like Cs^+, Rb^+ or K^+, the glass molar volume increases with cation addition. For cations presenting an ionic radius lower than that of O^{2-}, like Na^+ and Li^+, V_m of silicate glasses decreases both with the cation size and its amount. A similar behavior is observed in alkaline-earth silicate glasses. In Ca and Mg silicate glasses, V_m varies almost linearly with the glass SiO_2 (Figure 5). In Figure 5, a dotted straight line is drawn between SiO_2 and MgO with MgO with Mg in 6-fold coordination, and it is clearly observed that the V_m of Mg-silicate glasses are below this line, which suggests that the CN of Mg is significantly less than 6 in amorphous magnesium silicates. Such an interpretation agrees with ^{25}Mg Nuclear Magnetic Resonance (NMR) spectroscopy that shows that Mg is essentially in four-fold coordination in silicate glasses (Fiske and Stebbins, 1994; Georges and Stebbins, 1998, Kroeker and Stebbins, 2000, Shimoda et al., 2007a,b), as well as with XANES at the Mg *K*-edge (Trcera et al., 2009) while Ca is essentially in six fold coordination in silicate glasses as shown by XANES at the Ca *K*-edge (Neuville et al., 2004b, Cormier and Neuville, 2004; Ispa et al., 2010; Cicconi et al., 2016). These gentle variations may indicate that Ca and Mg remain almost in the same

[4] Cation size are given in Whittaker and Muntus (1970) and molar volumes are from Robie et al. (1979).

coordination number, CN, in silicate glasses, this CN being slowly affected by the SiO_2 content or by the variation in the number of bridging oxygens around Si.

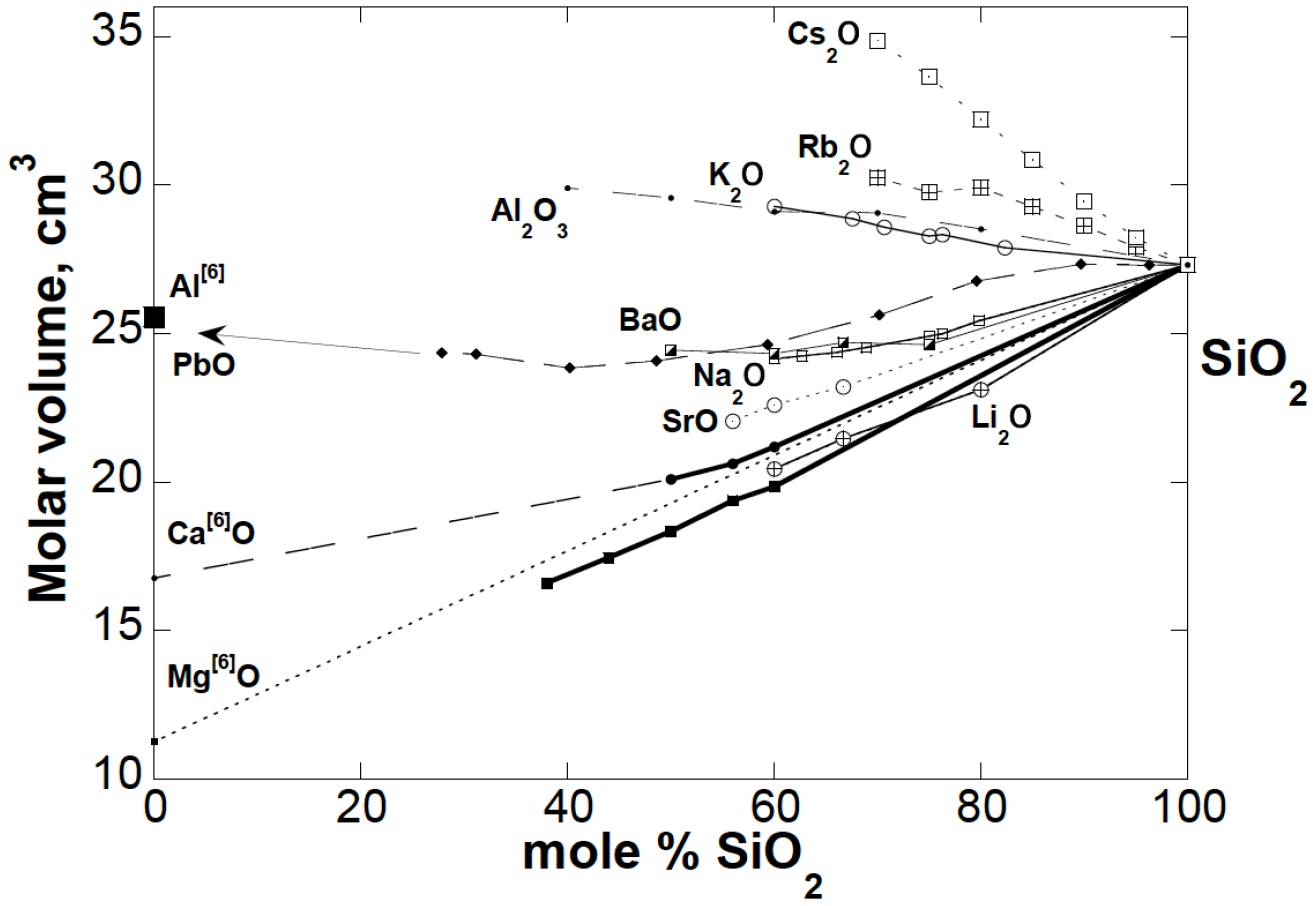

Figure 5: *Molar volume of glasses at room temperature: data for Ca, Mg, Na, K, Li silicate glasses are original data from Neuville, Sr and Ba Novikov (2017) Rb, Cs O'Shaughnessy et al., (2017, 2020); Pb-silicate (Ben Kacem et al., 2017) and Al-silicate glasses (Wang et al., 2020). Molar volume of $^{[6]}Al$ corresponds to Al_2O_3, and MgO and CaO are from Robie et al. (1979). Density of MA44.00 and MA38.00 glasses are respectively 2,807 and 2,881, Raman spectra of these two glasses are given by Neuville et al. (2014).*

Viscosity of silicate melts

In Figure 6A, the viscosity of SiO_2 and soda silicate melts are plotted as a function of reciprocal temperature. Silica shows the highest viscosity of all glass compositions, as well as a strongly linear behavior indicating an Arrhenian behavior (slope is equal to an activation energy).

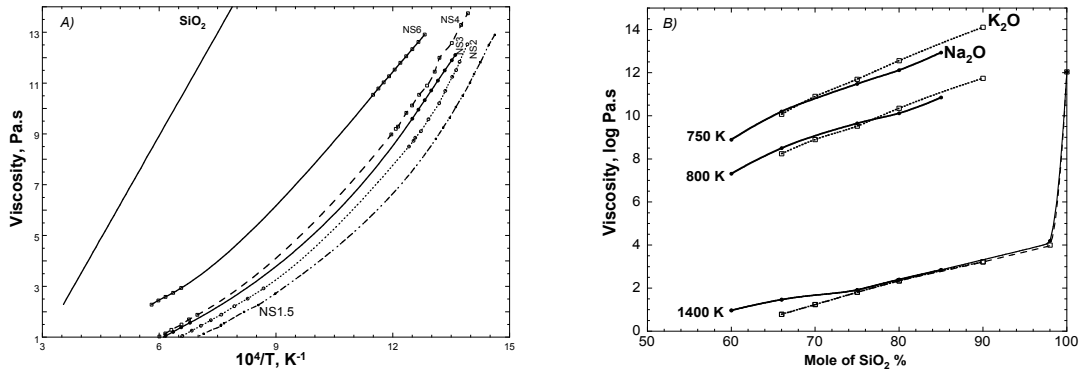

Figure 6: *A) viscosity versus reciprocal temperature (SiO_2 NS6, NS4, NS3, NS2, NS1.5, data from Neuville, 2006, and Le Losq et al., 2014). NSx: x* corresponds to the ratio of SiO_2/Na_2O in mole percent (e.g. NS4: x = 4 = 80/20 - 80 % SiO_2 and 20 % Na_2O)*; B) viscosity versus SiO_2 content for Na- and K-silicate glasses (data from Poole, 1948, Bockris et al., 1955, Neuville, 1992, 2006).*

The fact that silica easily forms a glass, albeit a strong one with a very high viscosity, directly indicates that Si is a network former cation. Other elements, presenting lower valence and larger ionic radius, can play different roles in the glass structure. For instance, the introduction of Na_2O in silica glass yields to breaking the covalent Si-O-Si bridges, and, hence, to the formation of Non-Bridging Oxygens, NBO. Na is considered, in this case, as a network modifier cation. Na fits into the glass structure as cations linked to the surrounding oxygens by bonds that are much more ionic and thus weaker than Si-O covalent bonds. Thus, the structure of sodium silicate glasses is weaker than that of vitreous silica. This translates into a lowering of the viscosity at given temperature when adding Na_2O in SiO_2 (Figure 6A). Furthermore, the introduction of Na_2O in silica glass produces a non-Arrhenian behavior that increases with *x* for the *NSx* glass; *x* corresponds to the ratio of SiO_2/Na_2O in mole percent (Figure 5A). When viscosity varies with 1/T following an Arrhenian behavior, it follows this equation:

$$Log\ \eta = A + B/T\ , \qquad (4)$$

with *A* the viscosity at infinite temperature and *B* an activation energy. This equation can only be used for a few chemical compositions like SiO_2, GeO_2, $NaAlSi_3O_8$ or $KAlSi_3O_8$. An Arrhenian behavior implies that the activation energy, *B*, is independent of temperature, and, hence, that the process underlying melt viscous flow remains the same regardless of temperature. For melts showing a strong non-Arrhenian behavior like NS3, the activation energy term, *B*, decreases from 2000 kJ mol^{-1} at 1000 K down to 300 kJ mol^{-1} at 1800 K. In such conditions, it is no longer possible to use the Arrhenian

equation. For this reason, Tamman, Vogel and Fulcher proposed the so-called TVF equation (Vogel, 1921; Fulcher, 1925, Tamman and Hesse, 1926) to link viscosity and temperature:

$$Log\ \eta = A + B/(T-T_1), \quad (5)$$

A, B and T_1 are just fitting parameters without physical meaning. The TVF equation is very useful to fit and interpolate viscosity data at low and/or at high temperature (Neuville and Richet, 1990). This equation has been used in many different papers and is at the basis of several viscosity models (Bottinga and Weill, 1971; Shaw, 1972; Persikov 1991; Giordano et al., 2008; Giordano et Russell, 2018). The empirical parameters A, B, T_1 can be linked to glass structure (Giordano and Russell, 2018). However, while finding very practical applications, this equation remains purely empirical.

Aside from the empirical Arrhenius or TVF equations, the Adam-Gibbs equation, derived from the theory of Adam and Gibbs (1965), is one of the best candidates to fit and extrapolate viscosity measurements for silicate melts (Urbain, 1972, Wong and Angel, 1976; Scherer, 1984, Richet 1984, Neuville and Richet, 1990; 1991, Mauro et al., 2009). The strength of this equation is that it allows relating viscosity measurements to heat capacity and configurational entropy data (Urbain, 1972; Wong and Angell, 1976; Scherer, 1984, Richet, 1984). The Adam-Gibbs theory and equation will be discussed in more details in the next section. No other equation allows relating thermodynamic to dynamic variables in a simple way.

The variations observed and described previously for sodium silicate glasses are similar for all alkali oxides, as for instance visible for K_2O in Figure 6B. Generally, the addition of a few percent of alkali in silica glass produces an important viscosity decrease of a few orders of magnitude (Lecko et al., 1977). Ten mole percent of alkali oxides decreases the viscosity by ~ 10 orders of magnitude at 1400 K, this decrease being larger at low temperature near the glass transition temperature. After 10 mol% of added alkali oxides, the decrease in viscosity with increasing alkali content becomes less pronounced and the viscosity varies almost linearly at high temperature. These viscosity variations for more than 10% of added alkali are well correlated with increases in thermal expansion and heat capacity of the liquid which vary almost linearly as a function of chemical change at high temperature (Bockris et al., 1955; Lange and Carmichael, 1987; Lange and Navrotsky 1992).

2.2 ideal mixing: mixing alkali or alkaline-earth in silicate glasses and melts

In section 2.1, we observed that molar volumes, as well as viscosity and glass transition temperature of alkali and alkaline-earth silicate glasses all changes with the addition of network modifiers. Mixing different metal cations (like Ca and Mg, or Na and K) in silicate glasses results in large variations in their properties, such as large decreases of their glass transition temperatures or large increases in their electrical conductivity (Day, 1976). This is the so-called mixed alkali effect, MAE, reviewed many times (Richet, 1984, Neuville and Richet, 1991, Allward and Stebbins, 2004; Cormier and Cuello, 2013, Le Losq and Neuville, 2013, Le Losq et al., 2017, Bødker et al., 2020) in the literature for alkali silicate glasses since the work of Day (1976).

In this section, we show and introduce some terminology about mixing elements and their effect on the structure and macroscopic properties of melts and glasses. Ca and Mg are very important elements in Earth and material sciences, and it thus it is particularly important to understand how they mix in silicate melts. To understand this, we can look at how viscosity varies along the $CaSiO_3$-$MgSiO_3$ binary. Neuville and Richet (1991) have shown that at constant temperature, the viscosity of $(Ca,Mg)SiO_3$ composition is always lower than the viscosity of the end-member, $CaSiO_3$ or $MgSiO_3$ (Figure 7A).

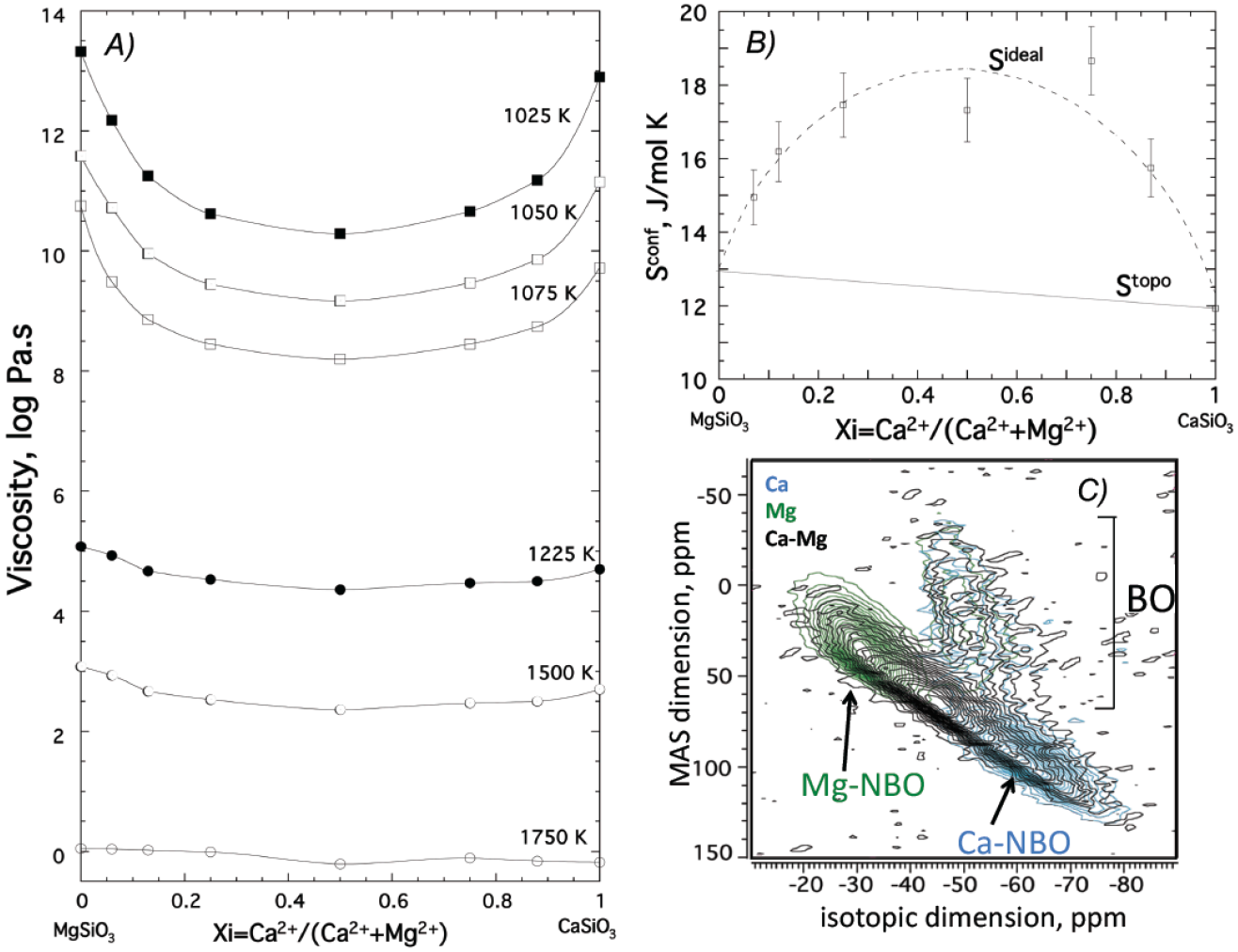

Figure 7: *A) Viscosity versus x_i=Ca^{2+}/(Ca^{2+}+Mg^{2+}) at constant temperature and B) configurational entropy for Ca/Mg mixing data from dashed line correspond to the total configurational entropy and full line to the topological variation of the entropy see text (Neuville and Richet, 1991) C) ^{17}O triple-quantum NMR spectrum redrafted from Allwardt and Stebbins (2004).*

By using the Adam-Gibbs equation, it is possible to determine the configurational entropy, S^{conf}. Adam and Gibbs (1965) theory of relaxation processes is based on the idea that transporting matter in a viscous liquid requires a cooperative change in the fluid configuration. A liquid with zero configuration entropy would be analogous to a perfect crystal, and no material displacement could occur since a single configuration would be available. The viscosity would then be infinite. If only two configurations were possible, a movement of matter could only occur if all the atoms of the liquid changed position simultaneously. The probability of such a cooperative movement would be very low and viscosity extremely high, but no longer infinite. More generally, as S^{conf} grows, cooperative configurational changes can occur independently of each other in increasingly smaller volumes of the liquid. At the same time, viscosity decreases and is predicted by:

$$\log \eta = A_e - B_e/TS^{conf}(T), \quad (6)$$

where A_e is a pre-exponential term and B_e a measure of the Gibbs-free energy barriers hindering configurational rearrangements in the liquid. $S^{conf}(T)$ can be written as:

$$S^{conf}(T) = S^{conf}(Tg) + \int_{Tg}^{T} \frac{Cpconf(T)}{T} dt, \quad (7)$$

And

$$C_p^{conf}(T) = C_{pl}(T) - C_{pg}(T_g), \quad (8)$$

where C_{pl} and C_{pg} are the heat capacity of the liquid and the glass.

C_p^{Conf} is the melt configurational heat capacity, equal to the difference between the heat capacity of the liquid C_{pl} and the heat capacity of the glass at T_g, $C_{pg}(T_g)$ (Richet et al., 1986). Those values can be measured or modelled with the existing parametric equations (Stebbins et al., 1984; Richet and Bottinga 1984; Richet 1987; Tangeman and Lange 1998; Russell and Giordano 2017), see for examples and details Neuville (2005, 2006), Le Losq et al. (2014) and Le Losq and Neuville (2017). One may also note that $C_{pg}(T_g) \sim 3R$, the Dulong and Petit limit (Petit and Dulong, 1819), such that it can be easily estimated from this simple calculation (Richet, 1987). The configurational heat capacity is a very important term, in particular, the higher Cp^{conf} is, the faster S^{conf} increases with T, and the lower the B_e/S^{conf} ratio.

The importance of these differences between configurational Cp is illustrated in Figure 1, where in the case of $NaAlSi_3O_8$, the liquid Cp^{conf} represents less than 10% of that of the glass, and deviations from Arrhenius behavior are small. On the contrary, $CaSiO_3$ or $Mg_3Al_2Si_3O_{12}$ have a Cp^{conf} representing 30% of the Cp of the glass, and the viscosity versus 1/T curves depart significantly from a straight line. Because of the importance of Cp^{conf}, it is therefore imperative to know the heat capacity of liquids and glasses for a given temperature and chemical composition. We can note that the configurational heat capacity $C_p^{conf}(T)$ depends essentially on the heat capacity of the liquid, C_{pl}, and in the case of alkaline-earth silicate melts, C_{pl} is independent of T and varies mostly linearly with melt composition (Stebbins et al., 1984, Richet and Bottinga, 1985, Lange and Navrotsky, 1992). This explains the pseudo-linear variations of viscosity observed at high temperature (1750 K, Figure 7A).

However, near T_g, the melt viscosity depends strongly on $S^{conf}(T_g)$, which shows large non-linear variations with melt composition. This explains the large, non-linear viscosity changes at supercooled temperature upon mixing alkaline-earth elements in silicate melts (Figure 7A). Using equation 6 in conjunction with viscosity data and heat capacity values (from data or models), S^{conf} can be calculated. S^{conf} along the $CaSiO_3$-$MgSiO_3$ binary is plotted in Figure 7B. To reproduce S^{conf} variations with composition, it is necessary to look at the contributions to $S^{conf}(T_g)$ in equation 7. S^{conf} records topological contributions from the melt structure (bond angle and inter-atomic distance distributions, etc.) as well as

excess entropy arising from chemical mixing effects. It thus is common to express S^{conf} as the addition of those two sources (Neuville and Richet, 1991):

$$S^{conf}(T_g) = S^{topo} + S^{mix} \qquad (9)$$

with S^{mix} the term embedding all mixing contributions and S^{topo} the entropy arising from the topology of the glass network. The topology of the network for the two end-members is distinctly different and is also different compared to the crystalline analogues.

S^{topo}, the topological configuration entropy can be approximated as a linear variation of the configurational entropy of the end-members and calculated as $\Sigma\ x_i\ S^{conf}_i(Tg)$, with $S^{conf}_i(Tg)$ the configurational entropy of $CaSiO_3$ and $MgSiO_3$ glasses (Neuville and Richet, 1991). This S^{topo} term corresponds to a mechanical mixing between the two end-members without necessary chemical or physical interaction. S^{topo} can be expressed from the glass structure and varies linearly with composition (Le Losq and Neuville, 2017).

S^{mix} corresponds to a chemical mixing term that can be ideal or non-ideal. In the case of Ca/Mg mixing, the simplest hypothesis that can be made is that $S^{mix} = S^{ideal}$, and thus can be written as:

$$S^{ideal} = -n \sum R\ x_i\ ln\ x_i, \qquad (10)$$

where R is the perfect gas constant and n is the number of atoms exchanged per formula units, 1 in this case, $x_i = Ca^{2+}/(Ca^{2+}+Mg^{2+})$. From a thermodynamic point of view, the ideal solution implies that end-members components mix randomly in solution.

The excellent agreement (Figure 7B) between entropies obtained from viscosity measurements and values predicted using eqs 6 to 10 shows that the ideal mixing hypothesis for *Ca/Mg* is consistent with the data. It should be noted that the mixing effect is predominant near T_g. The configuration entropy of the intermediate compositions is therefore much higher than that of the end-members, explaining the minimum in viscosity observed upon Ca/Mg mixing. When temperature increases, the entropy of the end-members increases rapidly and S^{mix}, which is constant, eventually becomes small compared to $\Sigma\ x_i\ S^{conf}_i(T_g)$ in eq. (9). Therefore, at high temperatures, S^{mix} is negligible and this results in a quasi-linear variations in viscosity, driven by the linear variation of C_{pl} upon *Ca/Mg* mixing.

These macroscopic conclusions about Ca/Mg mixing are in very good agreement with nanoscale investigations made by ^{17}O NMR (Allwardt and Stebbins, 2004) and neutron diffraction and RMC (Cormier and Cuello, 2013). From neutron diffraction, the silicate network shows small but significant changes with the Mg/Ca exchange and a significant intermixing of Ca and Mg can be observed (Cormier and Cuello, 2013). From another point of view, ^{17}O NMR spectra of the diopside glass $(CaMg)SiO_3$ shows that only one broad non-bridging oxygen atom (NBO) peak is visible, and encompasses the entire range of chemical shifts ranging from Ca-NBO to Mg-NBO. Comparison of the isotropic projections from 3QMAS NMR to 1D spectra predicted using a random model show that Ca/Mg mixing in Ca/Mg-

574 silicate glasses is generally highly disordered (Allwardt and Stebbins, 2004), except maybe near the glass
575 transition temperature where a more ordered glass is possible as shown by neutron diffraction made on
576 $CaSiO_3$ glass by Gaskell et al. (1985).
577
578 *Validity of the viscosimetry approach to determine $S^{conf}(T_g)$*
579 We have just shown that it is possible to determine configurational entropies using viscosity
580 measurements and the AG theory. Are those values of $S^{conf}(T_g)$ truly representative of the glass residual
581 entropy? To answer this question, we can compare $S^{conf}(T_g)$ obtained from calorimetric measurements to
582 those obtained from fitting viscosity data. Data from 11 very different compositions, including B_2O_3,
583 SiO_2 or $KAlSi_3O_8$, show very good agreement between $S^{conf}(T_g)$ values retrieved from viscosity
584 measurements or calorimetric measurements (Figure 8). This thus validates the use of eq. 6 to determine
585 $S^{conf}(T_g)$ of melts.

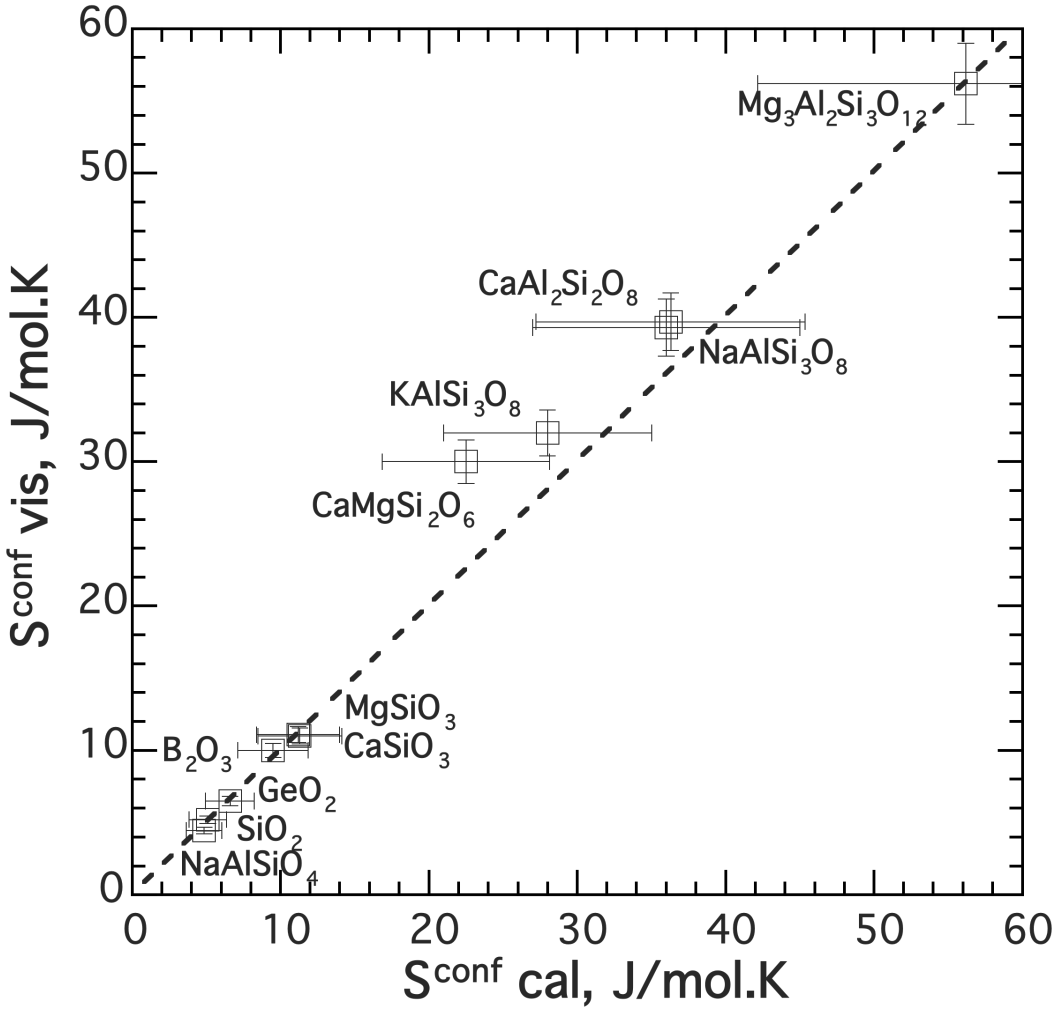

586
587 *Figure 8: viscosimetry configurational entropy versus calorimetry configurational entropy for 10*
588 *different oxide glasses for which determination of calorimetric measurements are possible. Calorimetric*

data are from Richet (1984) for SiO_2, $NaAlSi_3O_8$, $KAlSi_3O_8$, de Ligny and Westrum (1996) for GeO_2 and B_2O_3, Richet et al; (1991) for $NaAlSiO_4$, Tequi et al. (1991) for $Mg_3Al_2Si_3O_{12}$, and Richet et al. (1986) for $MgSiO_3$, $CaSiO_3$, $CaMgSi_2O_6$ and $Ca_2Al_2Si_2O_8$. Viscosity data are from Hetherington et al. (1964) and Urbain et al. (1982) for SiO_2, Neuville and Richet (1991) and Le Losq and Neuville (2013) and Le Losq et al. (2017) for alkali and alkaline-earth silicate and aluminosilicate compositions, from Fontana and Plummer (1966) for GeO_2, and from Eppler (1966), Macedo et Litovitz. (1965), Napolitano et al. (1965) for B_2O_3.

In the case of Na/K mixing in silicate melts, only one set of measurements is available from Poole (1948). Using those data, Richet (1984) proposed that an ideal, random Na/K mixing occurs in silicate melts, and viscosity can be modelled using the ideal mixing calculation of S^{conf} ; some differences between calculated and measured viscosity in the supercooled silicate melts are visible in Richet (1984) work, however they arise from the way the data and model are represented. The more recent study of Le Losq and Neuville (2017) resolved this, showing that it is clearly possible to model the viscosity of Na-K silicate melts while assuming a random mixing of the alkalis (see section 2.4).

2.3 Mixing alkali and alkaline-earth elements in silicate glasses

Most industrial and geologic glasses are silicate and aluminosilicate glasses containing a mixture of alkali and/or alkaline-earth elements. Igneous rocks (Morey and Bowen, 1925) as well as nearly 90 % of industrial glasses contain mixtures of alkali and alkaline-earth elements. We can cite the particular case of soda-lime silica glasses, extensively used for the construction of conventional windows and container glasses. The importance of $M^{2+}O$-M^{+}_2O-SiO_2 glasses (with M^+ an alkali and M^{2+} an alkaline-earth element) further increased recently because they also are used for the development of bioactive glasses (Hench, 1991 and Kim et al. 1995, Clupper and Hench, 2003, Hill and Brauer, 2011; Brauer, 2015). Given the importance of alkali and alkaline-earth metal cations in glasses, many studies were performed to understand the $M^{2+}O$-M^{+}_2O mixing in silicate glasses. They are essentially focused on the glass mechanical properties or devitrification (Morey, 1930; Frischat and Sebastian, 1985; Koike and Tomozawa, 2007, Koike et al., 2007), on glass structure (Buckerman and Müller-Warmuth, 1992, Jones et al., 2001; Lockyer et al., 1995; Lee and Stebbins, 2003; Lee et al., 2003, Neuville 2005, 2006, Hill and Brauer, 2011; Brauer, 2015; Moulton and Henderson, 2021 and reference therein) or thermodynamic properties (Natrup et al., 2005; Neuville 2005, 2006, Richet et al., 2009b; Inaba et al., 2010, Sugawara et al., 2013). Given the above-mentioned importance of $M^{2+}O$-M^{+}_2O-SiO_2 glasses, we will in this section bring new insights to the effect of $M^{2+}O$-M^{+}_2O mixture on the properties of silicate glass and melt.

623 *2.3.1 Glass formation domains*

624 The substitution of alkali elements by alkaline-earth elements allows extending the glass forming
625 domain of silica glasses to lower silica contents (Figure 9), and, more generally, it allows improving
626 many glass properties (Moore and Carey, 1951, Imaoka and Yamazaki 1963, Tomozawa, 1978; 1999;
627 Gahay and Tomozawa 1989, 1984, Neuville, 2005, 2006). For $M^{2+}O$ and $M^{+}O_2$ bearing silicate glasses,
628 the vitrification domain starts near 50 mol% silica in most cases. For Mg silicates, it starts at 45.7 mol%
629 (Moore and Carey, 1951). It was generally accepted that the presence of Mg-O bonds allows preserving
630 somehow the continuity of the silicate network, with Mg acting to some extent as a network former
631 (Moore and Carey, 1951), an idea in agreement with the low coordination number of Mg discussed
632 previously. In the case of CaO-Na_2O-SiO_2 glasses, the first phase diagram was made by Morey and
633 Bowen (1925). It revealed the domain where glasses can be formed, but also an immiscibility domain in
634 which phase separation is observed. This immiscibility domain is very large near the CaO-SiO_2 binary,
635 extending between 62 and 100 mol% of silica. It decreases rapidly with addition of Na_2O in the glass
636 (Morey and Bowen, 1925, Greig 1927, Hudon and Baker, 2002a,b). In the immiscibility domain, different
637 phases exist: cristobalite, SiO_2, wollastonite $CaSiO_3$, sodium disilicate $Na_2Si_2O_5$, devitrite $Na_2Ca_3Si_6O_{16}$,
638 and a non-defined compound $Na_2Ca_2Si_3O_9$. The proportion of these phases vary as a function of the bulk
639 composition and the cooling rate (Morey and Bowen, 1925, Greig 1927, Tomozawa, 1978; 1999; Gahay
640 and Tomozawa 1989; Hudon and Baker, 2002a,b; see also Schuller chapter in Neuville et al., 2017).
641
642 Similar observations can be made in the other M^{+}_2O-$M^{2+}O$-SiO_2 systems, with M^{+}=Li^{+}, Na^{+}, K^{+} and
643 M^{2+}=Mg^{2+}, Ca^{2+}, Sr^{2+}, Ba^{2+}. Generally, a pyrosilicate phase, $M^{2+}SiO_3$, and one or two phases
644 $M^{+}_yM^{2+}_xSi_zO_u$ crystallize at high silica contents (> 70 mol%, *x,y,z,u* are different proportions of each
645 crystalline phases), except for M^{2+}=Ba^{2+} where the glass forming domain is large but mostly
646 unconstrained. Bender et al. (2002) achieved the synthesis of Ba silicate glasses up to the BS7
647 (BaO/SiO_2=7 in mol %) composition, and Frantz and Mysen (1995) investigated some of those glass
648 compositions by Raman spectroscopy.
649
650 To summarize, in all of the M^{+}_2O-$M^{2+}O$-SiO_2 ternary diagrams, the glass forming domains are
651 relatively small and essentially exist at silica contents higher than 50 mol%, with exception of barium
652 silicates. In the case of sodium and potassium silicates, a large zone of high hygroscopicity exists below
653 the glass forming domain, typically between 66 and 50 mol % of silica for sodium silicate glasses and
654 between 70 and 50 mol % for potassium silicate glasses (Tomozawa, 1978; 1999; Gahay and Tomozawa
655 1989). In general, one should be careful with potassium silicate glasses that are always highly
656 hygroscopic.

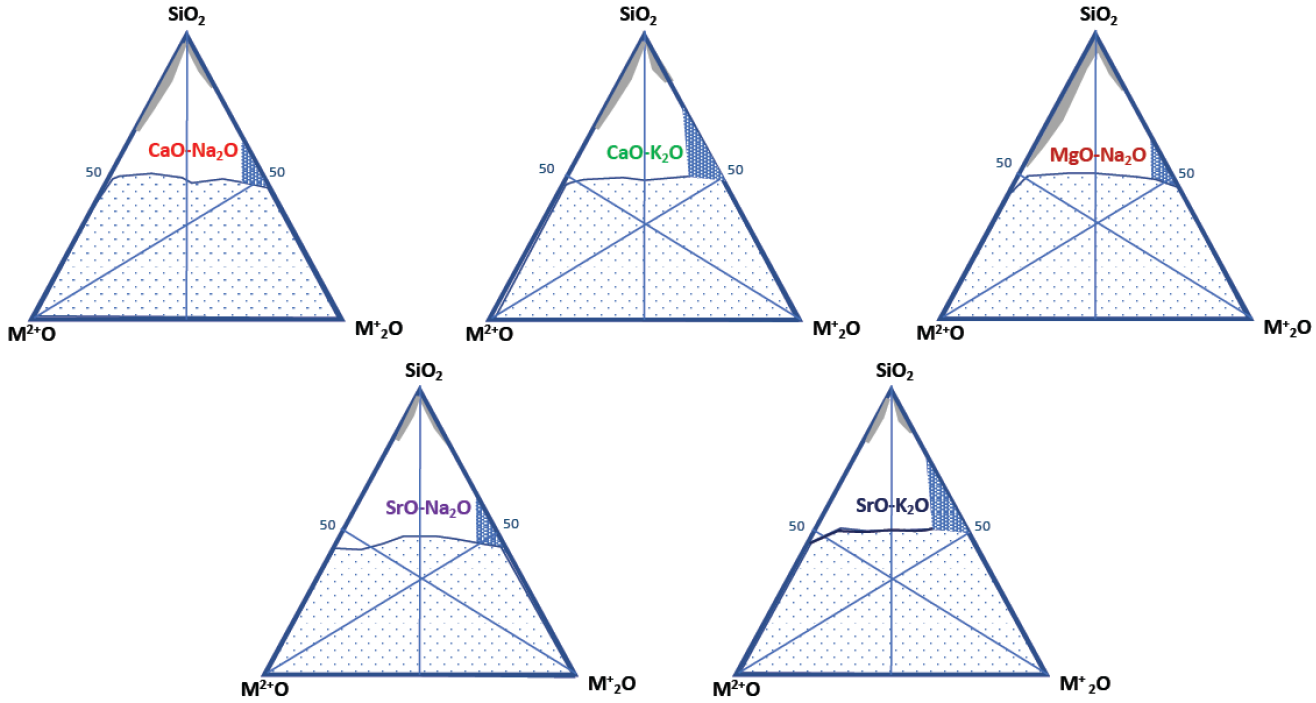

Figure 9: *The upper part of the ternary diagram corresponds to the glass forming region of glass between $M^{2+}O$ and $M^{+}{}_2O$, with M^{2+}=Mg^{2+}, Ca^{2+}, Sr^{2+} and M^{+}=Na^{+}, K^{+} (redrafted from Imaoka and Yamazaki, 1963 and Levin et al., 1964). The white areas are the glass making domain, the light dotted areas are the crystallization domains, the dark dotted lines correspond to the glass making domain, but strongly hygroscopic, and the gray areas to unmixed glass.*

2.3.2 Viscosity variations

Figure 10A shows viscosity measurements of silicate melts for M^{2+}-Na mixing with M^{2+} = Ca^{2+}, Sr^{2+}. Ca- and Sr-silicate melts show similar behavior. The addition of those elements produces a large increase in melt viscosity at constant temperature, in agreement with previous measurements (English, 1923). The lack of measurement between 10^2 and 10^9 Pa·s results from the very rapid rate of crystallization in this viscosity-temperature range for mixed alkali and alkaline-earth silicate glasses (Meiling and Uhlmann, 1977; Mastelaro et al. 2000, Neuville, 2005, 2006). In the Figure 10B, we clearly observe that addition of 10 mole % Na_2O in an alkaline-earth silicate melt has a stronger effect on melt viscosity than addition of 10 mole % $M^{2+}O$ to a soda-silicate melt composition. This indicates that a sodium silicate glass network can incorporate alkaline-earth elements more easily than the opposite. A striking difference exists in the behavior of the viscosity between pure Na-silicate melts and pure alkaline-earth silicate melts (CN60.00 or SN60.00). Indeed, at constant viscosity and near *Tg* (Figure 10B), i.e. near 1000 K, the viscosity of the end-member compounds differ by 10 orders of magnitude. This difference decreases

with temperature: it is less than 0.5 order of magnitude at 1600 K. Furthermore, at 1600 K, the viscosity of the Na_2O-$M^{2+}O$-SiO_2 melts decreases almost linearly with $Na_2O/(Na_2O+M^{2+}O)$. Similar behaviors were already observed by English (1923) in the same system with 75 mole % SiO_2 and 25 mole % Na_2O, and with a substitution of Na_2O by up to 12 mole % CaO.

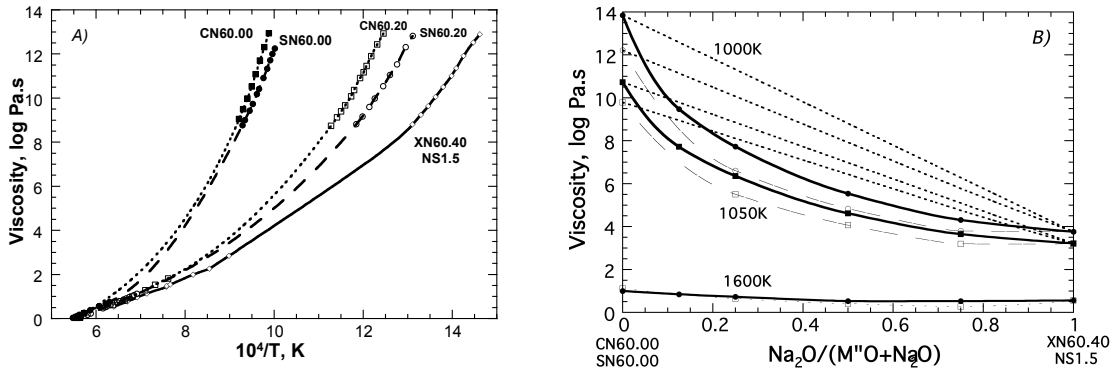

***Figure 10**: A) Viscosity versus 1/T for silicate melts ranging from the pure alkaline-earth silicate melt) to pure soda silicate (XN60.40) composition names are: XN60.Y, X=C or S for the Ca or Sr system, Y correspond to Na_2O content, 60 to SiO_2 in mole percent, and X= 100-(60+Y) all in mole percent. B) Viscosities of Na/M^{2+} silicate melts versus $Na_2O/(Na_2O+M^{2+}O)$ at constant temperature, M^{2+}=Ca, Sr, dashed lines correspond to the linear viscosity variation at 1000 K, 1050 K and 1600 K, solid and open symbols correspond to the CaO-Na_2O-SiO_2 and SrO-Na_2O-SiO_2 systems, respectively compiled from Neuville (2006, 2005).*

The viscosity variations observed in Figure 10 can be understood using equations 6 to 9. It is possible to determine how configurational entropy varies upon the mixing of Na_2O with M^{2+} in the glasses (Figure 11A). S^{conf} can be decomposed in S^{topo} and S^{mix} (eq. 9). S^{topo} is equal to the sum of endmembers. S^{mix}, in the case of M^{+}/M^{2+} mixing, has a complex expression that depends on the way the cations mix into the glass structure.

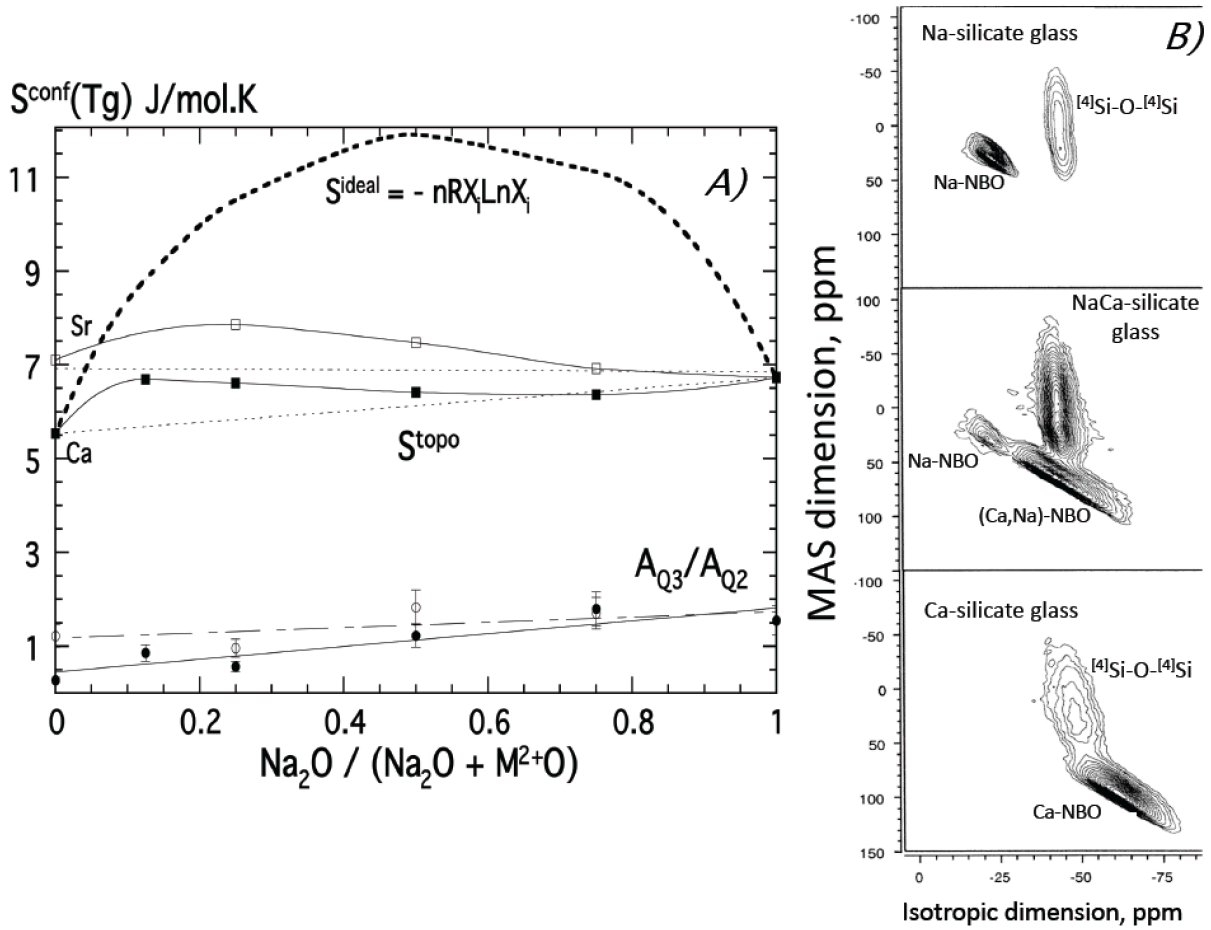

Figure 11: *A) $Na_2O/(Na_2O+M^{2+}O)$ dependence of configurational entropy, $S^{conf}(T_g)$, A_{Q3}/A_{Q2} ratio for in black symbol CaO and in open symbol for SrO (entropy are in J/mol.K and A_{Q3}/A_{Q2} without units and are calculated from the Q^3 and Q^2 areas of the Raman spectra, see Neuville (2005, 2006) for more detail). B) ^{17}O 3QMAS MAS spectra for Ca-Na silicate glasses at 9.4 T redrafted from Lee and Stebbins, (2003).*

Between the calcium and sodium silicate glasses, $S^{conf}(T_g)$ varies non-linearly with $Na_2O/(Na_2O+CaO)$. It increases rapidly with increasing $Na_2O/(Na_2O+CaO)$ to 0.2, then it slightly decreases with further substitution Ca^{2+} by Na^+. Similar observations are made in the $SrO\text{-}Na_2O\text{-}SiO_2$ system (Neuville, 2005). The observed variations strongly depart from the predictions made by the ideal model given in equation 10 (Figure 11A). In the case of Na^+ and Ca^{2+}, or of Na^+ and Sr^{2+}, it is clear that, as their $S^{conf}(T_g)$ variations are close to linear trends, those atoms do not mix randomly in the silicate melts. The fits of $S^{conf}(T_g)$ presented in Figure 11A thus require the use of a non-ideal mixing model. To model S^{mix} in the case of a non-ideal mixing of alkali and alkaline-earth elements, Neuville (2005, 2006) proposed to use the equation:

$$S^{mix} = W_{NM}\, x_n\, y_c^3, \quad (11)$$

where $x_n = Na_2O/(Na_2O+M^{2+}O)$ and $y_c = 1-x_n$, and W_{NM} is a constant.

713

714 *2.3.3 Structure of mixed glasses*

715 Equation (11) implies a significant change in the residual entropy that originates from a re-arrangement
716 of the glass structure as Ca^{2+} is replaced by Na^{+}. Spectroscopic methods that probe the glass structure
717 allow us to investigate such structural changes. ^{23}Na and ^{17}O Nuclear Magnetic Resonance (NMR)
718 spectroscopy data shown a non-random distribution in the case of Na^{+}-Ca^{2+} mixing, with in particular a
719 prevalence of Na^{+}-Ca^{2+} pairs in the system (Figure 11B), and several partially resolved non-bridging
720 oxygen peaks such as Na^{+}-NBO, and mixed peaks (Na^{+}, Ca^{2+})-NBO (Lee and Stebbins, 2003). The
721 observed fractions of Na^{+}-NBO are smaller than those predicted by random distributions of Na^{+} and Ca^{2+},
722 suggesting preference for dissimilar pairs (Lee and Stebbins, 2003) which is also in good agreement
723 (Florian et al., 1996; Lee 2005, Lee and Stebbins 2002 and Lee et al., 2003). In the previous chapter,
724 Raman spectroscopy soda and lime silicate glasses were shown in Figure 9. Different Q^n contributions
725 are visible in those spectra. From these Q^n contributions, the ratio of the area between Q^3 and Q^2 units,
726 A_{Q3}/A_{Q2} can be calculated. Results of such calculation are plotted in Figure 11A. It shows that the fraction
727 of Q^3 units in the glass increases with increasing the $Na_2O/(Na_2O+M^{2+}O)$ ratio. $M^{2+}O$ silicate glasses are
728 thus richer in Q^2 and Q^4 units than alkali silicate glasses (Frantz and Mysen, 1995, Neuville 2005, 2006),
729 because increasing the ionic field strength of metal cation in the glass shifts to the right the equilibrium
730 of the reaction:

731 $$Q^3 \Leftrightarrow Q^2 + Q^4, \qquad (12)$$

732 This observation will be used in section 2.4 for highlighting how one can build models of the structure,
733 entropy and viscosity of silicate melts. Huang et al. (2016) investigated Ca_3SiO_5 composition by using
734 $^{17}O \rightarrow {}^{29}Si$ CP-HETCOR NMR experiment and they proposed that free oxygen can also play a small role
735 structure and properties in the mixed glasses, what is possible but this experiment must be considered
736 with caution, firstly it is a particularly difficult composition to manufacture and secondly, only the
737 nominal compositions are given and not those analyzed.

738

739 *2.3.4 Network polymerization*

740 The substitution of 30 mol% of CaO by Na_2O in an alkaline-earth silicate glass results in a moderate
741 increase of ~ 0.9 J mol^{-1} K^{-1} of $S^{conf}(T_g)$ (Figure 11A). This indicates an increase in the structural disorder
742 in the glass, possibly linked to change in the glass network polymerization. Structural changes that may
743 account for the entropy behaviour may be discerned in the Raman spectra of the glasses. In particular,
744 the ratio of the areas of Raman bands assigned to Q^3 and Q^2 units, A_{Q3}/A_{Q2}, varies with
745 $M^{+}{}_2O/(M^{+}{}_2O+M^{2+}O)$, indicating a change in the Q^n speciation distribution (Neuville, 2006). There is a
746 distinct increase of this ratio with adding Na_2O in the alkaline-earth silicate glasses. In the case of Na/Ca

747 and Na/Sr mixing, Raman spectroscopy observations shown in Figure 11A are in good agreement with
748 previous observations by Raman spectroscopy (McMillan, 1984; McMillan et al., 1982; Frantz and
749 Mysen, 1995) and by ^{17}O NMR (Maekawa et al., 1991; Buckerman and Müller-Warmuth, 1992; Jones
750 et al., 2001, Lee and Stebbins, 2003, Lee et al., 2003), all showing a decrease in Q^3 fraction upon
751 substitution of alkali by alkaline-earth element in silicate glasses. Moreover, the increase in Q^2 units with
752 adding alkaline-earth elements in soda silicate glasses can be correlated to increasing Boson peak
753 frequency and intensity (Neuville, 2006).
754 Note that below 250 cm^{-1}, there is only a scattering continuum and the Raleigh tail of the exciting line,
755 except at very low frequency where there is the so-called boson peak (Malinovsky and Sokolov, 1986;
756 Buchenau et al., 1986). This peak has been ascribed to excitations associated with rotational motions of
757 almost rigid tetrahedra (Buchenau et al., 1986; Helhen et al., 2000, 2002). Helhen et al. (2002) consider
758 that this peak, observed for different silicate glasses, increases in intensity and shifts to higher frequency
759 with higher distortion of the SiO_4 tetrahedra. Several others interpretations are proposed: - Champagnon
760 and collaborators proposed that Boson peak can be link with structural homogeneity in the glass
761 (Champagnon et al., 2009), and the other hand Chumakov and collaborators proposed that Boson peak
762 can be attributed to some fluctuation of disorder in glass (Chumakov et al., 2014) and finally Schirmacher
763 and collaborators proposed an intermediate interpretation by considering that the Boson peak can
764 corresponds to the spatial fluctuations of elastic constants caused by the structural disorder of the
765 amorphous materials (Schirmacher and Ruocco, 2020, Schirmacher et al., 2015). If we consider that
766 molecular dynamic simulations provided by Cormack and coworkers suggest that Si-NBO bond length
767 is about 0.05Å shorter than the Si-BO bond length (Henderson, 1995; Cormack and Du, 2001; Du and
768 Cormack 2004)[5], we can propose that Q^2 units are more distorted than Q^3 or Q^4 units. This implies that
769 $Q^4$and Q^0 units are regular tetrahedra with Q^4 bigger than Q^0 and they are less distorted than the Q^1, Q^2,
770 Q^3 units species (Nakamura et al., 2013). It is probable that Q^2 units are the more distorted tetrahedra
771 with 2 distances T-BO and 2 distances T-NBO which can be in good agreement with the variation of the
772 frequency of boson peak. So, we proposed that the variation on the Boson peak observed as a function
773 of chemical change in simple systems with cation substitution can be attributed to tetrahedra distortion
774 as observed on SiO_2 glass with pressure. This variation can also result of structural heterogeneity produce

[5] Du and Cormack (2004) proposed from MD simulation that when the alkali content vary between 10 and 50 mole percent the d(Si-BO) vary between 1.625 and 1.629Å and d(Si-NBO) varies between 1.559 and 1.579 Å. Henderson (1995) proposed from EXAFS measurements that d(Si-O) equal 1.61±0.02 Å and 1.58±0.02 Å for NS1.5 glass which is in good agreement with MD.

775 by the fact that soda silicate glasses are richer in Q^3 species than lime-silicate glasses. These structural
776 heterogeneities can also be close the idea of percolation channels proposed by Greaves (1985).
777
778 *2.3.5 Fragility*
779 Angell (1991) proposed a classification of liquids between strong and fragile: a strong liquid shows a
780 linear variation like SiO_2 in the diagram *log η versus* T_g/T whereas this linear relation is not preserved in
781 a fragile liquid (Figure 12). The melt fragility, *m*, is related to its thermodynamic properties via the
782 relationship:
783 $$m = B_e/S^{conf}(Tg) * T_g * (1 + Cp^{conf}(T_g)/S^{conf}(T_g)) \quad , \qquad (13)$$
784 In the case of the M^+_2O-$M^{2+}O$-SiO_2 system, the viscosities of the alkali- alkaline-earth silicate melts
785 are plotted as a function of T_g/T in Figure 12. The strongest liquid is the pure soda silicate, XN60.40
786 (NS1.5), whereas the most fragile liquids are the pure alkaline-earth silicate melts. The Ca- and Sr-silicate
787 melts have similar fragility, despite the Ca-silicate melt being more viscous than Sr-silicate melt.
788 Intermediate chemical compositions mixing Na^+ with Ca^{2+} or Sr^{2+} present an intermediate behavior
789 between end-members. The behavior of the melt fragility correlates well with melt C_p^{conf} values, which
790 decrease of ~ 20 % upon replacing M^{2+} with Na (M^{2+} = Ca^{2+} or Sr^{2+}; Neuville, 2005, 2006). This
791 observation on the decrease of the C_p^{conf} is in good agreement with the increase of the $\Delta Cp = C_{pl}/C_{pg(Tg)}$
792 which varies between 1.2 for the Na-silicate glass up to 1.27 and 1.29 for Ca- and Sr-silicate glasses.
793 Note that, Angell (1991) proposed that ΔCp vary between 1.1 and 1.3 for a strong and fragile liquid
794 respectively.

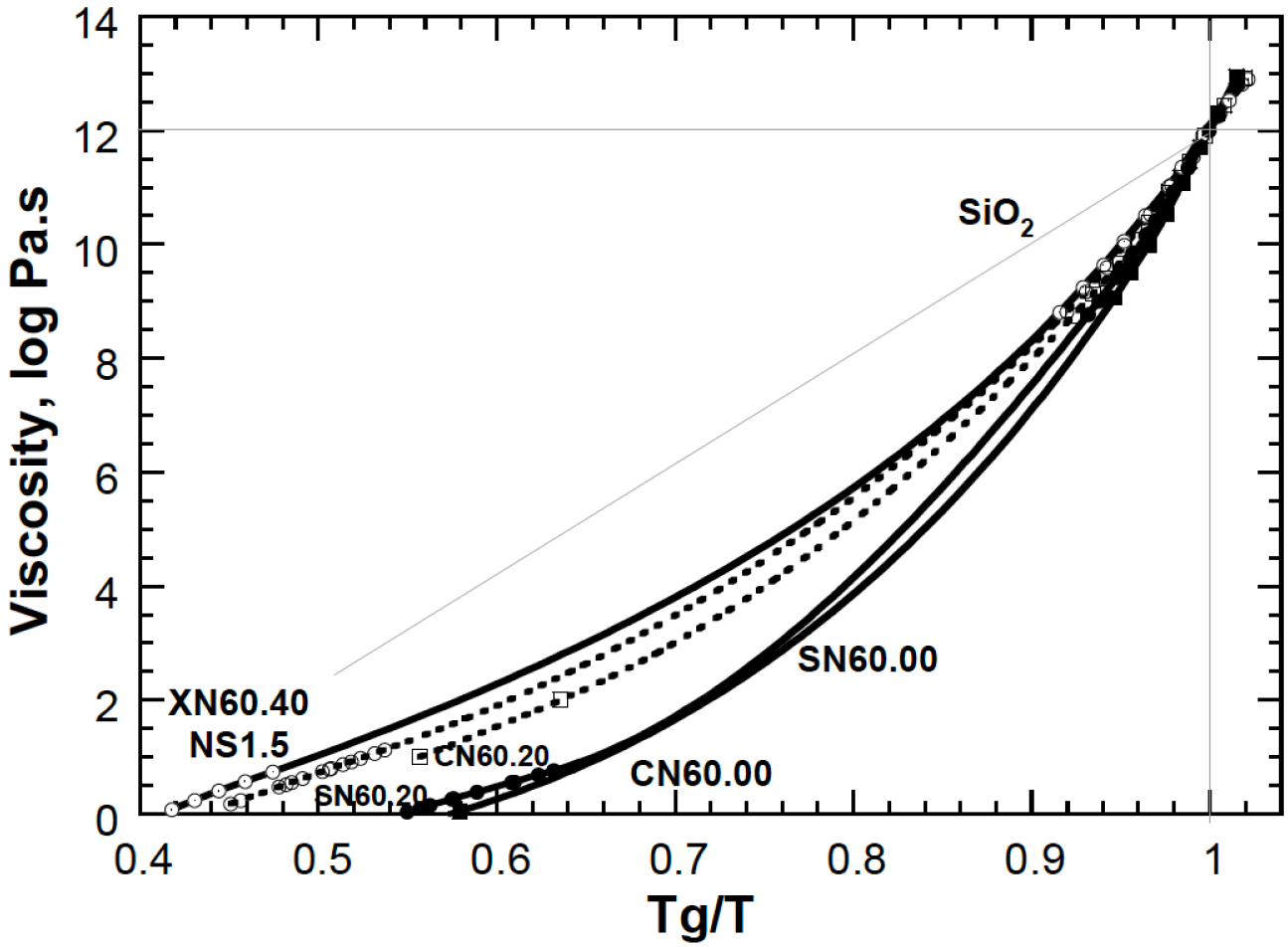

***Figure 12**: Viscosity of soda-$M^{2+}O$ silicate glasses versus T/T_g. Error bars are smaller than symbol size, from Neuville (2005, 2006).*

2.3.6 Melt configurational entropy, fragility, Q^n speciation, mobility and network connectivity

The distribution of cations in the glass network can have important implications for transport properties such as conductivity, viscosity and fragility. In the case of the Na/Ca substitution in silicate melts, Roling and Ingram (2000) have shown that the mobility of Ca^{2+} cations is enhanced upon their replacement by Na^+. This replacement of Ca^{2+} by Na^+ produces a positive coupling effect on the movements of divalent cations that correlates well with the increase in $S^{conf}(T_g)$ (Figure 11A). Conversely, the activation energies related to movements of Na^+ is slightly changed. The cation mobility strongly depends on the glass structure, and the structural changes taking place during the Na/Ca substitution in the Ca-silicate glass enhance the mobility of Ca^{2+}. The modification in network topology will provide new types of empty sites that could be used for Ca movements (Cormier and Neuville, 2004). The mobility of the divalent cation is then assisted by positive coupling with the more mobile monovalent cation (Magnien et al., 2004, 2008).

To summarize the observations made in the case of the mixing between alkali, M^{+}, and alkaline-earth, M^{2+}, elements in silicate glasses and melts:

- alkali and alkaline-earth cations do not mix randomly,
- increased alkali content increases the formation of Q^3 species,
- diffusivity increase with alkaline-earth element (Roling and Ingram, 2000),
- fragility increases with alkaline-earth content,
- the distortion of the tetrahedra suggested by the boson peak variation and the distortion of the network increases with increasing MO content,
- the proportion of Q^2 species increases with $M^{2+}O$ content and in the same way, the intensity and the frequency position of the boson peak increase. The fact, that the alkaline-earth silicate glasses around than 60% of silica correspond to a mixing of Q^2 and a small amount of Q^4 species, may be the origin of the unmixing observed for more than 60% of SiO_2 in the $M^{2+}O$-SiO_2 binary system (see Figure 9). These two interconnected Q^n species can also be an image of the percolation channels (Greaves et al., 1981, Greaves, 1985, Frischat et al., 2001, Le Losq et al., 2017).

2.4 Silicate glasses and others network formers

2.4.1 Lead

The replacement of SiO_2 by PbO produces a small decrease in the glass molar volume until the Si/Pb ratio reaches a value of 0.5. Further PbO addition results in a molar volume increase. The PbO amorphous molar volume value can be obtained by extrapolation and is 25.0 cm^3 (Robie et al., 1979; see arrow in Figure 5) which is similar to the molar volume of Litharge, PbO with Pb^{2+} in four-fold coordination. Variations in the molar volume of lead silicate glasses correlate well with structural observations made via Raman spectroscopy (chapter 2, this volume, and Ben Kacem et al., 2017). For small amounts of lead oxide added to silica glass (<20 mole %), Pb is essentially in six-fold coordination and its introduction into silica results in the formation of non-bridging oxygens, clearly visible in the Q^n species distribution in the Raman spectra (Ben kacem et al., 2017). This is accompanied by a decrease in melt viscosity and glass transition temperature. At PbO concentrations higher than 20 mol%, a mixture of essentially two lead species, in 4- and 6-fold coordinations, exists. Kohara et al. (2010) and more recently Sampaio et al. (2018) mentioned that Pb can be distributed between 3-, 4-, 5- and 6-fold coordination but recent X-Ray diffraction shows that Pb is essentially distribute in 4- and 6-fold coordination (Drewitt et al., this issue). Pb in four-fold coordination can be considered as a weak network former (Fayon et al., 1998, 1999; Feller et al., 2010; Ben Kacem et al., 2017) as $^{[4]}Pb$ creates a network of interconnected tetragonal pyramid PbO_4 (Morikava et al., 1982). This is visible in Raman spectra, where an intense band at 140 cm^{-1} can be

assigned to Pb-O-Pb covalent bonds (see chapter 3 and Ben Kacem et al., 2017). This band at 140 cm-1 is clearly at higher frequency than that observed in alamosite, $PbSiO_3$, at 110 cm^{-1} and attributed to Pb in 6-fold coordination (Worrell and Henshall, 1978; Ben Kacem, 2017, Pena et al., 2017). The coexistence of network former PbO_4 and network modifier PbO_6 entities agree with the pair correlation function obtained from the X-ray diffraction data (see chapter 3, Figure 6B (Drewitt et al. 2021)), which show that the proportion of PbO_4 increases with decreasing SiO_2/PbO. The mixing of the tetragonal pyramid PbO_4 with SiO_4 tetrahedra is probably mechanical in nature, i.e. the two polyhedra cohabit and are interconnected but their mixture does not result in an excess of entropy as indicated by the linear decreases of the glass transition temperature between 30 and 80% of SiO_2 (Figure 13). The fast decrease in T_g upon addition of ~10 mol% PbO probably relates to the network modifier role of PbO_6 octahedra, containing some NBOs in their first coordination shell.

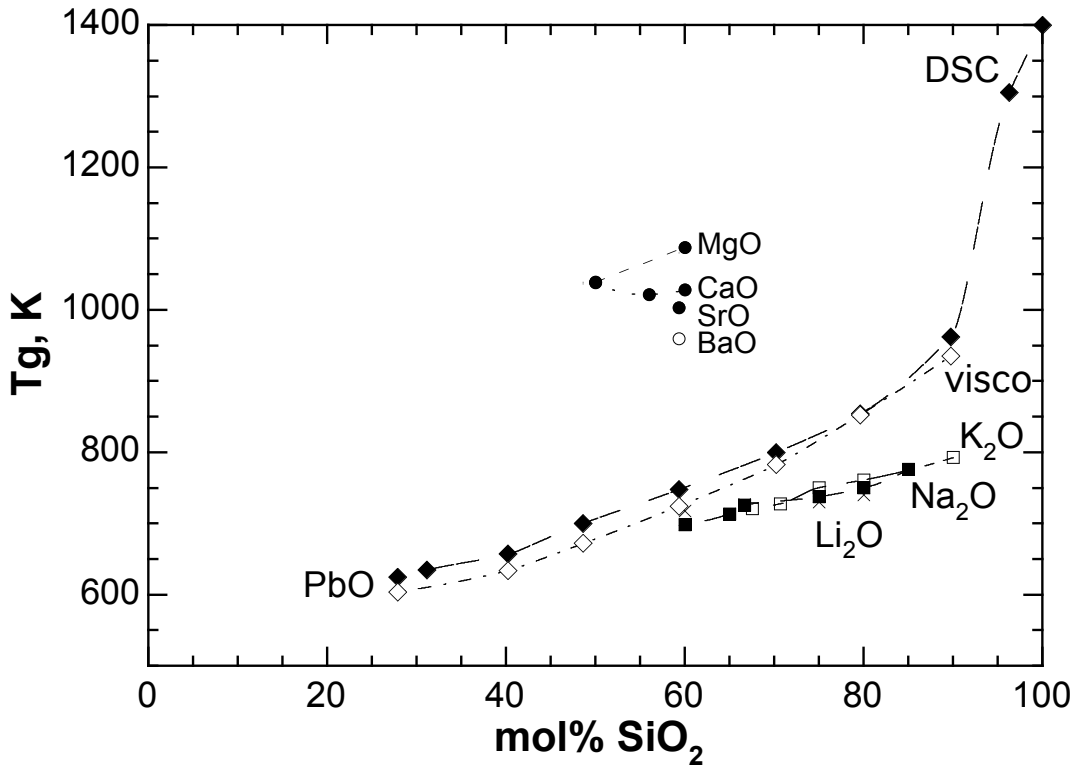

Figure 13: *Glass transition temperature as a function of the fraction of SiO_2 in PbO-SiO_2 glasses. Data for Ca^{2+}, Mg^{2+}, Na^+, K^+, Li^+ silicate glasses are original data from Neuville, Ca50 and Mg50 (Neuville and Richet, 1991), Ca60 and NS1.5, NS2, NS4 from Neuville (2006), NS3 from Le Losq et al. (2014); Sr60 from Neuville (2005) and Pb-silicate glasses open circle are from viscosity measurements and full circle are from DSC measurements. (Ben Kacem et al., 2017). Note that all Tg are obtained using viscosity measurements to be comparable except those obtained by Ben Kacem with DSC.*

The introduction of PbO thus produces the transformation of Q^n units into Q^{n-1} units as PbO_6 are network modifier units. The appearance of these Q^{n-1} species is documented by changes in the high frequency envelope (800 - 1200cm^{-1}) of the Raman spectra of the glasses (Worrell and Henshall, 1978; Ben Kacem et al., 2017). The Raman spectra of PbO-SiO_2 glasses corresponds to the combination of two distinct endmember Raman signals: that of a lead-silicate glass network with Q^{n-1} species, and that of an amorphous lead network characterized by a strong peak at 140 cm^{-1}. The relative abundances of these signals, and of their associated networks, vary as a function of the SiO_2/PbO ratio and this is in good agreement with observation made using ^{17}O NMR by Lee and Kim (2015). Lee and Kim (2015) also observed a small amount of free oxygen as early mention by Sampaio et al. (2018), but this small amount cannot explain the T_g and viscosity variations.

In this sense, lead is an example of an amphoteric[6] element that plays two different roles, network former or network modifier, depending on melt chemical composition. Another example of an element presenting such behavior is Fe^{3+}, which, depending on its coordination, plays different structural roles (Moretti, 2005). Indeed, while Fe^{3+} in 4- or 5-fold coordination can be considered as network formers, Fe^{3+} in 6-fold coordination behaves as a network modifier in silicate melts. It can be found in the literature that such elements are "intermediate" and often aluminum is associated with this terminology. However, the story is more complex than this, and Al^{3+} does not really present amphoteric behavior per se as highly coordinated Al species are not surrounded by NBOs such that $^{[4]}Al$ is exclusively a network former element. Its behavior is however complex, as we shall see in the sections below.

2.4.2 Al in silicate glasses

A well-known feature of silicate mineral structures is that Si cations can be replaced isomorphously by aluminum cations, provided that either mono or divalent cations can ensure charge compensation of Al polyhedra to maintain local neutralization of electrical charges in the structure. As such, those mono or divalent cations are called charge compensators. However, it is also possible to obtain alumina-silica glasses without the presence of charge compensator cations. From a research point of view, this is very interesting because Al_2O_3-SiO_2 glasses are important materials for the understanding of how network former elements mix. Al_2O_3-SiO_2 glasses have a very high liquidus (Sossman, 1933), and are difficult to synthesize except by fast quench or sol-gel methods (e.g. see Wang et al., 2020). With those methods, it is possible to obtain Al_2O_3-SiO_2 glasses in three different regions, near 15 mol%, 50 mol% or 60 mol%

[6] An amphoteric element can react both as an acid or a base; see Moretti (2005) for details on this concept for silicate melts.

of silica. The molar volume of xAl_2O_3-(1-x)SiO_2 glasses calculated from density measurement (Wang et al., 2020) varies linearly between 27.3 up to 31 cm^3 for 60 % of Al_2O_3 (Figure 6).

From the data on Al_2O_3 (corundum), the molar volume of Al in six-fold coordination is 25.57 cm^3 (Robie et al., 1979). The molar volume of Al in five-fold coordination is unknown, but the extrapolation of the Al_2O_3-SiO_2 line in Figure 5 yields a value of ~32 cm^3 at 0 mol % of SiO_2. Poe et al. (1992) proposed that Al_2SiO_5 glass is composed by 50% of $^{[5]}$Al, 40% of $^{[4]}$Al and 10% of $^{[6]}$Al.

However, no information on the geometry of the $^{[5]}$Al oxygen polyhedra is available: it could be a tetragonal pyramid, or a trigonal bi-pyramid. The present data do not allow assessment of this problem, but it is possible to make an assumption: the geometric shape of $^{[5]}$Al will depend on the nearest charge compensator cation. For example, the smaller the quadrupolar moment, Cq, observed in ^{27}Al NMR is, the more $^{[5]}$Al will look like a square base pyramid. The role of $^{[4]}$Al, $^{[5]}$Al and $^{[6]}$Al in the glass and melt structure will be discussed later in section 3.

2.5 Silicate melts: how can we use existing structural knowledge to model melt properties

With the above information from the traditional glass forming ranges, we understand that we know for silicate melts and glasses:

- the glass has a network of Qn units, whose concentrations can be determined via NMR or Raman spectroscopy (Farnan and Stebbins, 1990; Stebbins et al., 1992; Dupree et al., 1986; Maekawa et al., 1991; Mysen, 1990; Mysen and Frantz, 1993; 1994; Ispa et al., 2010; Zhang et al., 1996; Sen et al., 2003; Davis et al., 2010; O'Shaughnessy et al., 2020; Nesbitt et al., 2018, 2021)
- glass and melt heat capacities, which can be calculated, and
- their rheological properties.

It has been a longstanding goal to link those observations via a single model that could predict the properties and structure of glasses and melts. A pioneering start was the work of Mysen (1995), who proposed to calculate the melt configuration heat capacity from partial heat capacity values $C_p^{conf}{}_{Qn}$ assigned to each Q^n unit with a fraction x_{Qn}:

$$C_p^{conf} = \Sigma x_{Qn} C_p^{conf}{}_{Q^n}. \quad (14)$$

Links between melt thermodynamic parameters, rheology and structure were further established by subsequent publications (Neuville and Mysen, 1996; Neuville 2006; Mysen 1990, 1995, Le Losq et Neuville, 2013, 2017, Le Losq et al., 2015, 2017; Russell and Giordano 2017). Recently, Le Losq and Neuville (2017) demonstrated how, using the Adam and Gibbs theory and Q^n values from NMR spectroscopy, it is possible to determine with a high precision the viscosity of Na_2O-K_2O-SiO_2 melts. In this section, we will show how such a model can be constructed, and what opportunities for extension

are envisioned. The application of such modeling for aluminosilicate melts will further be discussed in section 3.

Using a principle similar to that of equation (14), we may be able to calculate values of $S^{conf}(T_g)$ and B_e in eqs. 6 to 9 from partial values assigned to Q^n units in the glass, i.e. in the melt at the glass transition temperature. This is possible because B_e is temperature-independent (Adam and Gibbs, 1965), and $S^{conf}(T)$ can be estimated from $S^{conf}(T_g)$ and $C_p{}^{conf}$, which can be easily determined from viscosity data and modeled in silicate melts, respectively. This implies that we can use glass structural data to build a model for melts. However, we need to be able to model precisely how the distribution of Q^n units vary with glass composition. Fortunately, the distribution of Q^n units mostly depends on (i) the glass silica concentration, and (ii) the ionic field strength (IFS) of network modifier metal cations. Numerous ^{29}Si NMR spectroscopy data were acquired on silicate glasses and allow us to know precisely how Q^n units distribute depending on glass composition. They allow, in particular, determining the equilibrium constants of the Q^n dissociation reactions

$$2Q^n = Q^{n-1} + Q^{n+1}, \qquad (15)$$

which is at play in silicate glasses and melts. This explains the deviations of the Q^n distribution measured compared to silicate minerals, where binary combinations of Q^n units are observed (e.g. Q^4-Q^3, Q^3-Q^2, etc.). In glasses and melts, randomness implies that the Q^n distribution departs from the binary model. The existing ^{29}Si NMR and Raman data allow one to estimate how the melt composition influences such deviation. In Figure 14, we collected K_{eq} equilibrium constants for the dissociation of Q^3 units and of Q^2 units, and reported them as a function of the ionic field strength. In this Figure, most data are from NMR spectroscopy because data interpretation from ^{29}Si NMR 1D and 2D methods (Edén, 2012) is less subject to debate, despite some possible complications that highlight that the determination of Q^n unit distribution always is an arduous task (Pedone et al. 2010; Charpentier et al. 2013). Indeed, Raman data requires the use of Raman cross sections, determined by calibration against ^{29}Si NMR data, to transform the area of Raman peaks assigned to different Q^n units into concentrations of those Q^n units. This is a first barrier as Raman cross-sections are not straightforward to obtain, a second one being the fit of the spectra that can be a topic of debate (Nesbitt et al., 2018, 2021; Bancroft et al., 2018). The very few K_{eq} values from Raman data used in Figure 14 do not come from possibly controversial traditional peak fitting methods, but from the use of linear alternative least square methods to retrieve partial Raman spectra for the different Q^n units in binary silicate glasses, a method developed by Zakaznova et al. (2007) and Malfait et al. (2007, 2009). While it is very powerful for binary silicate glasses, it relies on composition-specific, constant Raman signal shapes for the different Q^n units. This hypothesis is valid in binary systems, but this method is limited because (i) partial Raman spectra for one binary system (e.g.

963 Na_2O-SiO_2) cannot be used for others and (ii) this starting hypothesis becomes void for ternary and more
964 complex systems. This is because partial Raman spectra and Raman cross-sections differ depending on
965 the network modifier present into the glass (e.g. Malfait et al., 2009; Woelffel et al. 2015).

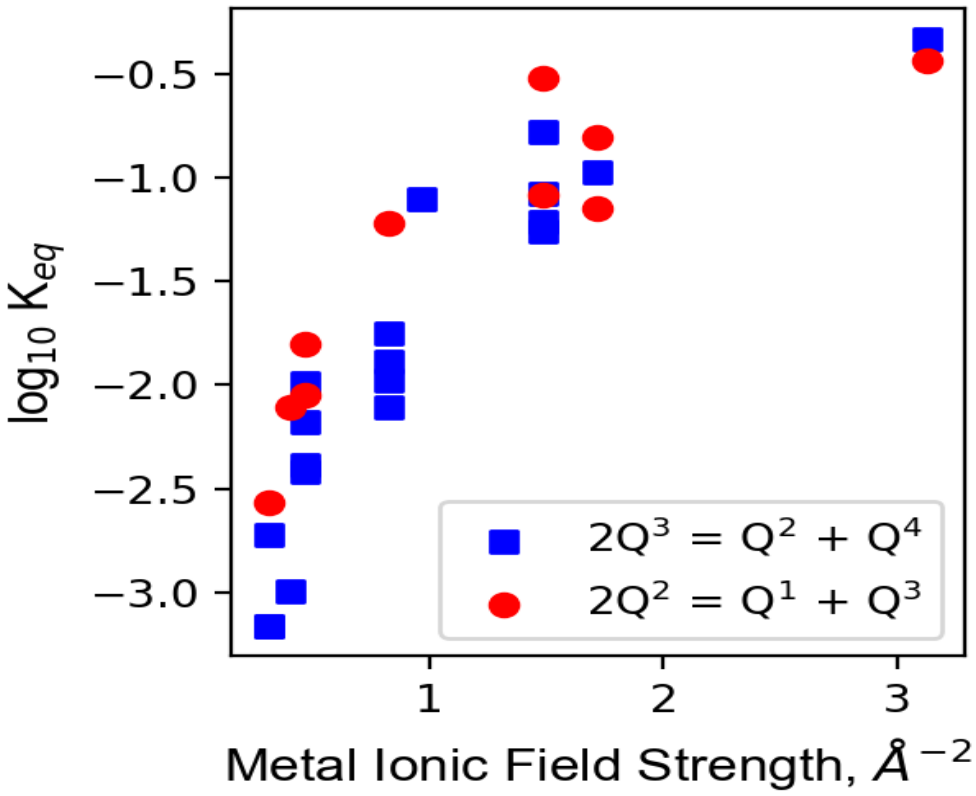

966 ***Figure 14***: *Equilibrium constants of the dissociation of Q^3 and Q^2 units represented as a function of the*
967 *metal ionic field strength. Metal IFS was calculated assuming a coordination number of 6 and ionic*
968 *radius from Whittaker and Muntus (1970). Equilibrium constants were calculated from the data of*
969 *Emerson (1989), Emerson and Bray (1994), Maekawa et al. (1991), Bray et al. (1991), Zhang et al.*
970 *(1996, 1997), Schneider et al., (2003), Voigt et al. (2005), Larson et al. (2006), Malfait et al. (2007),*
971 *Zakaznova-Herzog et al. (2007), Sen et al. (2009), Malfait et al. (2009), Davis et al. (2010) and Herzog*
972 *and Zakaznova-Herzog (2011).*
973
974
975 An idea that arises when seeing Figure 14 is to parametrize the K_{eq} values as a function of the mean
976 ionic field strength of metals cations in silicate glasses. Indeed, K_{eq} values for Q^3 and Q^2 units change
977 systematically depending on the ionic field strengths of the metal cation in the glass structure. It thus
978 seems possible to calculate K_{eq} values from the mean ionic field strengths of metal cations in the glass.
979 For ternary and more complex silicate glasses, this relies on the fact that mixing different cations in

980 silicate glasses affects linearly the distribution of Q^n units. Fortunately, this is a good approximation.
981 Indeed, from ^{29}Si and ^{23}Na MAS NMR spectroscopy, the Q^n unit distribution upon Rb-Na mixing in
982 alkali trisilicate glasses does not systematically change (Hater et al., 1989). This was also reported during
983 Na and Li mixing in $(Na,Li)_2Si_2O_5$ glasses (Ali et al., 1995, Sen et al., 1996). From ^{6}Li, ^{7}Li and ^{29}Si static
984 NMR spectroscopy data, Bray et al. (1991) observed a linear change of the Q^3 units fraction upon mixing
985 Li and K in disilicate glasses. The ^{29}Si static NMR data from Emerson and Bray (1994) further suggest
986 a slight departure from linearity of the Q^3 unit fraction when mixing $Na_2Si_2O_5$ and $Cs_2Si_2O_5$ glasses. Such
987 interpretation may be consistent with ^{17}O Dynamic Angle Spinning NMR data from mixed $Na_2Si_2O_5$-
988 $K_2Si_2O_5$ glasses (Florian et al., 1996), showing slightly non-linear changes of the fractions of Bridging
989 (BO) and Non-Bridging (NBO) oxygen anions with changes in the glasses K/ (K + Na) ratios. Such
990 observation agrees with the recent report of Le Losq and Neuville (2017), which showed that the Raman
991 areas of Q^n units in alkali trisilicate glasses vary linearly within error bars.
992
993 From the above review, it thus should be possible to calculate K_{eq} values for Q^3 and Q^2 unit
994 dissociation given the mean IFS of metal cations present in the silicate glass. However, despite a good
995 correlation, scattering is visible in Figure 14. Such scattering results from second order effects that may
996 be related to some local peculiarities of the effect of each cation on K_{eq} values as well as our lack of a
997 perfect understanding of the coordination number of each cation. To circumvent this problem, we propose
998 to calculate the mean K_{eq} values in silicate glasses based on the combination of K_{eq} values assigned to
999 each cations (from their calculation in the binary $M^x_{2/x}O$-SiO_2 systems):
000
001 $$K_{eq}\ glass = \sum K_{eq}^i\ x_i\,, \qquad (16)$$
002 where x_i is the fraction of a given cation relative to the sum of all cations. Assuming linear variations
003 in the Q^n unit fractions upon mixing different cations, a valid hypothesis given existing data as indicated
004 previously, this will allow obtaining the most precise model for the variations in Q^n units in Al-free
005 silicate glasses (the case of aluminium deserves its own section, such that its effect will be discussed in
006 section 3). K_{eq}^i values determined for each system are provided in Table 1, based on the data reported in
007 Figure 14.
008

Metal cation	K_{eq} $2Q^3 = Q^2 + Q^4$	K_{eq} $2Q^2 = Q^1 + Q^3$
Li	0.09(5)	0.2(2)
Na	0.012(4)	0.06(-)

K	0.006(3)	0.012(5)
Rb	0.001(-)	?
Cs	0.001(-)	0.003(-)
Mg	0.464(-)	0.364(-)
Ca	0.106(-)	0.156(-)
Ba	0.078(-)	?

Table 1: *mean values of the K_{eq} coefficients for the dissociation of Q^3 or Q^2 units in M^+O_2-SiO_2 or $M^{2+}O$-SiO_2 glasses, calculated from the data presented in Figure 14. Standard deviations from the mean are provided in parenthesis, when possible.*

Now that we can calculate the fractions of Q^n units for various silicate compositions, it opens doors to calculate the terms of the Adam and Gibbs equation: B_e and $S^{conf}(T_g)$. Le Losq and Neuville (2017) leveraged such ability for K_2O-Na_2O-SiO_2 melts with 60 to 100 mol% SiO_2, taking into account the ideal mixing of Na and K in silicate melts (Richet, 1984) when developing equations for $S^{conf}(T_g)$ and B_e. For $S^{conf}(T_g)$, they assumed that, added to the topological entropy S^{topo}, excess entropies arise from the ideal Si mixing between the different Q^n units $S^{mix}{}_{Si}$ and random mixing of Na and K into the glass network $S^{mix}{}_{Na\text{-}K}$, such that:

$$S^{conf}(T_g) = S^{topo} + S^{mix}{}_{Si} + S^{mix}{}_{Na\text{-}K}\,, \qquad (17)$$

with

$$S^{topo} = \sum_{n=2}^{3} x_{Q^n_{Naenv}} S^{conf}_{Q^n_{Naenv}} + \sum_{n=2}^{3} x_{Q^n_{Kenv}} S^{conf}_{Q^n_{Kenv}} + x_{Q^4} S^{conf}_{Q^4}\,, \qquad (18)$$

$$S^{mix}_{Si} = \frac{-x_{Si}}{x_O} * 2 * R * \sum_{n=2}^{4} x_{Q^n} ln\left(x_{Q^n}\right)\,, \qquad (19)$$

and

$$S^{mix}_{Na-K} = \frac{-(x_{Na}+x_K)}{x_O} * 2 * R * \left(X_K ln(X_K) + (1-X_K) * ln(1-X_K)\right)\,, \qquad (20)$$

with x_{Si}, x_O, x_{Na} and x_K the atomic fractions of Si, O, Na and K respectively, $X_K = K/(K+Na)$, R the gas constant, and x_{Q^n} the Q^n fractions. We note that, as Le Losq and Neuville (2017) investigated melts with NBO/T lower than 1.5, equations above were limited to Q^2 to Q^4 units. In addition, in the topological contribution (equation 18), $Q^n{}_{Naenv}$ and $Q^n{}_{Kenv}$ units with their associated $S^{conf}_{Q^n_{Naenv}}$ and $S^{conf}_{Q^n_{Kenv}}$ values are distinguished; those are the Q^n units, with n < 4, that have NBO bonded preferentially to Na or K, respectively. This is an approximation introduced to take into account the fact that Q^n units with NBO

bonded to Na or K may present different S^{conf} values, as shown by the difference of $S^{conf}(T_g)$ between sodic and potassic silicate glasses.

For the calculation of B_e, the link between $S^{conf}(T)$ and B_e needs to be considered. Indeed,

$$B_e = \frac{\Delta\mu s_c}{k_B}, \qquad (21)$$

and

$$S^{conf}(T_g) = \frac{N_A}{z\ (T_g)} s_c \ , \qquad (22)$$

with $\Delta\mu$ the Gibbs free-energy barrier opposed to the cooperative rearrangements of molecular subunits of size $z\ (T_g)$ and intrinsic entropy s_c , k_B the Boltzmann constant and N_A the Avogadro constant (Adam and Gibbs, 1965; Richet, 1984). s_c represents the entropy of the molecular subunits involved in the melt viscous flow and relaxation process. It appears in both eqs. (21) and (22), yielding a strong correlation between $S^{conf}(Tg)$ and B_e (Neuville and Richet, 1991). From eqs. (20) and (22), we can write

$$B_e = \frac{\Delta\mu z\ (T_g) S^{conf}(T_g)}{R}, \qquad (23)$$

with R the perfect gas constant (=$N_A k_B$). From eq. (23) and considering that $\Delta\mu$ and s_c are temperature-independent (Richet, 1984), B_e should be expressed similarly to $S^{conf}(T_g)$, from the melt structure recorded at T_g in glasses. Considering that, Le Losq and Neuville (2017) assumed that B_e can be expressed as the sum of partial molar B_e terms for the different Q^n_{Menv} and Q^4 units, with additional non-linear contributions arising from the role of $S^{conf}(T_g)$ in eq. (23). The latter non-linear contributions are obtained by directly injecting eqs. (19) and (20) with K_1 and K_2 scaling terms in the expression of Be:

$$B_e = \sum_{n=2}^{3} x_{Q^n_{Naenv}} B_{e_{Q^n_{Naenv}}} + \sum_{n=2}^{3} x_{Q^n_{Kenv}} B_{e_{Q^n_{Kenv}}} + x_{Q^4} B_{e_{Q^4}} + K_1 S^{mix}_{Si} + K_2 S^{mix}_{Na-K} \qquad (24)$$

Using this model, Le Losq and Neuville (2017) showed that it is possible to calculate the viscosity of the alkali silicate melt with a mean square error of 0.2 log Pa·s. This error is much lower than those of parametric models, typical presenting root mean squared errors on their parametrization datasets of ~ 0.6-0.7 log Pa·s (e.g. Hui and Zhang, 2017; Giordano et al., 2008).

Le Losq and Neuville (2017) used cubic splines for interpolation of the Q^n distribution in their model. With the approach presented in this chapter, it is possible to replace this by the K_{eq}-based model for Q^n distribution in silicate melts in order to improve the future deployment and development of such a thermodynamic viscosity model. Preliminary tests yield good predictions with standard errors of 0.3 log

Pa·s, a value slightly higher than the initial value of 0.2 log Pa·s from Le Losq and Neuville (2017). This difference arises from the fact that the initial cubic spline modeling of the Q^n distribution in K_2O-Na_2O-SiO_2 melts is slightly more accurate than the global structural model based on the K_{eq} values calculations. Differences are in the range of 1-2%. This actually highlights how sensitive a model can be to melt structure: an error of only 1-2 % alters measurable the accuracy of the model.

3. Aluminosilicate glasses and melts

Aluminum is a key element in Earth and material sciences because it is present, in various amounts, in most geologic and industrial glasses, and it drastically affects their properties. Generally, a well-known feature of the structure of silicate minerals is that silicon ions may be replaced isomorphously by aluminum ions provided that either mono or divalent cations are available to maintain local neutralization of electrical charges in the structure (Putnis, 1992). This feature is clearly visible in tectosilicates that present an interconnected three-dimensional silica-like tetrahedral structure, in which the mono or divalent cations are accommodated in the framework free volumes. In these minerals, the ratio $R=M^{+}_2O/Al_2O_3$ or $M^{2+}O/Al_2O_3$ is unity. The metal cations play charge compensator roles, and no non-bridging oxygens are present. This is also generally the case in tectosilicate glasses, albeit some possible minor amounts of NBOs may be present (Stebbins and Xu, 1997). However, an additional complexity in aluminosilicate glass is the variable coordination number of Al. Indeed, while Al mostly substitutes for Si in the SiO_4 tetrahedra in silicate glass, it also is found in five and six-fold coordinations, in proportions that depend on melt chemical composition, system pressure and temperature, and glass-forming cooling rate (Ohtani et al., 1985; Risbud et al., 1987; Murdoch et al., 1985; Mc Millan, et al., 1982; Merzbacher et al., 1990, 1991; Lacy, 1963; Merzbacher and White, 1991; Coté et al., 1992, Stebbins and Xu, 1997, Sato et al., 1991; Allward and Stebbins, 2005a,b, 2007, Allwardt, et al., 2004; 2007; Stebbins et al., 2000, 2008; Stebbins, 2008; Henderson et al., 2007; Lee 2005, Lee and Stebbins, 2000, 2002, 2009; Neuville et al., 2004ab, 2006, 2008a,b, 2010; Le Losq et al., 2014). The varying coordination number of Al raises the question of its role in the melt structure depending on its coordination. Indeed, following the terminology proposed by Zachariasen (1932), while Al in four-fold coordination is a network former, Al in six-fold coordination should be a network modifier, and Al in five-fold coordination should probably also be considered as a network modifier. We will review such questions, and more generally the connection between aluminosilicate melt structure and properties in this section.

3.1 Molar volume, coordination number and structure

Density and molar volume are properties easy to measure in glasses, and bring important pieces of information regarding their internal structure, and by extension, that of the melt at the glass transition.

Variations in the molar volumes of alkali and alkaline-earth silicate and aluminosilicate glasses as a function of silica concentration show similar trends, except for the heaviest elements, like potassium, cesium and rubidium (Figure 15). From silica glass with V_m=27,31cm^3, it is found that generally the molar volume decreases with the decrease in SiO_2, except for K-, Cs-, Rb- silicate glasses. For the same SiO_2 content, the magnitude of the decrease of the molar volume depends on the ionic field strength of the metal cation: it is moderate for Na^+ and very important for Mg^{2+} (for example V_m of Ca silicate =21,21cm^3 and 24,14cm^3 for Na-silicate, both at 60 mol % of SiO_2 – note that we compare Ca and Na silicate glass and not Mg-silicate at 60 of silica, because this glass is made with a high cooling rate, and its fictive temperature is probably very different than that for the Na-silicate glass). In the case of potassium, V_m always increases regardless of the glass aluminum content. For other cations, V_m variations in aluminosilicate glasses are more complex. First, the M^{2+}/Al or M^+/Al ratio directly influences the variations of V_m with the glass silica concentration. Secondly, a general concave trend of the V_m *versus* SiO_2 relationship is observed according to previous work (Seifert et al., 1982, Doweidar et al., 1999, Doweidar 1999). Taking the SiO_2-$CaAl_2O_4$ binary mixture as an example, and starting from silica, V_m decreases with silica decrease until 50 mol% SiO_2 (V_m=25,81cm^3 for anorthite glass), and then increases up to a value of ~27 cm^3 for the pure $CaAl_2O_4$ end-member for example. Such non-linear V_m trends indicate that V_m modelling in aluminosilicate glasses cannot be obtained from a linear combination of partial V_m values assigned to the different oxides. To circumvent this problem, several papers have modelled the density of glass and melts as a function of their expected Q^n speciation (Doweidar, 1999, Doweidar et al., 1999) or other entities like partial volume of oxide components (Lange, 1996, 1997, Bottinga and Weill, 1970).

One of the most important pieces of information arising from V_m data analysis is the possibility to provide knowledge regarding the coordination numbers of metal cations as well as aluminum. We have mentioned, in section 2.1 (Figure 5), that metal cations' CNs remain almost constant in silicate glasses. It is also well known that the molar volume of the SiO_4^{4-} tetrahedra doesn't change a lot as a function of the Q^n species because the d(Si-BO) or d(Si-NBO) vary less than 0.05Å (Cormack and Du, 2001; Du and Cormack 2004). This variation corresponds to a variation of around 3% on the distance between Si-BO and Si-NBO which causes a variation of the volume of the tetrahedra between 12.4 and 9.3% as a function of the amount of alkali content respectively 10 and 50%, if we used the distances given by Cormack and collaborators. In the case of aluminum, the molar volume of AlO_4^{5-} tetrahedra doesn't change because Al-O distances stay almost constant as a function of the different Q^n species for Al[7], and the most important change in the molar volume of Al units come from the change in the coordination of Al and

[7] The distance Al-O increases from 1.76 up to 1.86 Å when the coordination number of Al changes from 4 to 6 (Cormier et al., 2000, 2003, Hennet et al., 2016). This implies that Al-O distance vary smaller when Al change of Q^n species in tetrahedra.

not of the Q^n species of Al. If we consider that the volumes vary very slightly in the ternary diagrams this implies that the molar volume variation observed between silicates and aluminosilicates glasses is produced essentially by changes in coordination number of alkaline or alkaline-earth. Before discussing this, we will quantify the different proportions of aluminum.

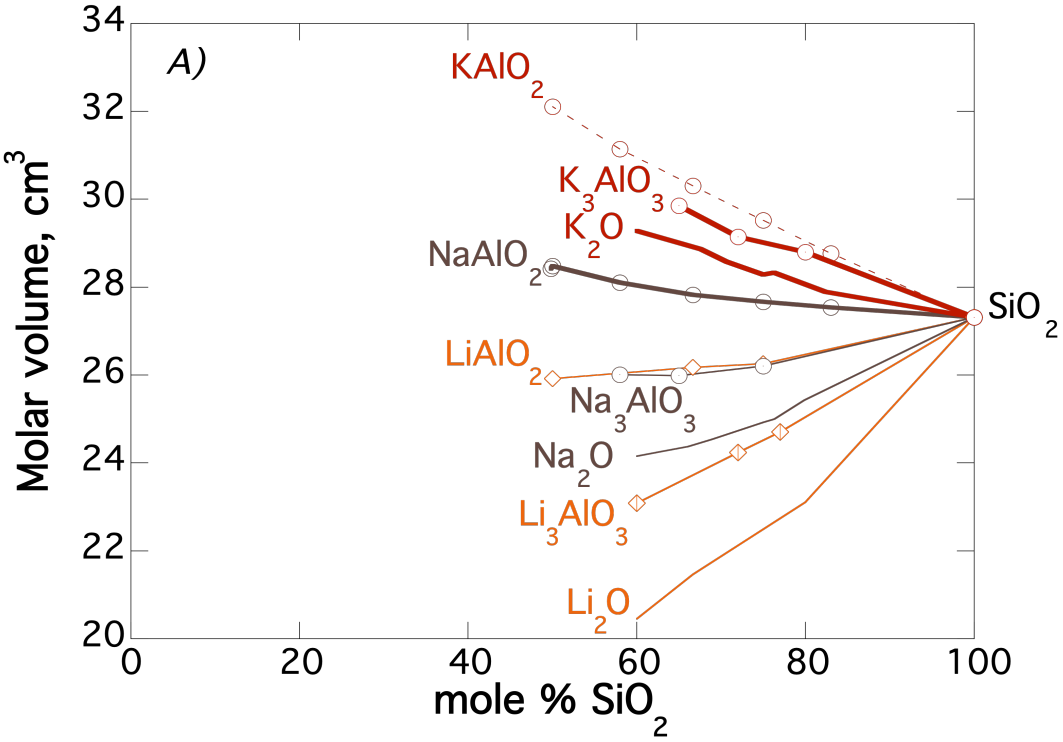

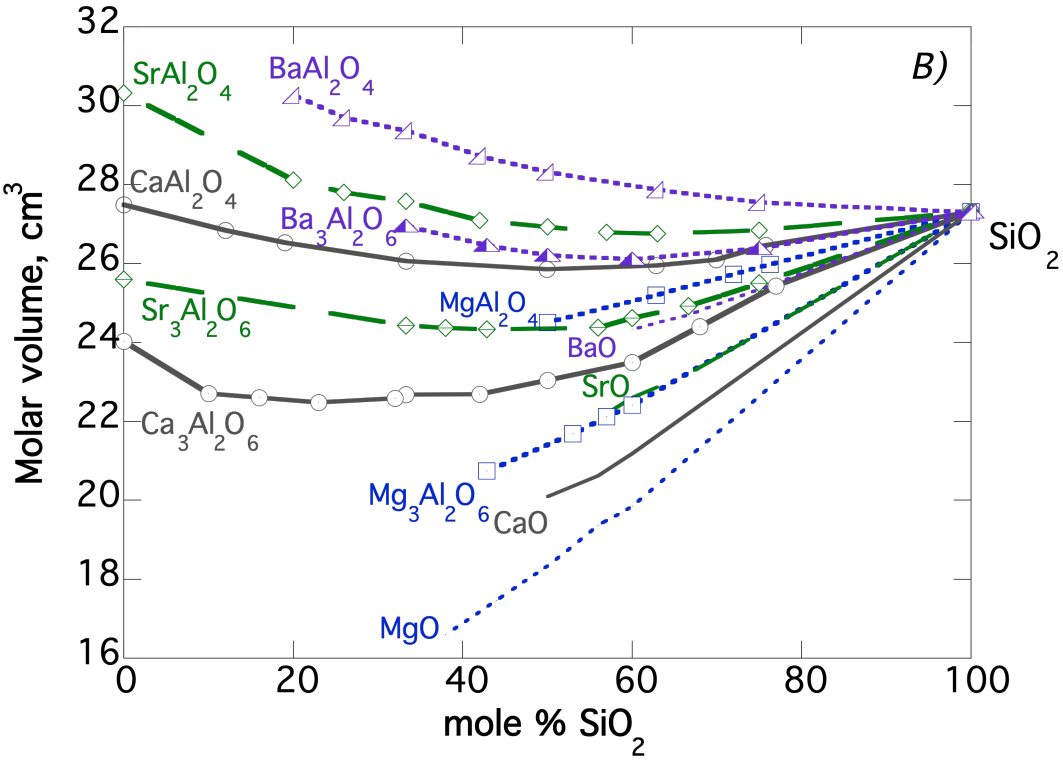

***Figure 15**: A) molar volume for alkali and B) for alkaline-earth silicate and Al-silicate glasses, data for NAS, KAS compositions (Le Losq et al. 2017, 2015, Neuville, 1991, 2006), LAS (Strukelj, 2008), MAS, CAS system (Neuville, 1992), SAS data from Novikov et al., (2017), BAS original data and from Novikov (2017).*

3.2 Proportion of Al in five-fold coordination

Given the role of Al coordination on V_m and other melt/glass properties, it is clear that Al coordination should be quantified. Fortunately, through ^{27}Al NMR spectroscopy, several studies allow drawing a picture of Al coordination variations with composition, temperature and pressure.

The presence of $^{[5]}$Al is systematically observed in the middle of the ternary diagrams of Li aluminosilicate, and alkaline-earths aluminosilicate, including peralkaline glasses in which Al in five-fold coordination is not expected considering the stoichiometry (Neuville et al., 2006, 2007, 2008b, 2010). Moreover, the proportion of $^{[5]}$Al is always maximum for glasses with about 50 mol % of SiO_2 (Neuville et al, 2004, 2006, 2008, Novikov et al., 2017). On the contrary, Na or K tectosilicate and peraluminous glasses have small concentrations of Al in five-fold coordination, which becomes undetectable in peralkaline compositions (Stebbins and Farnan, 1992; Allwardt et al., 2005a,b; Lee et al. 2009; Le Losq et al., 2014). The variation of NMR chemical shift values for $^{[5]}$Al and $^{[6]}$Al sites with SiO_2 content are less dependent on silica content than $^{[4]}$Al sites (Figure 13b, from the previous chapter). The NMR chemical shift values are directly related to the inter-tetrahedral angle or the first-neighbor cations (Stebbins and Farnan, 1992). This can imply that $^{[5]}$Al and $^{[6]}$Al sites are more connected with Al in four fold coordination than with Si in different Q^n species which does not respect the Lowenstein rule's, but in the majority of studies this rule is avoided (Neuville et al., 2008a, 2010, Lee and Stebbins, 2009, Hiet et al., 2009). 2D NMR ^{27}Al-^{29}Si correlations (Lee and Stebbins, 2009, Hiet et al., 2009) show that $^{[5]}$Al is more connected with Si than with Al in lanthanium aluminosilicate glasses (Florian et al., 2007). Highly coordinate Al species, especially $^{[5]}$Al, are likely to have a positive formation enthalpy and their abundance in the melt is expected to increase with increasing temperature as observed by some authors (Neuville et al., 2008b; Stebbins, 2008). However, the ^{27}Al NMR spectra at high temperature shifts to lower ^{27}Al chemical shift values with increasing temperature, this can be interpret as resulting from the appearance of $^{[5]}$Al and $^{[6]}$Al contributions located at lower chemical shifts than that of $^{[4]}$Al (Kanehashi and Stebbins, 2007, Thompson and Stebbins, 2011, 2012, 2013). Signatures of Al in high coordination are also clearly visible using X-ray absorption spectroscopy at the Al *K*-edge (Neuville et al., 2008b). In the case of CA50.25 (anorthite melts composition), Neuville et al (2008b) show an increase from 8% up to 22% of $^{[5]}$Al between room temperature and 1900 K, in good agreement with high

temperature Al NMR (Stebbins, 2008). A significantly higher proportion of $^{[5]}$Al is observed in magnesium aluminosilicate glasses than in the others aluminosilicate systems on the tectosilicate join (Neuville et al., 2008b, Novikov et al., 2017, Figure 23B) which can be explained by the promotion of highly coordinated Al species with the presence of metal cations with relatively high ionic field strength, as shown in boroaluminate by Bunker et al., (1991) and in La-aluminosilicate glass compositions (Florian et al. 2007). Such an idea agrees with the increase in the disorder when the cation field strength decreases (Mysen et al., 1982; Murdoch et al., 1985; Sharma et al, 1985; Navrotsky et al., 1982, 1985; Lee and Stebbins 2000, 2002, Neuville et al. 2008a, Wu and Stebbins, 2009; Lee et al., 2016, Le Losq et al., 2017).

Several papers on ^{27}Al NMR spectroscopy have shown that, for R = M/Al varying between infinity and 1 (silicate to tectosilicate compositions), Al is essentially in four-fold coordination (Risbud et al., 1987, Murdoch et al., 1985; Merzbacher et al., 1990, 1991; Merzbacher and White, 1991; Coté et al., 1992, Stebbins and Xu, 1997, Stebbins et al., 2000, 2008; Neuville et al., 2004ab, 2006, 2007, 2008a, McMillan and Kirkpatrick, 1992; Massiot et al., 2008; Lee and Stebbins, 2009, 2016; Richet et al., 2009a; Le Losq et al., 2014; Novikov et al., 2017; Florian et al., 2018, Charpentier et al., 2018). In the CAS system, 93 % of Al is in 4-fold coordination, and the proportion of $^{[5]}$Al increases slowly up to 7% for the anorthite glass composition on the tectosilicate join (Neuville, et al., 2006). In the MAS system, the proportion of $^{[5]}$Al is a little higher, 12% for Mg-anorthite glass (Neuville et al., 2008a). For all others M^{+} or M^{2+} Al-silicate systems, the proportion of $^{[5]}$Al is lower and the amounts decrease with increasing *z/r* (*z* : cation charge and *r* atomic radius, see Neuville et al., 2008a or Stebbins et al., 2008, Novikov et al., 2017). Figure 16 A and B show the total amount of $^{[5]}$Al in mol % in the CAS and MAS system.

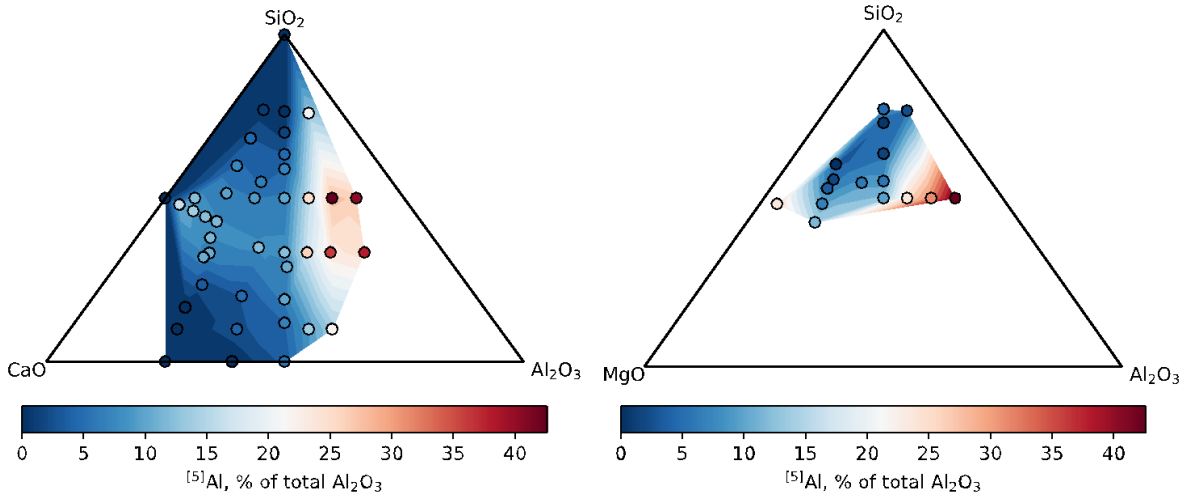

***Figure 16**: Percentage of $^{[5]}$Al of total Al_2O_3 in the CAS (left) and MAS (right) systems. Data from Neuville et al. (2004, 2006, 2007, 2008b, 2010, Massiot et al., 2008; Licheron et al., 2011).*

196

197 *3.3 Molar volume, AlO_4^{4-} and implications for the coordination number of metal cations*

198 In the previous sections, we saw that the molar volume of Si in the different Q^n species can vary by
199 less than 10% when *n* varies from 4 to 0 and that the molar volume of Al stays almost constant for Al in
200 four-fold tetrahedra. Despite this, the molar volume V_m of a lime aluminosilicate glass with 50% of SiO_2
201 (wollastonite to anorthite glasses) can vary from 20 to 25.9 cm^3 between the wollastonite and anorthite
202 compositions, this represents an increase of 25 %. This increase is 12 % between silicate glasses and the
203 glasses on the R = 3 join, and of 12 % again between the join R = 3 and the join R = 1 with $R=MO/Al_2O_3$
204 with M=Mg, Ca. This huge increases of V_m is a maximum at 50 mol % silica.

205 In the case of calcium aluminate glasses, the molar volume difference between C3A ($Ca_3Al_2O_6$) and
206 CA ($CaAl_2O_4$) glasses is only 6.8 % (Figure 15B). In Figure 15B, the increase of molar volume between
207 join R=3 and 1 can also result from a change in the coordination number of calcium because the aluminum
208 stays in four-fold coordination between C3A and CA glasses. In this case, Ca varies between regular
209 octahedra where Ca is in 6-fold coordination to a distorted site in 7-8-fold coordination (Cormier et al.,
210 2001, 2003, Neuville et al., 2008b, 2010, Cicconi et al., 2016; Drewitt et al., 2012, 2017, Jakse et al.,
211 2012; Takahashi et al., 2015; Hennet et al., 2016).

212

213 Generally, the coordination number of alkali or alkaline-earth elements is difficult to determine, but
214 changes in the *Vm* of a glass can inform us about CN changes. For instance, the abovely variation in the
215 CN of Ca is in good agreement with the changes observed via XANES at the Ca *K*-edge in Ca
216 aluminosilicate glasses (Neuville et al., 2004b, 2008, Cormier and Neuville, 2004; Cicconi et al., 2016).
217 In particular, Cicconi et al. (2016) observed a shift to greater energy and a decrease in intensity of the
218 pre-edge in the XANES spectra at the Ca *K*-edge between wollastonite to anorthite glasses. This shift
219 can also be correlated with the new peak ω_2 observed in the depolarized Raman spectra, VH, (see Figure
220 13, chapter 3 this volume, Drewitt et al., 2021). The peak ω_2 decreases when R goes from infinity to 1
221 (to silicate to tectosilicate glasses)

222

223 In the case of the NAS system (Na_2O-Al_2O_3-SiO_2), the peak ω_2 is also clearly visible for silicate
224 glasses in the VH Raman spectra and it disappears for $R=Na_2O/Al_2O_3=1$ (Hehlen and Neuville, 2015).
225 This peak ω_2 exists in all silicate glasses with M^+=Na, K and M^{2+} =Mg, Ca, Sr, Ba (Hehlen and Neuville,
226 2015, 2020) and it's intensity decreases when Al replaces M^+ or M^{2+}. In the NAS glass system, a shift is
227 also observed in the chemical shift, δ, of ^{23}Na NMR between NS3 and albite glass (Le Losq et al., 2015)
228 following a trend that can be correlated with variations in XANES at the Na *K*-edge between the NS3
229 and albite glasses (Neuville et al., 2004).

In the case of the SAS (SrO-Al_2O_3-SiO_2) system, Novikov et al. (2017) also observed some change in the first XANES oscillation which can also be attributed to a change in CN of strontium.

To summarize, ^{23}Na NMR, XANES at the Na, Sr, Ca *K*-edge, and depolarized Raman spectra, (VH), all show changes that can be correlated with an observed increase in the molar volume between silicate and tectosilicate glasses. V_m varies between 4% and 16% with changing the M^+/Al or M^{2+}/Al ratio at a given silica content and depends clearly on the metal cation size. The V_m changes can be assigned to changes in the coordination of metal cations as their role in the aluminosilicate network varies with the M/Al ratio. Similarly, features observed in NMR, XANES or Raman spectroscopies can be directly correlated with such change in the role of alkali or alkaline-earth elements between network modifier and charge compensator. The concept of network modifier and charge compensator was introduced by Zachariazen but never really demonstrated. Now, with the technical evolution of spectroscopy methods, but with measuring the molar volume determined from density measurements, it is possible to have an idea of the role alkaline elements.

In Figure 17, the molar volume of various glasses is shown as a function of mole percent of Al_2O_3 at constant silica. The glass compositions vary between $MSiO_3$ up to Al_2SiO_5, M=Mg, Ca, Sr, Ba. Four trends are clearly visible for the four alkaline-earth aluminosilicate glass families. In the case of $MgSiO_3$-Al_2SiO_3, the molar volume varies almost linearly with Al_2O_3 (the linear variation corresponds to the dashed line). This can imply:

- i) that the coordination number of Mg is almost constant in this system and is not really affected by the Mg/Al substitution, an idea in good agreement with XANES at the Mg K-edge (Trcera et al., 2009);

-ii) that the molar volume depends on the proportion of Al in five-fold coordination.

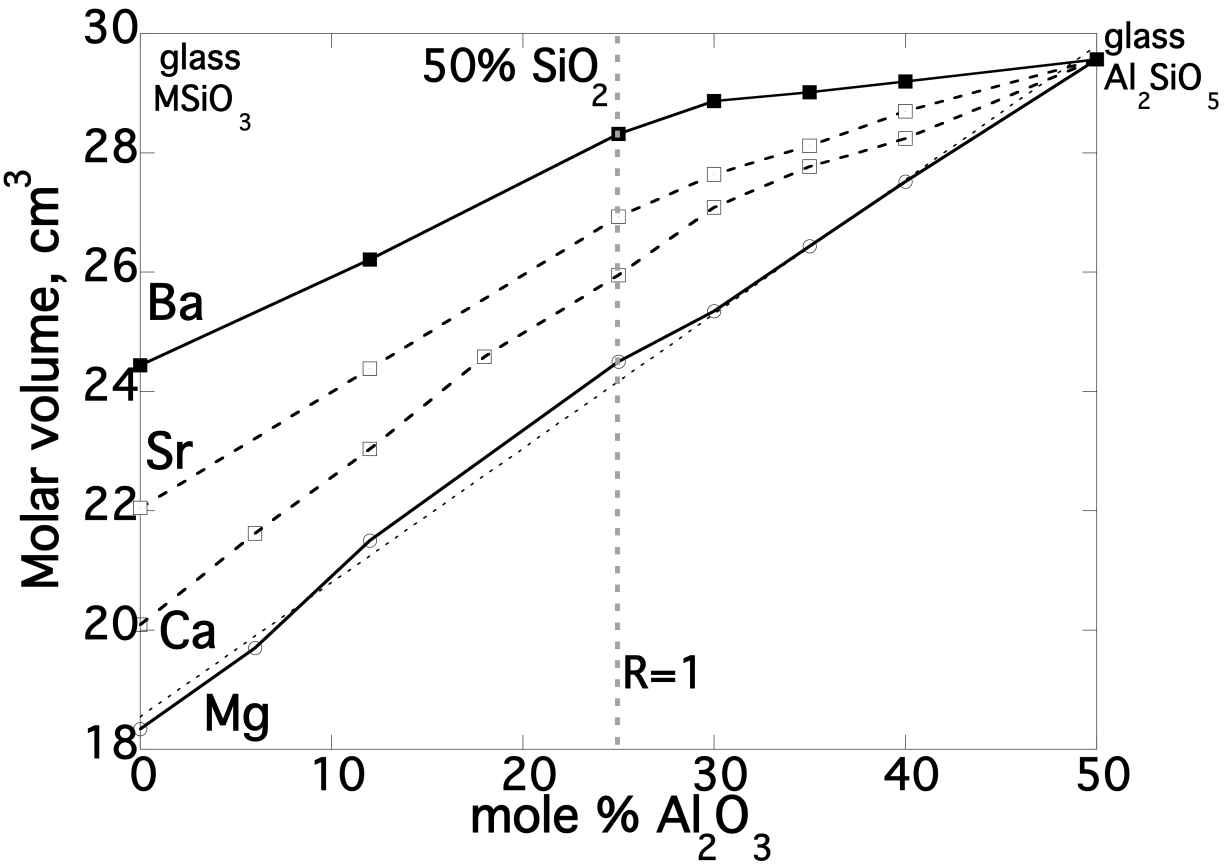

*Figure 17: molar volume at constant SiO_2 = 50 mol% for four alkaline-earth aluminosilicate glass compositions. (The dashed line between $MgSiO_3$ and Al_2SiO_5 glasses correspond to this equation 18.547+0.22497*Al_2O_3). Values are calculated from density measurements from Neuville (1992) for Ca and Mg system peralkaline compositions, Neuville et al. (2006, 2008) for Ca and Mg Per-aluminate compositions, Novikov et al. (2017) for Sr compositions, Novikov (2017) for Ba compositions and Al_2SiO_5 are from Wang et al. (2020).*

For the Ca, Sr and Ba aluminosilicate glasses the changes observed in the slopes near 25 mol % of Al_2O_3 correspond to the tectosilicate line ($R=M^{2+}O/Al_2O_3 = 1$), characterized by an increase in the proportion of $^{[5]}$Al in the glass (Neuville et al., 2006, 2008, Novikov et al., 2017, Novikov 2017). This Figure clearly shows two domains, one where V_m is affected by aluminum, the peraluminous domains, and one where V_m depends on an increase in the coordination of the alkaline-earth element, the peralkaline domain (Cicconi et al., 2016; Novikov et al., 2017).

3.3 Glass transition temperature

In general, a decrease in T_g occurs with decreasing SiO_2 content at all R ratios ($R=M^+O_2/ Al_2O_3$ or $M^{2+}O/Al_2O_3$) (Figure 18). It is particularly important at silica contents between 100 and ~75 mol%. In

detail, this T_g decrease is more significant in Al-free silicate melts than in tectosilicate glasses; the lower R, the lower the effect of changing SiO_2 on T_g. Typically, at *R=1* in tectosilicate compositions, the decrease in T_g is of ~300 K for $MAl_2Si_2O_8$ glasses, and 200 K and 300 K for respectively $KAlSiO_4$ and $NaAlSiO_4$ glasses. The large contrast between T_g variations in Al-free silicate and tectosilicate glass compositions results from the changing role of metal cations upon aluminum addition into the melt network. Indeed, while in silicate glasses, alkali and alkaline-earth elements are network modifiers that break the 3D tetrahedral network, in aluminosilicate glasses they ensure the charge compensation of AlO_4^- tetrahedral units and thus participate in increasing melt polymerization. This translates to higher T_g along the M^+AlO_2-SiO_2 or $M^{2+}Al_2O_4$-SiO_2 binaries than along the M^+O_2-SiO_2 or $M^{2+}O$-SiO_2 binaries.

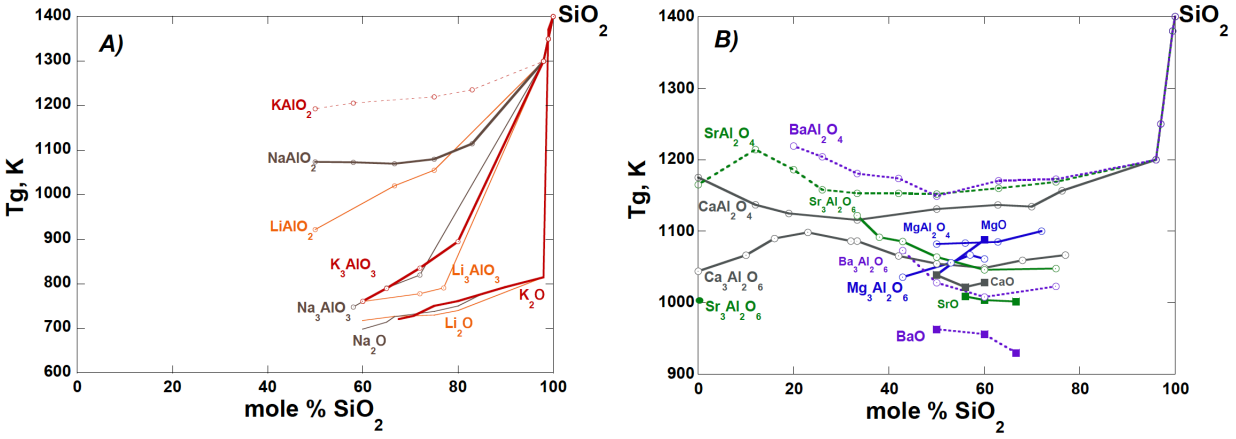

Figure 18: Glass transition temperature T_g, in K, of silicate and aluminosilicate glasses with alkali elements (A) and alkaline-earth elements (B). The glass transition temperatures were determined from viscosity measurements, i.e. they correspond to the temperature at which log η = 12 Pas. Data from Neuville (1991) for Li, K silicates; Neuville (2006) and Le Losq et al. (2014) for sodic systems, (Neuville, 1992) for Ca and Mg, Novikov et al. (2017) for Sr and Novikov (2017) for Ba.

3.4 Link between structure and properties of aluminosilicate melts: example of the CaO-Al_2O_3-SiO_2 system

To discuss and illustrate the links between glass structure and glass/melt properties, the CaO-Al_2O_3-SiO_2 (CAS) glass system will be taken as an example in the following. The CAS system has the advantage having the largest glass forming domain (Neuville et al., 2006). The observations and interpretations made in this system can be extended to other ternary system. In general, in the CAS system, an important decrease in T_g is observed with decreasing SiO_2 content, which results from network depolymerization, except at $R = 1$. In the latter case, melt polymerization is almost constant and the decrease in T_g results from the formation of weaker Si-O-Al bonds as Al substitutes for Si in Q^4 units (Navrosky et al., 1985;

299 Neuville et al., 2004, Cormier et al., 2001, 2005, Hennet et al., 2016). T_g varies by about four hundred
300 degrees between pure SiO_2 (T_g ~ 1480 K; Richet and Bottinga 1984) and the center of the ternary system
301 (T_g = 1115 K for CA33.33, M^{2+}AX.Y where M^{2+}=alkaline-earth element and A=Al_2O_3, X = SiO_2% i.e.
302 33.3 mol%, Y= %Al_2O_3 and M^{2+}O=(100-(X+Y) in this case, CaO=33.3%). At *R=1*, glasses with less
303 than 30 mol% SiO_2 display a continuous increase in T_g upon decreasing SiO_2 content, and T_g reaches a
304 new local maximum for the $CaAl_2O_4$ composition at 1175 K; the minimum in T_g at *R=1* is centered
305 between 40 and 50 mol% SiO_2. The observed behavior in T_g at R = 1 results from the competition between
306 Si and Al as network formers. As indicated by the difficulty of forming glasses at high Al concentrations
307 (e.g. along the SiO_2-Al_2O_3 binary) as well as a lowering of T_g with addition of Al. Al can be considered
308 as a relatively poor network former compared to Si. This is further corroborated by variations in the melt
309 fragility (i.e. the derivative of the melt viscosity as a function of T at T_g): the strongest existing melt is
310 SiO_2, and Al-rich melts have higher fragility, with the most fragile being $CaAl_2O_4$ in the CAS system
311 (Figure 19). This is also in good agreement with the variation of the Cp^{conf} of SiO_2 and $CaAl_2O_4$, which
312 varies between 8.2 to 13.8 J/mol K. This ΔCp between liquid and glass at Tg can be expressed in term of
313 *Cpl/Cpg* ratio as proposed by Angel (1991). This ratio varies between 1.1 for SiO_2, the strongest melt to
314 1.37 for $CaAl_2O_4$, the more fragile melt in Figure 19.
315

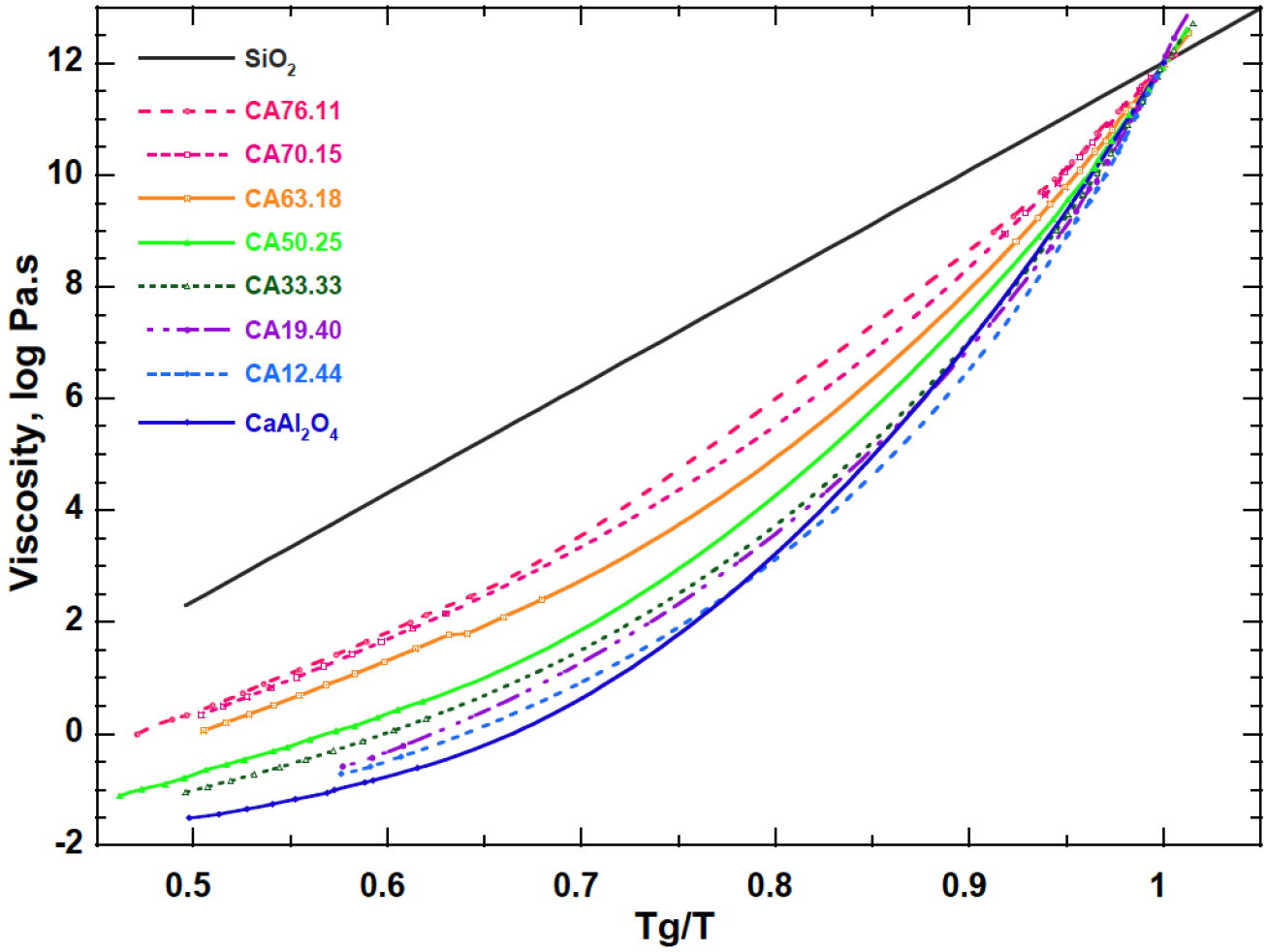

Figure 19: "Angel plot" showing log η versus T_g/T for melts with R=CaO/Al₂O₃=1 in the CAS system.

As mentioned previously, the CAS system presents one of the largest glass-forming domains. Indeed, it is possible to quench glasses even without silica, e.g. like the C12A7 composition (CXAY with C=CaO, A=Al_2O_3, X and Y are their relative proportions), using classic quench rates. With increasing quench rates, e.g. via laser levitation heating, it is possible to make glasses between C3A and CA1.5 (from 75 down to 40 mol% CaO). In this condition, the addition of a small amount of SiO_2 in CaO-Al_2O_3 glasses extends the glass forming ability and lowers the melt liquidus temperature. Other macroscopic properties are also markedly changed with silica introduction in CaO-Al_2O_3 melts/glasses, suggesting extensive structural modifications. For instance, an anomalous behavior of T_g is clearly observed at low silica content, with a maximum in T_g visible at ~20 mol% SiO_2 along the $Ca_3Al_2O_6$-SiO_2 binary (Figure 18B; Higby et al., 1990; Neuville 1992; Neuville et al., 2004; Cormier et al., 2005; Neuville et al., 2010). Note that this anomalous behavior of T_g results from the change in the polymerization of Al which varies between Q^2 to Q^4 species along the join $R=3$ between C3A and CA20.40 glasses (Neuville et al., 2004, Cormier et al., 2001, 2003, 2005).

To explore further the properties of CAS glass compositions, viscosity along the join R=1 ($CaAl_2O_4$ – SiO_2 binary) is plotted in Figure 20. At high temperatures, viscosity decreases constantly with addition of $CaAl_2O_4$ (Figure 20B). At supercooled temperatures, near T_g, melt viscosity decreases by ~ 7 orders of magnitude with adding 30 mol% $CaAl_2O_4$ to silica, then a further addition of 30 mol% $CaAl_2O_4$ yields a decrease in viscosity of 1 order of magnitude. Between 40 and 0 mol% SiO_2, melt viscosity increases ~ 5 orders of magnitude. The deviation from a linear variation (Figure 20B) is 4 orders of magnitude at 1175 K, and less than 2 orders of magnitude at 1900 K. It thus decreases with increasing temperature. These changes thus deviate strongly and negatively from a linear variation, particularly at undercooled conditions. Such behavior may originate from mixing between Si and Al in Q^4 units that occurs in such tectosilicate melts (Seifert et al., 1982), this mixing resulting in excess entropy and leading to non-linear, convex variation of the melt viscosity as a function of the *Si/(Si+Al)* ratio (e.g., Neuville and Mysen, 1996).

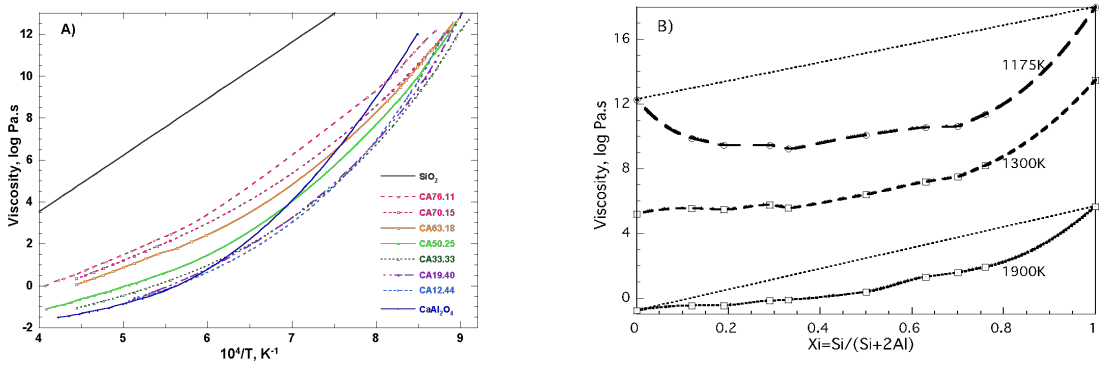

Figure 20: A) Viscosity of melts between silica and $CaAl_2O_4$ compositions, CAX.Y mean: X=SiO_2 %, Y=Al_2O_3, CaO=100-(X+Y). B) viscosity at constant temperature, 1150, 1200, 1800 K as a function of Xi=Si/(Si+2Al). SiO_2 data are from Hetherington et al. (1964) Leko, (1979) and Urbain et al. (1982), $CaAl_2O_4$ from Urbain (1983), Neuville (1992).

In all others glass systems, alkali or alkaline-earth aluminosilicate, viscosity shows similar behavior along the join *R=1*, an important decrease between 100 and 70% of SiO_2, and for lower silica content, a smaller decrease of the viscosity (Alkaline see Le Losq et al., 2017, Mg, Neuville 1992, Sr, Novikov et al 2017, Ba, Novikov 2017).

As already mentioned, the configurational heat capacity, Cp^{conf}, is required in order to determine the configurational entropy, $S^{conf}(T)$, from equations (6) and (7). In the CaO-Al_2O_3-SiO_2 system, the

configurational heat capacity can be determined from the difference between the heat capacity of the melt at T and that of the glass at T_g (equation 8). Several models exist, like those of Richet (1987) and Richet and Bottinga (1985), and allow one to calculate the configurational heat capacity with precision. The more recent works of Courtial (1993) and Richet and Neuville (1992) allow refining the heat capacity modelling in the CaO-Al_2O_3-SiO_2 system, with using the following partial molar heat capacity equations (J mol^{-1} K^{-1}) for the glass and liquid (the estimated uncertainties is about 1% for the partial molar heat capacities following Courtial and Richet, 1993):

$$C_{pg\ SiO_2} = 127.2 - 0.010777T - 431270/T^2 - 1463.9/T^{0.5}, \quad (25)$$

$$C_{pg\ Al_2O_3} = 175.46 - 0.005839T - 1347000/T^2 - 1370/T^{0.5}, \quad (26)$$

$$C_{pg\ CaO} = 39.159 + 0.01865T - 152300/T^2, \quad (27)$$

$$C_{pl\ SiO2} = 81.37, \quad (28)$$

$$C_{pl\ Al2O3} = 85.78 - 130.216T, \quad (29)$$

$$C_{pl\ CaO} = 86.05. \quad (30)$$

With these partial molar heat capacity terms, $C_p^{conf}(T_g)$ can be calculated easily and used for the calculation of $S^{conf}(T_g)$, which are plotted in Figure 21. It is clearly visible that $S^{conf}(T_g)$ of silica glass is almost the same than that of $CaAl_2O_4$, CA glass. Assuming that $S^{conf}(T_g)$ can be decomposed into topological and excess terms, we can model the observed variations as

$$S^{topo} = X_{SiO_2} S^{conf}(T_g)_{SiO_2} + (1 - X_{SiO_2}) S^{conf}(T_g)_{CaAl_2O_4}, \quad (31)$$

S^{topo} is thus assumed to vary linearly between the two end-members SiO_2 and $CaAl_2O_4$ glasses. This term S^{topo}, is independent of temperature and corresponds to a simple mechanical mixing between two entities. The term S^{ideal}, defined in equation 10, can be taken as equal to the entropy obtained from an ideal random mixing of two species, in this case Si and Al. At high or low concentration of silica, $S^{conf}(T_g)$ variations seem to follow the ones predicted assuming such an ideal mixing between Si and Al. This suggests that $CaAl_2O_4$ randomly replace Si_2O_4 in the melt/glass structure. However, between 33 and 75 percent of silica, $S^{conf}(T_g)$ variations depart from the predictions of this ideal mixing model. In this silica concentration range, a decrease of ~25 % in $S^{conf}(T_g)$ is observed, and there is a maximum difference of ~2.5 J mol^{-1} K^{-1} between $S^{conf}(T_g)$ values and the ideal model at around 50 mol% SiO_2 (Figure 21).

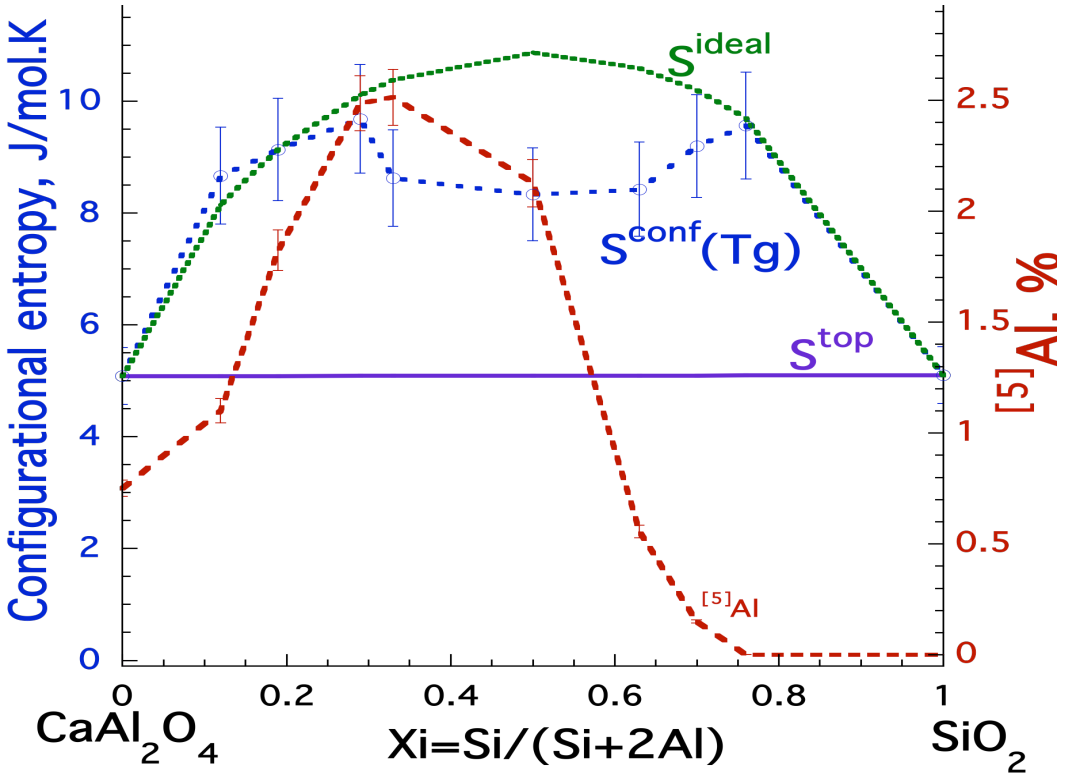

388

389 *Figure 21: Configurational entropy at the glass transition temperature, $S^{conf}(T_g)$ (Neuville, 1992), and*
390 *real proportion of $^{[5]}Al$ in mole percent in glasses along the SiO_2-$CaAl_2O_4$ binary (Neuville et al., 2004,*
391 *2004). Each $S^{conf}(T_g)$ value was calculated from the viscosity data obtained for each composition.*

392

393 The observed $S^{conf}(T_g)$ variations (Figure 21) suggest that :

394 –i) at low or high silica concentrations, Si and $^{[4]}$Al mix almost randomly in the melt/glass structure,

395 -ii) a deviation from ideal mixing exists at intermediate silica contents. The latter deviation can be
396 rationalized upon considering that Al in five-fold coordination represents around 2,5 % of total Al in the
397 CA50.25 glass.

398 Excess $^{[5]}$Al tends to decrease $S^{conf}(T_g)$ and in parallel increase the glass transition temperature, as
399 shown by Le Losq et al. (2014) in the Na_2O-Al_2O_3-SiO_2 system. A similar effect is potentially observed
400 here, with the presence of $^{[5]}$Al possibly producing a decrease in $S^{conf}(T_g)$ and also an increase in T_g
401 because $^{[5]}$Al and $^{[4]}$Si do not interact and do not mix randomly. One should be careful with extrapolating
402 such behavior because it is only valid close to the glass transition. Indeed, at high temperatures (close or
403 above the liquidus), Neuville et al (2008b) proposed that $^{[5]}$Al plays a role similar to $^{[5]}$Si, a transient
404 species ensuring the exchange of O atoms during viscous flow according to Stebbins (1991). Similarly,
405 in polymerized aluminosilicate networks, we can infer that five-fold coordinated network formers (Si or
406 Al) ensure cationic mobility at high temperature. In depolymerized networks, Q^1, Q^2 and Q^3 units ensure

network mobility (Stebbins, 1991; Farnan and Stebbins, 1990, 1994; Neuville et al., 2008b, Le Losq et al., 2014). Such assumptions agree well with the data near the C3A domain (see section 4). From Figure 21, it is further possible to make the assumption that $^{[5]}$Al plays a different role in silica-rich or alumina-rich glasses and melts. Indeed, in silica-rich networks (>60 mol% SiO_2), $^{[5]}$Al increases network connectivity and this results in a decrease in $S^{conf}(T_g)$. In an aluminate-rich network, a few percent of $^{[5]}$Al plays a role similar to $^{[4]}$Al, which exchanges randomly with Si.

Other systems show behaviors along the tectosilicate join similar to that previously presented for $CaAl_2O_4$-Si_2O_4. In particular, Raman spectra along all tectosilicate joints in the LAS, NAS, KAS, MAS, SAS, BAS systems show similar variations. They all present a linear decrease in the frequency of the bands assigned to T-O symmetric and asymmetric stretching of Q^4 units with decreasing SiO_2 concentration. This correlates very well with increasing ^{27}Al NMR chemical shifts with decreasing silica content in tectosilicate glasses (see Figure 12 previous chapter, Drewitt et al., 2021). Those Raman and NMR variations arise from the variation of the T-O distance between Si-O and Al-O, as the Si-O distance is shorter than the Al-O distance.

In the Figure 22, the viscosities of tectosilicate melts with 75 and 50 mol % silica are plotted as a function of T_g/T. The strongest glass in the Angell plot corresponds to the SiO_2 composition, and the more fragile the composition, the greater the curvature. The fragility of melts decreases from Mg, Ca, Sr to Ba for the alkaline-earth elements. Alkali tectosilicate compositions show similar fragilities at 50 mol % silica (Figure 22B). At 75 mol % (Figure 22A), Li and K tectosilicate compositions also present a similar fragility while the Na-tectosilicate composition is the strongest one.

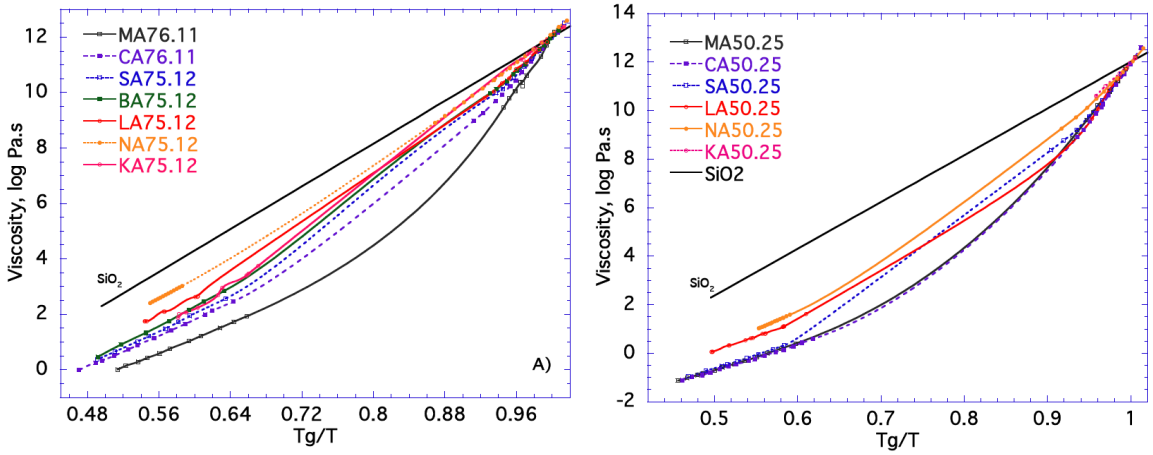

Figure 22: Viscosity of MAX.Y melts versus T_g/T, with M = Li_2, Na_2, K_2, Mg, Ca, Sr, Ba. X = SiO_2, Y = Al_2O_3, and MO=100-(SiO_2+Al_2O_3) in mole%, A) for 75 mole % of SiO_2, and B for 50 mole % of

SiO_2. (data are from Le Losq, 2012 for LAS, Le Losq et al., 2017, for NAS and KAS, Neuville 1991 for CAS and MAS, Novikov et al.2017, for SAS, and Novikov, 2018 for BAS).

3.5 From the CAS system to other chemical systems

For tectosilicate glasses and melts, the structure seems to present a random distribution and random substitution between SiO_4^{4-} and AlO_4^{5-} units, in violation of the Loewenstein's aluminum avoidance principle (Loewenstein, 1954). The Si/Al substitution is clearly confirmed by the linear variation of the chemical shift of the ^{27}Al NMR and of the frequency of the Raman band in the 800 - 1200cm^{-1} domain. We can propose that alkali or alkaline-earth elements are in the free-volumes of the Al_x-$Si_{(1-x)}O_2$ network, ensuring the charge compensation of AlO_4^{5-} units. The Figure 23 shows the proportion of $^{[5]}$Al in tectosilicate glasses versus SiO_2 content. The proportion of $^{[5]}$Al is a maximum in the middle of the ternary system, in the peraluminous domain for all ternary systems MAS (with S=SiO_2, A=Al_2O_3, M=Li_2O, Na_2O, K_2O, MgO, CaO, SrO, BaO), and increases with the decrease of z/r^2 (Lee and Stebbins, 1999, 2000, Allward et al, 2003, 2007, Stebbins, 2008, 2016; Stebbins and Farnan, 1992; Stebbins et al., 1999; Neuville et al., 2004, 2006, 2008, 2010, Le Losq et al., 2017, Lee et al., 2016; Novikov et al., 2017, Stebbins et al., 2008, Lee et al., 2009, Hiet et al., 2009, Alu et al., 2018). In the NAS and KAS system, $^{[5]}$Al is not detected in tectosilicate compositions, and it is only present in peraluminous domain (Allwardt, et al., 2003; Le Losq et al., 2014).

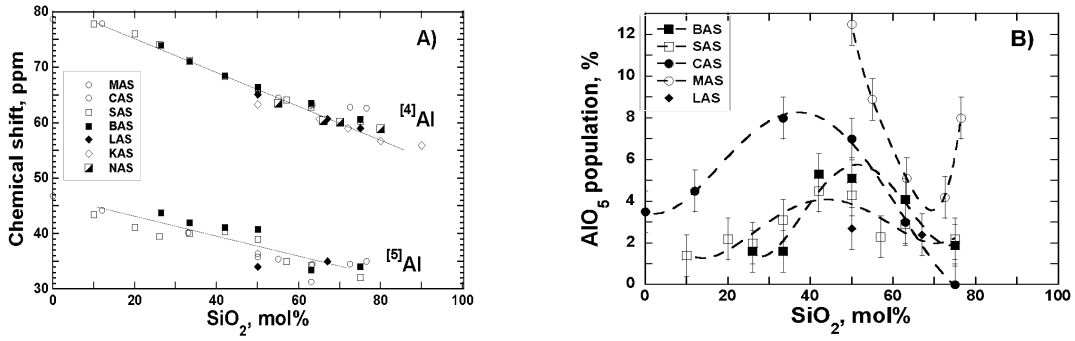

Figure 23: A) NMR chemical shift of $^{[4]}$Al and $^{[5]}$Al and B) proportion of $^{[5]}$Al in LAS, MAS, CAS, SAS, BAS system along the join R=1, the tectosilicate join (note that there is not $^{[5]}$Al in Na and K tectosilicate glasses). Data from Le Losq (2012), Neuville et al., (2008, 2006), Novikov et al., (2017), Novikov, (2017). Error bar are smaller than symbol size.

In tectosilicate glasses, the NMR chemical shifts of $^{[5]}$Al and $^{[4]}$Al decrease linearly with the silica content (Figure 23A), due to an increase in the mean T-O-T inter-tetrahedral angle as Al substitutes for Si in tetrahedral units (Stebbins and Farnan, 1992; Neuville et al., 2006, 2008). At a given silica content,

small variations in the ^{27}Al NMR chemical shift are observed, and correlate with the electronegativity and size of the first-neighbor metal cations in the glass structure. These variations arise from small changes in the Si/Al distribution and in the mean inter-tetrahedral T-O-T angle as the metal cation field strength and property changes.

In peralkaline glasses, the degree of polymerization plays a small role on the $^{[4]}$Al environment. Mysen et al. (2003) showed that, in sodium aluminosiicates, Al remains mostly in Q^4 units. Using Raman and viscosity data, Le Losq et al. (2014) corroborated such a view for this system. Other studies suggest that this remains true probably in most aluminosilicate compositions at silica contents higher than 40 mol% (Neuville et al., 2004b, 2008, Novikov et al., 2017); a strong preference of $^{[4]}$Al for the most polymerized structural units is expected according to experimental (Mysen et al., 1981; Cormier et al., 2000; 2005, Neuville et al., 2004b, 2008, Novikov et al., 2017) and numerical studies (Cormier et al., 2003, Cormier 2019).

3.6 Alkaline-earth mixing in aluminosilicate glasses and melts

The substitution of one alkaline-earth element by another has little affect on glass Raman spectra (Merzbacher and White, 1991, Neuville et al. 2008b). The Si/Al substitution actually has a greater influence on the aluminosilicate network than the alkaline-earth element substitution (see also chapter 3, this volume). In the case of Ca-Mg aluminosilicates, this agrees with an ideal mixing of Ca and Mg in aluminosilicates as inferred from macroscopic viscosity measurements (Neuville and Richet, 1991). This random distribution was confirmed by ^{17}O NMR data, which show that NBOs, are equally associated with Mg or Ca cations (Farnan and Stebbins, 1990, 1994; Allwardt and Stebbins, 2004). However, the network is more perturbed by the presence of Mg than by Ca because of the higher ionic field strength of Mg (Navrotsky et al., 1982; Roy and Navrotsky, 1985) and the Ca/Mg coordination number should play an important role. The coordination number of Mg is well characterized (Kroeker and Stebbins, 2000, Trcera et al. 2009, Fiske and Stebbins, 1994): it is 4 in silicate glasses, and increases up to 5-6 in aluminosilicate glasses, in agreement with glass molar volumes variations (Figure 15). Turning to Ca, in silicate glasses it is mainly located in distorted sites with 6-7 oxygen neighbors (Cormier et al., 2003, Neuville et al., 2004b, 2008, Cicconi et al., 2016). Its CN increases with substitution by Al as shown by the variation of the molar volume between $CaSiO_3$ and Al_2SiO_5 glasses (Figure 17). At high Al_2O_3 content ($R>=1$), in Ca/Mg aluminosilicate glasses, Ca is in 7-8 fold coordination (Shimoda et al., 2007a) whereas Mg is in 6-fold coordination (Shimoda et al., 2007b, Trcera et al. 2009), as corroborated by data like molar volume, X-ray diffraction spectra, XANES spectra at the Ca and Mg *K*-edge, and ^{43}Ca and ^{25}Mg NMR experiments (Kroeker and Stebbins, 2000, Trcera et al. 2009, Fiske and Stebbins, 1994).

494 The above discussion raises a paradox: Ca and Mg always have different coordination numbers but
495 seem to mix randomly in silicate and aluminosilicate melts and glasses. First, this may highlight the
496 difficulty determining alkali or alkaline-earth environments that are loosely held in large sites with fairly
497 irregular coordination (Cormier and Neuville, 2004, Neuville et al., 2008). Nevertheless, there is a
498 general consensus for lower coordination for Mg than Ca. The low Mg coordination number and the
499 possibility to have MgO_4 tetrahedra in Mg-silicate glass suggest that Mg will not be available for charge
500 compensation of Al in tetrahedral position. Alternatively, its small size favors its localization in network
501 tetrahedral cavities, yielding important distortions of the aluminosilicate network to accommodate such
502 Mg coordination, which could result in the formation of highly-coordinated Al. This interpretation might
503 justify the modifier role played by Mg despite their low coordination (Shimoda et al., 2007b, Guignard
504 and Cormier, 2008, Trcera et al. 2009), in agreement with recent NMR data suggesting that substitution
505 of Na by Mg in aluminosilicates in glass promotes melt depolymerisation (Sreenivasan et al. 2020).
506 Similar observations can be made regarding the role of Zn in silicate or aluminosilicate glasses (Novikov,
507 2017). The fact that the viscosities of the Mg or Zn glass compositions are lower than that of Ca glass
508 compositions for the same amount of SiO_2, confirms the role of network modifier of Mg and Zn while
509 they are preferably in 4-fold coordination. (Neuville, 1992; Neuville and Richet, 1991; Toplis and
510 Dingwell, 2004, Neuville et al., 2008).
511
512 In mixed CMAS glasses, Raman, NMR and neutron diffraction data (Allwardt and Stebbins, 2004,
513 Allwardt et al., 2003, Lee et al., 2003, Lee and Stebbins, 2003; Neuville et al., 2006, 2008, Guignard and
514 Cormier, 2008; Cormier and Coello, 2013, Cormier 2019) are in good agreement with random mixing
515 between Ca and Mg in the melt structure, as initially proposed by Neuville and Richet (1991). This
516 implies that intermediate CMAS melts can be considered as being derived from the random mixing of
517 their CAS and MAS end-members, e.g. $Ca_3Al_2Si_3O_{12}$ - $Mg_3Al_2Si_3O_{12}$ for garnet-like glasses and
518 $CaAlSi_2O_8$ - $MgAlSi_2O_8$ for anorthite-like compositions. An interesting observation is that Ca/Mg mixing
519 shows a random distribution and the network polymerization is not really affected by the Ca/Mg
520 substitution, but the proportion of $^{[5]}Al$ increases with the Ca/Mg substitution (Neuville et al., 2008b).
521
522

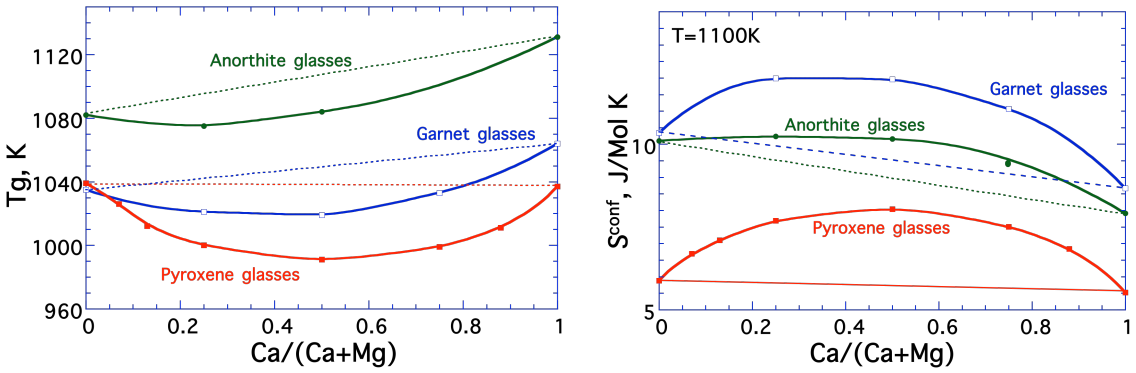

Figure 24: A) glass transition temperature and B) configurational entropy at 1100 K upon Ca/Mg mixing in pyroxene ($CaSiO_3$-$MgSiO_3$), garnet ($Ca_3Al_2Si_3O_{12}$-$Mg_3Al_2Si_3O_{12}$) and anorthite ($CaAl_2Si_2O_8$-$MgAl_2Si_2O_8$) glass compositions, with respectively 0, 12.3 and 25.0 mol% Al_2O_3. Data for pyroxene and garnet glasses are from Neuville and Richet (1991) and original data for anorthite glasses.

Unfortunately, knowledge regarding the mixing between Sr/Ca, Ba/Mg or more generally between an alkali with an alkaline-earth element in aluminosilicate compositions remain scarce, and it is not possible to propose a general conclusion. It is possible to say that Si and Al are almost randomly distributed in tectosilicate glass compositions, and metal cations are located in cavities of the 3D polyhedral network and ensure the charge compensation of the AlO_4^{5-} tetrahedra. This assumption is in good agreement with the linear variation of the *T-O* distances from 1.66 up to 1.76 Å between SiO_2 and $CaAl_2O_4$ glasses (Figure 13b, chapter 3, this issue). The *T-O* distances are also well correlated with the linear variation of the NMR chemical shift of ^{27}Al and the linear variation of the frequency of the Q^4 species along the tectosilicate joint (compiled in Figure 13a,b chapter 3, this issue). They may mix randomly like Ca and Mg, but a non-random distribution with increasing network segregation has also been reported in alkali tectosilicate melts (Le Losq et al., 2017). This highlights the complexity of the structure of aluminosilicate melts and glasses, a problem when considering the modelling of their properties. Other problems are the presence of excess NBOs, $^{[5]}Al$ and tri-coordinated oxygens (Stebbins and Xu, 1997, Le Losq et al. 2014). For instance, the presence of $^{[5]}Al$ can be important, reaching concentrations up to 12% of the Al_2O_3 in the middle of the MAS ternary system, and the presence of $^{[5]}Al$ results in increasing the glass transition temperature and decreasing configurational entropy. Metal cations could be located in cavities of the 3D polyhedral network, in a manner consistent with the Compensated Continuous Random Network model (Greaves and Ngai, 1995; Greaves and Sen, 2007; Le Losq et al., 2017); they ensure the charge compensation of the AlO_4^{5-} tetrahedra. In the potassium aluminosilicate ternary, a non-random distribution of Si and Al between framework units may be accompanied by an increasing segregation of metal cations in clusters or channels. This has been proposed to explain the variations in

the structure and properties of potassium tectosilicate melts, for instance (Le Losq and Neuville, 2013; Le Losq et al., 2017). This is a problem when considering the modelling of their properties, and a large number of approximation may be necessary as we shall see in the later section.

3.7 Models for alkali aluminosilicate melts

The above sections allow us to have a glimpse into the complexity of aluminosilicate melts. Even leaving aside the potential effects of parameters like $^{[5]}$Al, there is no data for the distribution of Q^n species in aluminosilicate melts because ^{29}Si NMR spectroscopy loses resolution with aluminosilicate compositions due to Si-Al interactions resulting in significant signal broadening and increased complexity of the peaks. Mysen et al. (2003) quantified the fractions of the different Q^n species in Na aluminosilicate glasses by modelling the ^{29}Si NMR data. Their findings allow us to constrain the K_{eq} value for the dissociation 2 $Q^3 = Q^2 + Q^4$ in sodium aluminosilicate glasses (Figure 25). We observe that Al introduction into the glass network promotes the dissociation of Q^3 units.

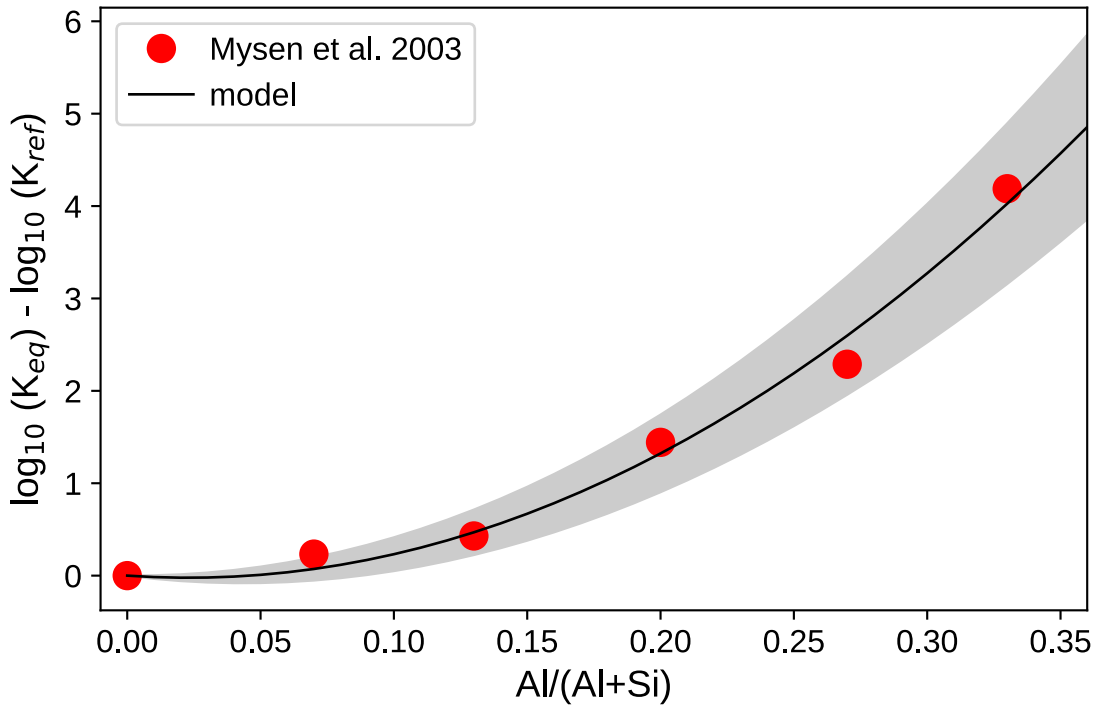

Figure 25: Relative value of the equilibrium constant K_{eq} of the reaction 2 $Q^3 = Q^2 + Q^4$ obtained from Q^n data in Na aluminosilicate melts calculated by Mysen et al. (2003), reported as a function of the Al/(Al+Si) ratio of glasses. K_{ref} is the value of K_{eq} in the glass without Al. The black line represents a polynomial modelling of the data, and the grey areas are the two-sigma confidence interval of the model predictions. Using this model, it is possible to estimate the Q^n distribution in alkali aluminosilicate glasses, but one must note that such relation remains unknown for other elements like K, Ca or Mg.

This result is the only experimental one to the knowledge of authors that could be used to model the Q^n distribution in aluminosilicates based on the principle of using partial K_{eq} values as highlighted in section 2.5. Other models (Doweidar, 1999 for example), like the associate solution one, are purely theoretical and remain unconstrained by experimental data, as they are not available. This does not prevent one from building models of glass and melt properties. For instance, Doweidar (1999) simply used a binary model for calculating the density of Na_2O-Al_2O_3-SiO_2 glasses from partial molar values of different Na-Q^n units. The structural model employed there is clearly not appropriate, but interestingly, this does not prevent a good prediction of glass densities. A better attempt to link melt composition, structure and viscosity is that of Starodub et al. (2019), who calculated the Q^n distribution in Na_2O-K_2O-Al_2O_3-SiO_2 melts from an associate solution model, and then linked the fractions of Q^n units and the concentrations of cations to the parameters of the Avramov-Milchev equation for calculation of melt viscosity. This is an interesting model, but it suffers from two problems. First, they did not select the viscosity data used for fitting their model, as they used the large SciGlass database, and the results of their model will thus suffer from the propagation of large errors affecting some experimental data. Secondly, the Avramov-Milchev (Avramov and Milchev, 1988) equation works well but it is less attractive than the Adam-Gibbs theory because it does not allow one to link the chemical, structural, thermodynamic and dynamic dimension of the problem.

An extension of the model presented in section 2.5 could allow one to circumvent such caveats. We will explore if such a model is possible to implement below for the Na_2O-K_2O-Al_2O_3-SiO_2 system. A first step would be to combine the silicate structural model (section 2.5) to the relationship presented in Figure 25. This will allow one to approximate the Q^n speciation in aluminosilicate glasses. Then, we need to know the effects of Na-K mixing in aluminosilicate melts and of Al concentration on the glass configurational entropy. Combining viscosity and Raman data with thermodynamic calculations, Le Losq et al. (2014) have shown that Al introduction in $NaSi_2O_7$ yields a rapid network polymerisation (Figure 26A) that is accompanied by a jump in glass configurational entropy and an increase in glass T_g (Figure 26B). At Al/(Al+Na) higher than 0.5, we see a continuous decrease in $S^{conf}(T_g)$ that is accompanied by increasing T_g.

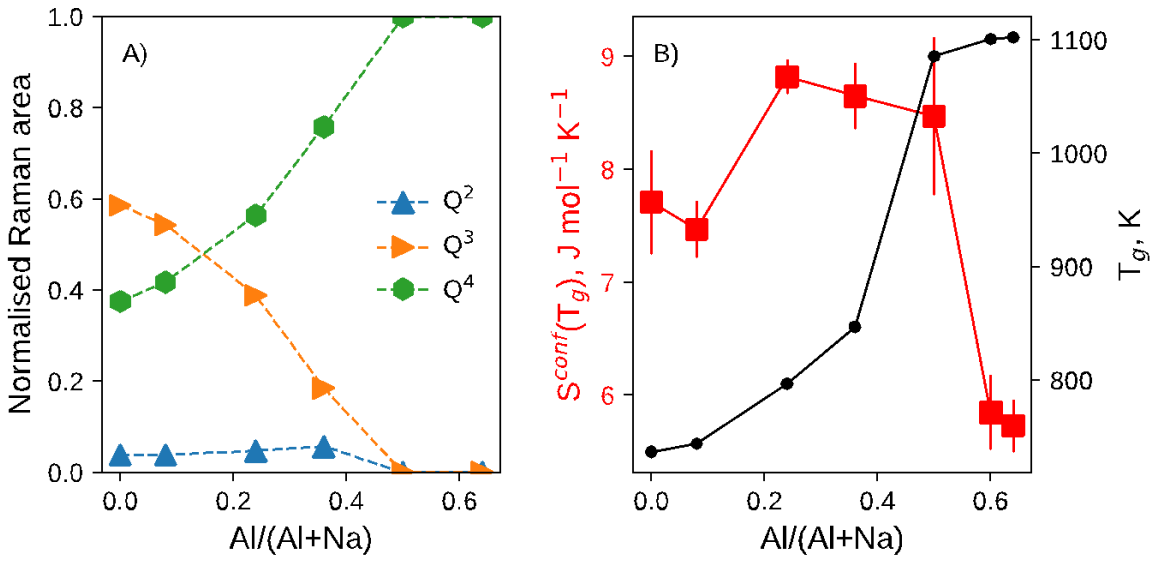

Figure 26: A) Fractions of the Q^n units Raman signal, and B) entropy and glass transition temperature of Na aluminosilicate glasses with 75 mol% SiO_2 but varying Al/(Al+Na) ratios. Data from Le Losq et al. (2014).

Variations in $S^{conf}(T_g)$ are thus complex functions of the melt Al/(Al+M) ratio. As an approximation, one could assume that Al and Si mix randomly in Q^4 units in the silicate network, as proposed for Na tectosilicate melts by Neuville and Mysen (1996). Note that it is important to remember that unlike the Ca or Mg aluminosilicate system, the ternary system Na_2O-Al_2O_3-SiO_2 does not contain Al in 5-fold coordination except in the peraluminous domain (Lee et al., 2003, Le Losq et al., 2014). This hypothesis implies that the Lowenstein Al-O-Al avoidance rule will not be respected, and is thus in contradiction with the interpretation of NMR data of Na aluminosilicate glasses (Lee and Stebbins, 1999, Lee et al., 2003). However, this hypothesis allows reproduction of the variations in configurational entropy observed when Al substitutes Si in Na aluminosilicate melts (Neuville and Mysen, 1996; Le Losq, 2012). One may thus consider it as adequate for the aim of building a model of configurational entropy variations. An additional point is to consider that Q^4_{Al} charged-balanced by Na ($Q^4_{Al,Naenv}$) or K ($Q^4_{Al,Kenv}$) probably present different partial configurational entropies (respectively $S^{conf}_{Q^4_{Al,Naenv}}$ and $S^{conf}_{Q^4_{Al,Kenv}}$). S^{topo} (eq. 16) could then be written as:

$$S^{topo} = \sum_{n=2}^{3} x_{Q^n_{Si,Naenv}} S^{conf}_{Q^n_{Si,Naenv}} + \sum_{n=2}^{3} x_{Q^n_{Si,Kenv}} S^{conf}_{Q^n_{Si,Kenv}} + x_{Q^4_{Si}} S^{conf}_{Q^4_{Si}} + x_{Q^4_{Al,Naenv}} S^{conf}_{Q^4_{Al,Naenv}} + x_{Q^4_{Al,Kenv}} S^{conf}_{Q^4_{Al,Kenv}}. \quad (32)$$

From this equation, we need to discriminate the fraction of charge-compensator and network modifiers (Na, K), in order to calculate the variation in the fractions of the Q^n units. This could be done easily assuming that the fractions of charge-compensator and network modifiers Na and K are just equal to the weighted average fractions of Na and K. This assumes no preference of Na and K to specific environments, an hypothesis that surely could be challenged.

We see that many hypotheses have been already proposed in order to start building a model to express $S^{conf}(T_g)$. This is without even considering the calculation of any entropy resulting from cationic mixing, S^{mix}. The picture becomes even more complex at this point. Indeed, while variations of $S^{conf}(T_g)$ upon mixing Na and K in silicate melts can be explained by a random mixing of those cations (Richet, 1984; see section 2.4, eq. 18): mixing Na and K in the presence of Al results in a different behaviour. Entropy variations upon mixing Na and K in tectosilicate melts (R=1) are far from ideal (Le Losq and Neuville, 2013). Viscosity, Raman, NMR and molecular dynamic simulation data all indicate that Na and K actually are present in different environments in tectosilicate melts (Le Losq et al., 2017), with K tending to be present in large percolation channels in the polyhedral Al-Si network. This was recently challenged by a new analysis of viscosity data along the SiO_2-(Na,K)AlO_2 binary by Robert et al. (2019). Those authors fitted viscosity data of mixed Na-K tectosilicate melts, leaving the A_e parameter (eq. 6) free. This yields results where it is possible to fit viscosity upon Na-K mixing in tectosilicate melts assuming a random Na-K distribution, like in silicate melts. In such cases, most of the variations in viscosity seemed to be explained by variations in A_e. While this is an interesting take on this problem, this is probably not a good representation of the reality. Indeed, many authors demonstrated that the pre-exponential term in viscosity equations converge to a singular value (Persikov, 1991; Giordano and Dingwell, 2003, Giordano et al., 2008, Giordano and Russell 2018). The A_e parameter is unlikely to vary largely in aluminosilicate melts (e.g. Russell and Giordano, 2005, 2017 and references therein). It thus seems improbable that A_e varies largely upon substitution of Na by K at fixed SiO_2 and Al_2O_3 contents. Raman spectroscopy data and molecular dynamic simulations (Le Losq and Neuville, 2013; Le Losq et al., 2017, Le Losq et al., 2019) further indicate that Na tectosilicate and K tectosilicate melts do not have the same structure, such that Na and K do not mix randomly in such systems. The mixing of Na- and K-tectosilicates thus appears to be of a mechanical mixing, and should accordingly yield a pseudo-linear variation of $S^{conf}(T_g)$. This agrees with conclusions from Le Losq and Neuville (2013) as well as Le Losq et al. (2017), which report pseudo-linear variations in $S^{conf}(T_g)$ upon Na-K mixing.

Considering that mixing Na and K compensators does not affect entropy, we need to consider three sources for the calculation of S^{mix} : (i) the ideal mixing of Si between different Q^n units, (ii) the

ideal mixing of Si and Al in Q^4 units and (iii) the ideal mixing of Na and K network modifiers. We thus have:

$$S_{Si-Al}^{mix} = -2\frac{x_{Si\in Q^4}+x_{Al}}{x_o}R\left[\frac{Al}{Al+Si}log\frac{Al}{Al+Si}+\left(1-\frac{Al}{Al+Si}\right)log\left(1-\frac{Al}{Al+Si}\right)\right], \quad (33)$$

with $x_{Si\in Q^4}$ the mole fraction of Si in Q^4 units,

$$S_{Si}^{mix} = \frac{-x_{Si}}{x_O} * 2 * R * \sum_{n=2}^{4} \quad x_{Q_{Si}^n} log\left(x_{Q_{Si}^n}\right), \quad (34)$$

and assuming a distribution of Na and K as charge-compensator and network modifier that varies linearly with Al/(Al+M), we finally have

$$S_{Na-Kmodifiers}^{mix} = MODS \times \left[-2R\frac{x_{Na}+x_K}{x_O}\left(X_K log(X_K)+(1-X_K)log(1-X_K)\right)\right], \quad (35)$$

with MODS the fraction of modifiers contributing to S^{mix}; MODS is equal to (1-Al/(Na+K)) for Al < (Na+K), and is equal to 0 for Al ≥ (Na+K).

The sum of equations 32 to 35 allows the calculation of $S^{conf}(T_g)$. B_e can be calculated following a similar logic to that used for silicate melts *(section 2.5)*:

$$B_e = \sum_{n=2}^{3} \quad x_{Q_{Si,Naenv}^n} B_{e_{Q_{Si,Naenv}^n}} + \sum_{n=2}^{3} \quad x_{Q_{Si,Kenv}^n} B_{e_{Q_{Si,Kenv}^n}} + x_{Q_{Si}^4} B_{e_{Q_{Si}^4}} +$$

$$x_{Q_{Al,Naenv}^4} B_{e_{Q_{Al,Naenv}^4}} + x_{Q_{Al,Kenv}^4} B_{e_{Q_{Al,Kenv}^4}} + K_1 S_{Si}^{mix} + K_2 S_{Na-Kmodifiers}^{mix} + K_3 S_{Si-Al}^{mix} \quad , \quad (36)$$

with K_1, K_2 and K_3being proportionality constants accounting for the influence of the intrinsic entropy in B_e (section 2.4; Le Losq and Neuville, 2017). A_e is left as a common parameter.

Using the equations described above, and selecting viscosity data from the literature for parameter tuning via least-square (see Figure 27), we are able to build a model for the viscosity of melts in the Na_2O-K_2O-SiO_2-Al_2O_3 system, with compositions from 50 mol% (in aluminosilicates; 60 in silicates) to 100 mol% SiO_2, and NBO/T ranging from 0 to 1.33. Root-mean-square-errors between viscosity predictions and measurements are equal or lower than 0.5 log Pa·s. This demonstrates that building a structural model of the properties of aluminosilicate melts is possible. However, the above model is

incomplete because it relies on many hypotheses, and does not take into account (yet) many specifics like the role of $^{[5]}$Al on $S^{conf}(T_g)$. Despite this, this is an encouraging step toward the construction of structural models that usually achieve a high degree of precision in the predictions they make. New developments in modelling the melt structure and in linking it with melt properties will surely allow improvements of such structural models in the future.

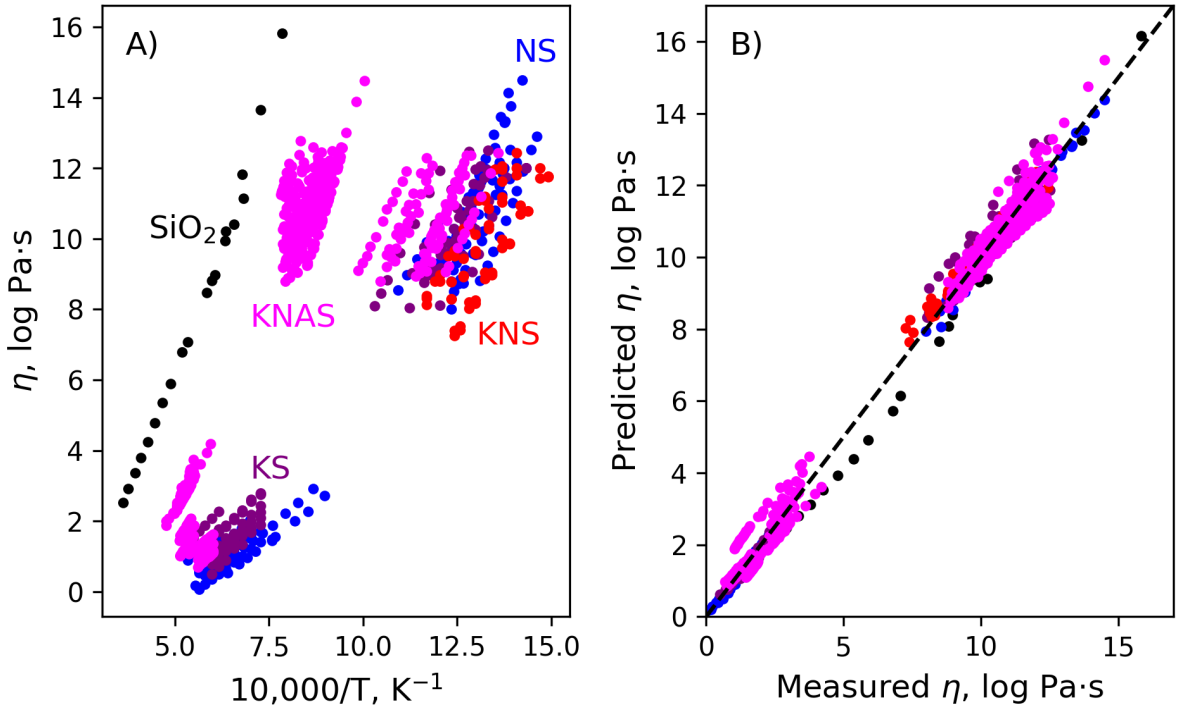

Figure 27. A) Viscosity data used for the model calibration. Data (n=817) are those compiled by Le Losq and Neuville (2017) for silicates (NS, KS, KNS and SiO_2), and for aluminosilicates (KNAS) they were compiled from Riebling (1966), Taylor and Rindome (1970), Urbain et al. (1982), Le Losq (2012), Le Losq and Neuville (2013), Le Losq et al. (2014), and Le Losq et al. (2017). The model parameters were optimised by No-U-Turn Markov Chain Monte Carlo sampling via the PyMC3 Python library. The root-mean-squared error between predictions and measurements is around 0.36 log unit.

4. Aluminate glasses and melts

Aluminate glasses and melts are of interest from a fundamental structural point of view: they contain only Al as a network former and, hence, allow better understanding of the role of Al in glasses and melts. The study of aluminate materials is also very important to understand the formation and evolution of parental bodies in the universe (Leger et al., 2009; Batalha et al., 2011). Aluminate materials further represent a technological material of interest because of their good IR transmission and ultralow optical losses (Higby et al., 1990) that make them attractive candidates for low loss optical fibers such as infrared

waveguides (Lines et al., 1989, King and Shelby, 1996). In addition, calcium aluminate glasses have been found to be photosensitive to ultraviolet radiations, leading to potential applications in photometric devices for information storage purposes (Hosono et al., 1985). They also have excellent mechanical properties, such that calcium aluminate glass fibres have been proposed for the reinforcement of cement composites (Wallenberger et al., 2004, El Hayek, 2017).

Looking at aluminate glasses allows one to better understand the fundamental role of aluminum in glasses and liquids, a task somehow difficult in aluminosilicate compositions because of the superposition of many complexities (see section 3). Numerous studies have probed the structure of calcium aluminate crystals, glasses and melts (e.g. McMillan and Piriou, 1983, Hannon and Parker, 2000, Benmore et al., 2003; Neuville et al., 2008, 2010, Licheron et al., 2011, Drewitt et al., 2012, 2017). From those, it appears that four compositional "domains" can be distinguished: Al_2O_3, Al_2O_3-CA, CA-C3A and C3A-CaO with CA=$CaAl_2O_4$, C3A=$Ca_3Al_2O_6$.

4.1 Al_2O_3

Crystalline Al_2O_3 has corundum structure with Al in 6-fold coordination (Rankin, 1915). Several studies, using ^{27}Al NMR at high temperature show that Al_2O_3 liquid is a mixture of 60% $^{[6]}$Al - 40% $^{[4]}$Al. This was confirmed more recently by XANES at the Al *K*-edge and FDMNES simulation (Neuville et al., 2009). Recently, Shi et al. (2019) proposed, from new X-ray diffraction at high temperature measurements, that Al is essentially in five-fold coordination in the Al_2O_3 liquid; this interpretation is based on the Al-O distance. The ^{27}Al NMR chemical shift is 53 ppm (Couture et al., 1990; Florian et al., 1995, Ansell et al., 1997), a value that can be interpreted as $^{[5]}$Al, or as a mixture of $^{[4]}$Al and $^{[6]}$Al. When assuming a mixture of $^{[4]}$Al and $^{[6]}$Al, the high temperature ^{27}Al NMR data allow determining an Al NMR relaxation time in excellent agreement with the relaxation time obtained from viscosity measurements (Urbain, et al. 1982). Besides, when comparing XANES data at the Al *K*-edge measured at high temperature in the liquid state to spectra simulated using the FDMNES code (Joly, 2001), the assumption of a mixture of $^{[4]}$Al and $^{[6]}$Al provides the best reproduction of the experimental data (Neuville et al., 2009). From all the high temperature NMR and XANES spectroscopies and/or neutron diffraction measurements, it is at the moment preferable to consider that, in liquid alumina, Al is present as a mixture of $^{[4]}$Al and $^{[6]}$Al.

We have essentially mentioned Al_2O_3 in its crystalline or liquid forms, however, some studies have shown that it is possible to obtain Al_2O_3 in its amorphous form, it is usually obtained by fast quenching and in thin film form (Lee et al., 2010; Kim et al., 2014). In that case, Al is essentially a mix of 4- and 5-fold coordination with a small amount of 6-fold coordination (Lee et al., 2010; Kim et al., 2014). The

742 difference between the Al coordination between glass and liquid state can be easily explained by the high
743 cooling rate.
744
745 *4.2 Al_2O_3-$CaAl_2O_4$ compositions.*
746 With the introduction of calcium (or others alkaline-earth elements) in alumina liquid, a first
747 crystalline phase can be found: grossite, $CaAl_4O_7$, called CA2, with AlO_4 tetrahedra only in Q^4 units
748 although one of the O atoms forms an "oxygen tricluster" which links three AlO_4 tetrahedra (Stebbins et
749 al, 2001, Iuga et al., 2005, Neuville et al., 2010). With increasing Ca content up to the $CaAl_2O_4$ crystal
750 composition, the amount of tricluster oxygen decreases and Al stays in four fold coordination. The
751 $CaAl_4O_7$ composition always crystallizes while $CaAl_2O_4$ (CA) can be quenched to a glass by fast quench
752 methods. In the CA glass, $^{[4]}$Al is dominant and $^{[5]}$Al representing 3,5 % of total Al (Neuville et al., 2006).
753 In the CA liquid, $^{[4]}$Al remains dominant but the proportion of $^{[5]}$Al increases up to around 40 mol % near
754 2000 K, as observed from XANES at the Al K-edge and neutron diffraction (Neuville et al., 2008a,
755 Drewitt et al., 2012). Oxygen triclusters also probably are present but remain unquantified during these
756 changes. The coordination of calcium, which is 7-fold in the glasses, increases in the melts as indicated
757 by the evolution of the pre-edge of Ca *K*-edge XANES spectra between room temperature and
758 superliquidus temperatures (Neuville et al., 2008a).
759
760 *4.3 CA-C3A compositions.*
761 For compositions between 50 > Al_2O_3 > 25 mol%, Al is only in tetrahedral coordination in both the
762 glasses and the crystals, with a number of bridging oxygens varying between 4 to 2 respectively for CA
763 and C3A (McMillan and Piriou, 1983, Neuville et al., 2004, 2006, 2010, Licheron et al. 2011, Drewitt et
764 al., 2017). In C3A crystal or glass ($Ca_3Al_2O_6$), Al can be found in Q^2 units, and, with increasing
765 temperature, Al *K*-edge XANES show very small changes (Neuville et al., 2008a). The later observation
766 implies that Al stays in Q^2 species with increasing temperature without creation of $^{[5]}$Al. The cationic
767 mobility is only insured by Q^2 species, and not by highly coordinated units as proposed by Stebbins and
768 Farnan (1992) for polymerized melts. Calcium cations in crystalline C3A and glass is in 6-fold
769 coordination, and, near 2000 K, a small pre-edge in Ca *K*-edge XANES spectra is observed; this implies
770 that the Ca coordination increases with increasing temperature (Neuville et al., 2008a).
771
772 *4.4 C3A-CaO compositions*
773 For compositions with Al_2O_3 < 25 mol%, no glass or stable crystalline phases are observed. The
774 knowledge of Al and Ca coordination in such conditions remains very scarce, if not non-existent.
775

4.5 Link with observations in other binary systems

In SrO-Al_2O_3 and BaO-Al_2O_3 systems, the liquidus temperatures are higher than in the CaO-Al_2O_3 system. This observation seems logical since there is agreement with an increase of liquidus temperature with increasing the size of the alkaline-earth elements in alkaline-earth aluminosilicate systems (Méducin et al., 2004, Licheron et al., 2011, Shan et al., 2018). Turning to MgO-Al_2O_3, Mg^{2+} forms a very stable spinel with alumina; it is not possible to quench the $MgAl_2O_4$ composition or other magnesium aluminate composition even with using fast-quench methods. In $MgAl_2O_4$ crystals, Mg and Al are in 4 and 6-fold coordinations, respectively, at room temperature and that can change with temperature (Andreozzi et al., 2000, Neuville et al., 2009).

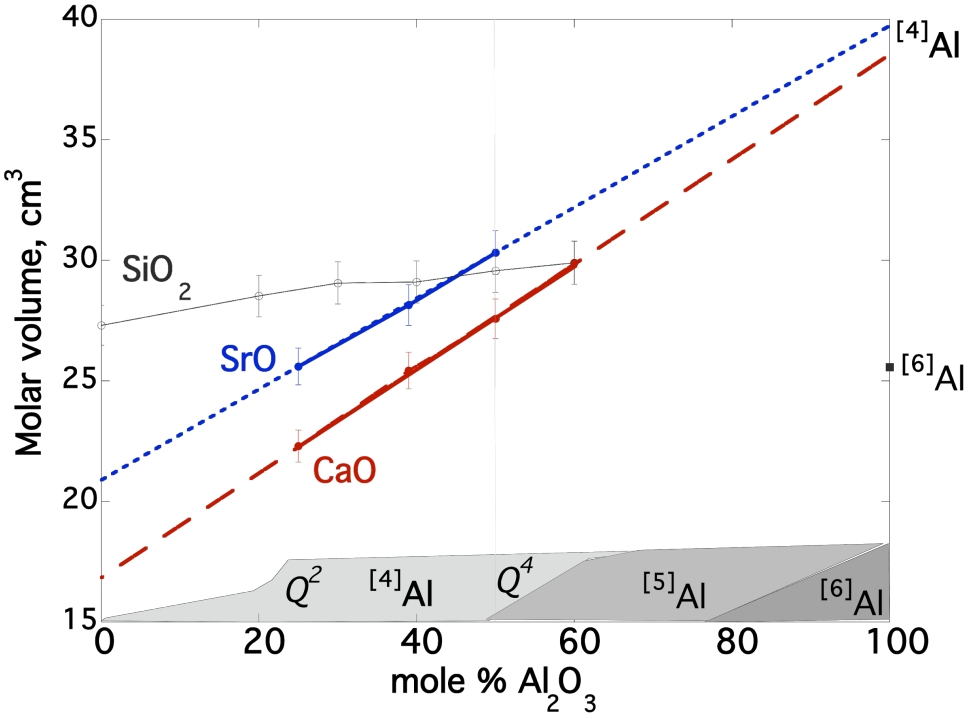

Figure 28: Coordination of Al between MO-Al_2O_3 and variation of molar volume of aluminate glasses. Molar volumes are calculated from the density measurements for Al_2O_3-SiO_2 (Wang et al., 2020), Al_2O_3-CaO (Neuville et al., 2006, 2010, Licheron et al., 2011), and Al_2O_3-SrO (Licheron et al., 2011). Solid lines correspond to fits of the data with a line, and dashed lines show the extrapolation of those fits to end members.

Figure 28 summarizes the evolution of the Al coordination in aluminate glasses and also shows how the molar volume of glass changes with Al_2O_3 content. The glasses *CxA* or *SxA*, with *x* varying between 3 and 1, are made by levitation and fast quench, and all these glasses show Al in 4-fold coordination (Neuville et al., 2006, 2008b, 2010, Licheron et al., 2010). For Ca or Sr aluminates, a linear variation of

the molar volume with the alumina content is observed between 25 and 50 mole percent of alumina, and Ca is in 6-fold coordination and Al in 4-fold coordination (Neuville et al., 2008b). If we consider linear extrapolations of these trends, it is possible to propose, considering only Al in four-fold coordination and Ca and Sr in 6-fold coordinations, that the respective partial molar volumes of Al_2O_3, CaO and SrO are respectively of 39.1, 17.0 and 21.0 cm^3 mol^{-1}. Such estimations are in very good agreement with the values proposed by Robie (1978) for the molar volume of CaO and SrO.

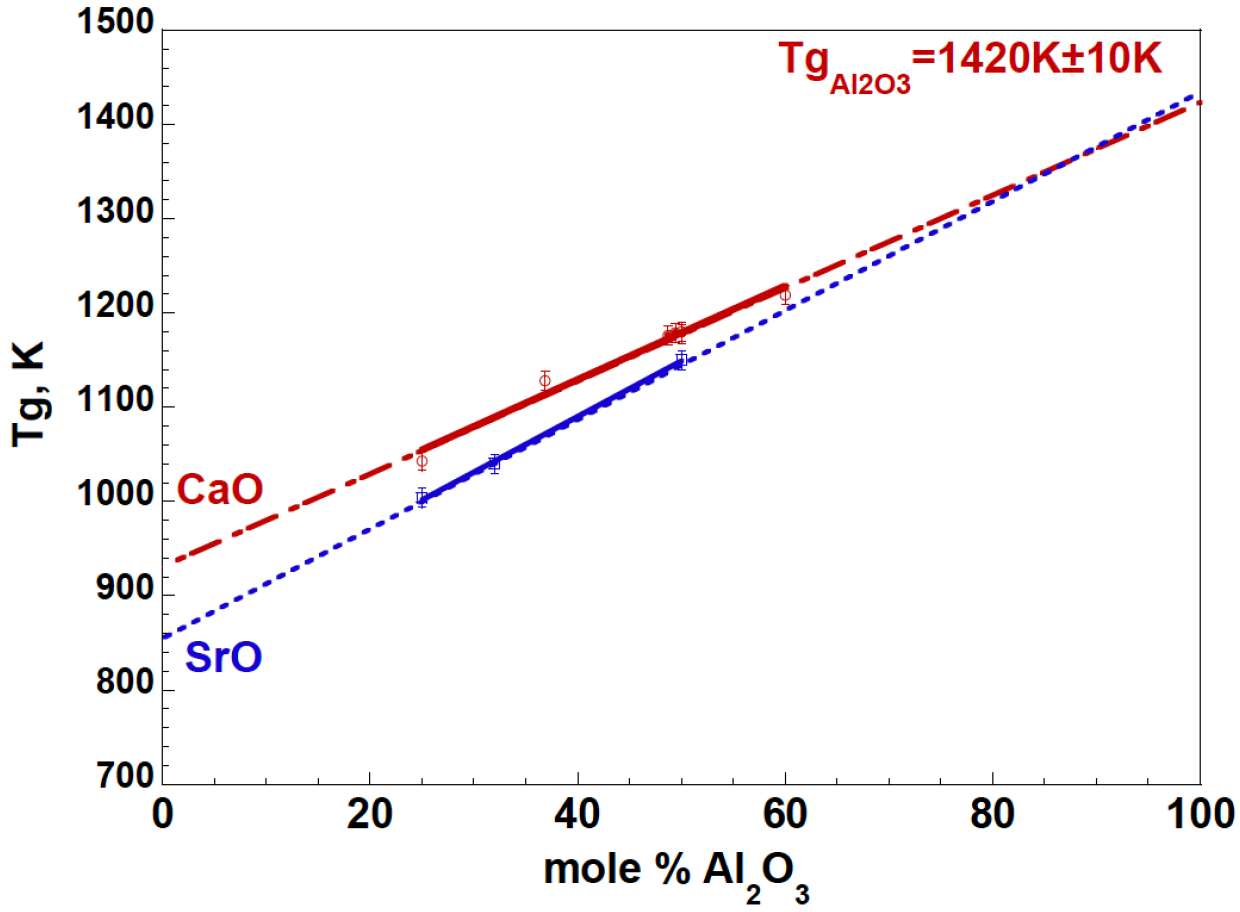

Figure 29: Glass transition temperature obtained from DSC measurements with and heating rate of 10°/min for aluminate glasses. Full line corresponds to linear variation fitting datas and dashed line corresponds to extrapolation up to end members.

To complete the observations made on the molar volume, the glass transition temperatures for *CxA* and *SxA* glasses were measured and plotted in Figure 28. The glass transition temperature of the different *CxA* and *SxA* glasses were obtained by DSC measurements with a heating rate of 10 °/min. Two linear trends are observed along the binaries CaO-Al_2O_3 and SrO-Al_2O_3. They converge to similar values when extrapolated to the alumina end-member. From this, we can propose an "apparent" partial glass transition temperature for Al_2O_3 at 1420 ± 10 K. Following this logic, we also propose partial T_gs for CaO and SrO

in 6-fold coordination at 932 ± 10 and 857 ± 10 K. The estimated Tg_i for Al_2O_3 with Al in four-fold coordination is in very good agreement with calculation of phase diagrams using CALPAHD program (Pitsch, et al. 2021 submitted).

Recently Shan et al (2018) made some calcium-strontium peraluminous glasses at 58% mole of Al_2O_3 using levitation device and fast cooling rate. They investigated macroscopic properties of these glasses and they showed that an ideal mixing term between Ca and Sr clearly exist to explain Vickers micro-hardness and glass transition temperatures variation between Ca/Sr aluminate glasses.

5. Conclusion and perspectives

Since the 1980s, it has been possible to study the structure of a liquid at high temperature by several spectroscopic methods: Raman, NMR, X-ray absorption and X-ray and neutron diffraction techniques. This allows us to understand the local order and the medium range order directly in the liquid state and thus be able to link the high temperature structure to the measurements of properties directly accessible at high temperature, like heat capacity, viscosity, conductivity, diffusivity. We have seen that this kind of approach is very promising because it allows us to have a global view of a glass and a liquid and thus to better understand the structural changes that take place in a liquid. This improved understanding of silicate glasses and liquids has great applications in both volcanology and geochemistry where we are better able to understand changes in eruptive dynamism, mass transfers and also chemical balances during crystallization processes for example. But this work allows also a better understanding of industrial processes during melting, glass-forming or even during the processes of glass-ceramic.

To summarize the changes that can occur in a cooling liquid, Figure 30, obtained for a composition of $Ca_3Al_2Si_3O_{12}$ liquid, shows both the changes that occur in the liquid state and during its cooling. We can see that at high temperature, beyond the liquidus, T_m, 1580K, the relaxation times obtained from the ^{27}Al NMR, τ_{NMR}, measurement of conductivity, τ_σ, or viscosities, τ_η converge and are similar. It simply means that in the liquid state all cations whatever their roles in the melts, move in relation to each other. From structural point of view, it is a liquid state, characterized by the particularly intense pre-edge of the XANES spectra at the Ca *K*-edge at high temperature. On the other hand, when the temperature decreases, there is a decoupling between the various relaxations, this means that the atoms begin to move differently, the network modifiers like Ca, continue to move as shown by the relaxation τ_σ, while the relaxation calculated from the viscosity measurements, τ_η, shows a strong increase, meaning that the tetrahedral network composed of tetrahedral SiO_4 and AlO_4 moves more slowly, which translates into an increase in the viscosity curve. This decoupling between the various families of atoms appears at about 1100K for this chemical composition, several orders of magnitude

separate the relaxation times obtained from the conductivity measurements, τ_σ, from those obtained from viscosity measurements, τ_η. These differences show, on the one hand, that the aluminosilicate network freezes with a significant increase of τ_η, and viscosity and that calcium atoms put themselves in a position close to that which they will have in the crystalline phase, as shown by the changes observed in the pre-edge of the XANES spectra at the Ca *K*-edge. In the end, we find that close to T_g, the Ca is probably in a crystallographic site almost identical to the one it will have in a crystal.

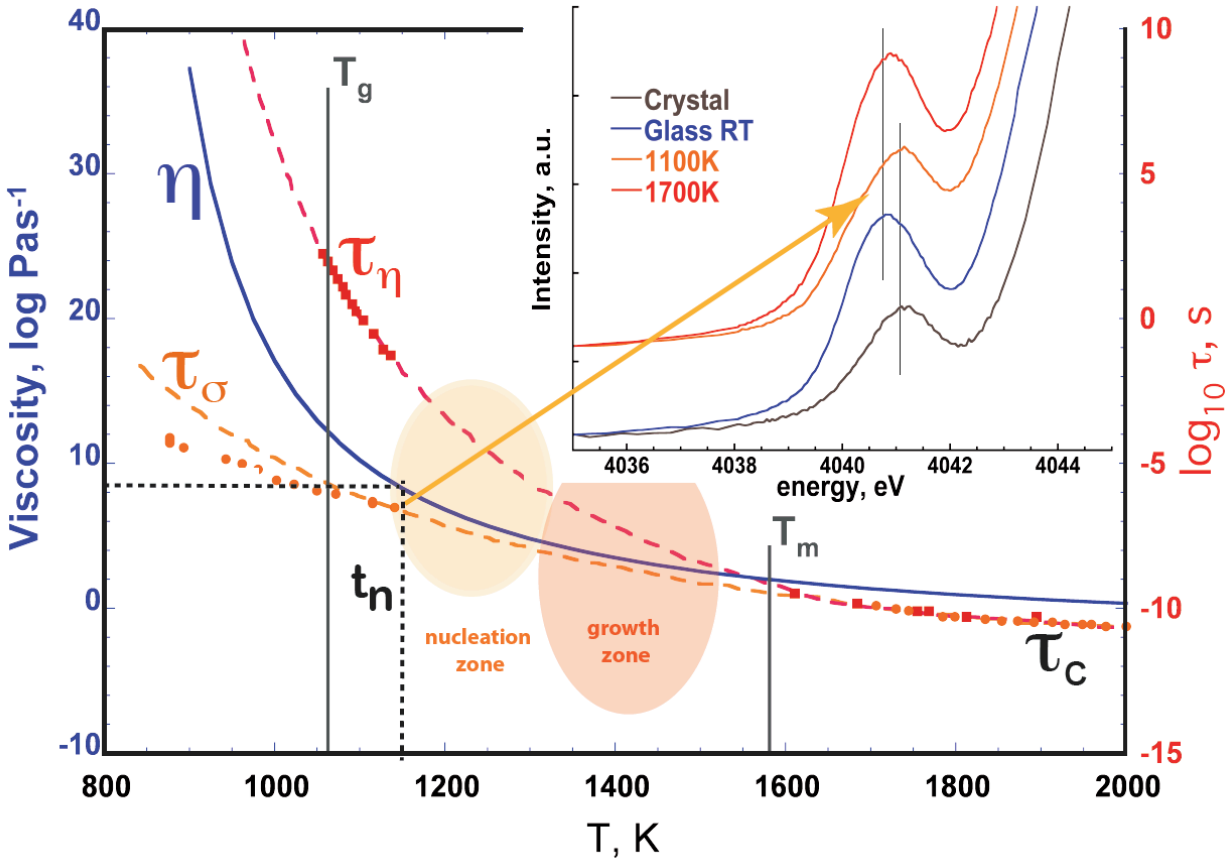

Figure 30: viscosity of $Ca_3Al_2Si_3O_{12}$ liquid from Neuville and Richet (1991), relaxation τ_η is calculated from viscosity measurements, τ_σ and τ_{NMR}, are from Gruener et al., (2001) and pre-edge XANES spectra at the Ca K-edge are from Neuville et al., (2008b)

Figure 30 completes the Figure 4 of this chapter, which helped to understand the links between potential movements in a liquid, various entropic states and viscosity, but this latter figure indicates that at high temperature all atoms can move quickly relative to each other and that at lower temperatures, atoms are in different potentials energy states and that changes will take more time.

In 2021, it is therefore possible and necessary to understand the structure and properties of a glass or/and a liquid throughout its history during a natural or industrial process. The current

computational techniques discussed in the following chapters can show and predict these different states, and it is easy to imagine that the new techniques based on Machine Learning will allow modeling of the structure, and physical properties and be able to predict them globally (Le Losq et al., 2021), this will have great consequences for both earth sciences and materials sciences.

6. References

Adam, G. and J.H. Gibbs, (1965) On the temperature dependence of cooperative relaxation properties in glass-forming liquids, J. Chem. Phys. 43 139–146.

Ali F., A.V. Chadwick, G.N. Greaves, M.C. Jermy, K.L. Ngai, M.E. Smith, Examination of the mixed-alkali effect in (Li,Na) disilicate glasses by nuclear magnetic resonance and conductivity measurements, Solid State Nucl. Magn. Reson. 5 (1995) 133–143.

Allu A., Gaddam A., Sudheer Ganisetti, Sathravada Balaji, Renée Siegel, Glenn C. Mather, Margit Fabian, Maria J. Pascual, Nicoletta Ditaranto, Wolfgang Milius, Jürgen Senker, Dmitrii A. Agarkov, Vladislav. V. Kharton, and Ferreira J. (2018) Structure and Crystallization of Alkaline-Earth Aluminosilicate Glasses: Prevention of the Alumina-Avoidance Principle. *The Journal of Physical Chemistry B*. *122*, 4737-4747

Allwardt, J.R., Lee, S.K., and Stebbins, J.F. (2003) Bonding preferences of non-bridging O atoms: evidence from 17O MAS and 3QMAS NMR on calcium aluminate and low-silica Ca-aluminosilicate glasses. American Mineralogist, 88, 949-954.

Allwardt J.R. and Stebbins J.F. (2004) Ca-Mg and K-Mg mixing around non-bridging O atoms in silicate glasses: An investigation using 17O MAS and 3QMAS NMR. American Mineralogist, 89, 777–784.

Allwardt, J.R., Stebbins, J.F., Schmidt, B.C., Frost, D.J., Withers, A.C., and Hirschmann, M.M. (2005a) Al coordination and density of high-pressure aluminosilicate glasses. American Mineralogist, 90, 1218-1222.

Allwardt, J.R., Poe, B.T., and Stebbins, J.F. (2005b) The effect of fictive temperature on Al-coordination in high-pressure (10 GPa) Na aluminosilicate glasses. American Mineralogist, 90, 1453-1457.

Allwardt, J.R., Stebbins, J.F., Terasaki, H., Du, L.D, Frost D.J., Withers, A.C., Hirschmann, M.M., Suzuki A., and Ohtani E. (2007) Effect of structural transitions on properties of high-pressure silicate melts: 27Al NMR, glass densities, and melt viscosities. American Mineralogist, 92, 1093-1104.

Andreozzi, G.B., Princivalle, F., Skogby, H. and Della Giusta, A. (2000) Cation ordering and structural variations with temperature in MgAl2O4 spinel: an X-ray single-crystal study. Americ. Mineral., 85, 1164-1171.

Angell C.A. ,1991. Relaxation in liquids, polymers and plastic crystals strong/fragile patterns and problems. J. Non-Cryst. Solids 131-133, 13-31.

Ansell, S., Krishnan, S., Weber, J. K. R., Felten, J. F., Nordine, P. C., Beno, M. A., Price, D. L. and Saboungi, M.-L. (1997) Structure of liquid aluminum oxide. Phys. Rev. Let., 78, 464-466.

Avramov I. and Milchev A. (1988) Effect of disorder on diffusion and viscosity in condensed systems. J. Non-Cryst Solids 104, 253–260.

Batalha, N.M., Borucki, W.J., Bryson, S.T., Buchhave, L.A., Caldwell, D.A., Jørgen Christensen-Dalsgaard, Ciardi, D., Dunham, E.W., Fressin, F., III, T.N.G., Gilliland, R.L., Haas, M.R., Howell, S.B., Jenkins, J.M., Kjeldsen, H., Koch, D.G., David W. Latham, Lissauer, J.J., Marcy, G.W., Rowe, J.F., Sasselov, D.D., Seager, S., Jason H. Steffen, Torres, G., Basri, G.S., Brown, T.M., Charbonneau, D., Christiansen, J., Bruce Clarke, Cochran, W.D., Dupree, A., Fabrycky, D.C., Fischer, D., Ford, E.B.,Jonathan Fortney, Girouard, F.R., Holman, M.J., Johnson, J., Isaacson, H., Klaus, T.C., Pavel Machalek, Moorehead, A.V., Morehead, R.C., Ragozzine, D.,Tenenbaum, P., Joseph Twicken, Quinn, S., VanCleve, J., Walkowicz, L.M., Welsh W.F., Devore, E., Gould, A., 2011. Kepler's First Rocky Planet: Kepler-10b. Astrophys. J. 729, 27. https://doi.org/10.1088/0004-637X/729/1/27

Bacon C.R. (1977) High-temperature heat content and heat capacity of silicate glasses: experimental determination and a model for calculation. Amer. J. Sci., 277, 109

Bancroft M., Nesbitt H.W., Henderson G.S., O'Shaughnessy C., Withers A.C. and Neuville D.R. (2018) Lorentzian dominated lineshapes and linewidths for Raman symmetric stretch peaks (800–1200 cm−1) in Qn (n=1–3) species of alkali silicate glasses/melts. Journal of Non-Crystalline Solids. 484, 72-83.

Ben Kacem I, Gautron L., Coillot D., Neuville D.R. (2017) Structure and properties of lead silicate glasses and melts. Chemical Geology, 461, 104-114.

Benmore C.J., Weber J K R, Sampath S, Siewenie J, Urquidi J and Tangeman J A (2003) A neutron and x-ray diffraction study of calcium aluminate glasses. J. Phys.: Condens. Matter 15 (2003) S2413–S2423.

Bockris J.O.M., Mackenzie J.D. and Kitchener E., 1955. Viscous flow in silica and binary liquid silcates. Farad. Soc. Lond. Trans. 51, 1734-1749.

Bødker M.S., Youngman R.E., Mauro J. and Smedskjaer M.M. (2020) Mixed Alkali Effect in Silicate Glass Structure: Viewpoint of 29Si Nuclear Magnetic Resonance and Statistical Mechanics. J. Phys. Chem. B, 124, 10292−10299. DOI: 10.1021/acs.jpcb.0c07980

Bottinga Y. and Weill D.F. (1970) Densities of liquid silicate systems calculated from partial molar volumes of oxyde components Amer. J. Sci., 269, 169

Bottinga Y. and D.F. Weill, The viscosity of magmatic silicate liquids: a model for calculation, Am. J. Sci. 272 (1972) 438–475

Bender S., Franke R., Hartmann E., Lansmann V., Jansen M., Hormes J. (2002) X-ray absorption and

photoemission electron spectroscopic investigation of crystalline and amorphous barium silicates. Journal of Non-Crystalline Solids 298, 99–108

Bray, P.J., J.F. Emerson, D. Lee, S.A. Feller, D.L. Bain, D.A. Feil, NMR and NQR studies of glass structure, J. Non-Cryst. Solids 129 (1991) 240–248.

Brauer D.S. Bioactive glasses - structure and properties. Angew Chem Int Edit. 2015;54(14):4160–81.

Brückner R. (1970) Properties and structure of vitreous silica. II. J. Non-Cryst. Solids 5, 177-216.

Buckerman W-A, Müller-Warmuth W., 1992. A further 29Si NMR study on binary alkali silicate glasses. Glastech. Ber. 65, 18-21.

Bunker, B.C., Kirkpatrick, R.J., Brow, R.K., Turner, G.L., and Nelson, C. (1991) Local structure of alkaline-eath boroaluminate crystals and glasses. II, 11B and 27Al MAS NMR spectroscopy of alkaline-earth boroaluminate glasses. Journal of the American Ceramic Society, 74,1430-1438.

Carmichael I.S.E., Nicholls J., Spera F.J., Wood B.J. and Nelson S.A. (1977) High-temperature of silicate liquids: application to the equilibration and ascent of basic magma. Phil. Trans. R. Soc. Lond., A. 286, 373.

Champagnon B., Wondraczek L., Deschamps T. (2009) Boson peak, structural inhomogeneity, light scattering and transparency of silicate glasses Journal of Non-Crystalline Solids, 355, 712–714

Charpentier T., Okhotnikov K., Novikov A., Hennet L., Fischer H., Neuville D.R., Florian P. (2018) Structure of strontium aluminosilicate glasses from molecular dynamics simulations, neutron diffraction and nuclear magnetic resonance studies. The Journal of Physical Chemistry. 122(41): 9567-9583. DOI: 10.1021/acs.jpcb.8b05721

Chumakov A. I., Monaco G., A. Fontana A. Bosak, R. P. Hermann, D. Bessas, B. Wehinger, W. A. Crichton, M. Krisch, R. Rüffer, G. Baldi, G. Carini Jr., G. Carini, G. D'Angelo, E. Gilioli, G. Tripodo, M. Zanatta, B. Winkler, V. Milman, K. Refson, M. T. Dove, N. Dubrovinskaia, L. Dubrovinsky, R. Keding, and Y. Z. Yue (2014) Role of Disorder in the Thermodynamics and Atomic Dynamics of Glasses. Physical Review Letters, 112, 025502

Cicconi M.R., de Ligny D., Gallo T. M., Neuville D.R. (2016) Ca Neighbors from XANES spectroscopy: a tool to investigate structure, redox and nucleation processes in silicate glasses, melts and crystals. American Mineralogist, 101, 1232-1236.

Clupper D.C., Hench L.L., 2003. Crystallization kinetics of tape cast bioactive glass 45S5. J. Non-Cryst. Solids 318, 43-48.

Cormack A.N. and Du J., 2001. Molecular dynamics simulations of soda-lime silicate glasses. J. Non-Cryst. Solids. 293-295, 283-289.

Cormier L. and Neuville D.R. (2004) Ca and Na environments in Na2O-CaO-Al2O3-SiO2 glasses: influence of cation mixing and cation-network interactions. Chem. Geol., 213, 103-113

968 Cormier L., Neuville D.R. and G. Calas (2000) Structure and properties of low-silica calcium
969 aluminosilicate glasses. J. Non-Crystal. Solids.274, 110-114.
970 Cormier L, Ghaleb D., Neuville D.R., Delaye JM, Calas G. (2003) Network polymerization of calcium
971 aluminosilicate glasses: a Molecular Dynamics and Reverse Monte Carlo study. J. Non-Crystal.
972 Solids., 332, 255-270.
973 Cormier L., Neuville D.R. and G. Calas (2005) Structure of low-silica calcium aluminosilicate glasses.
974 J. Amer. Ceram. Soc., 88, 2292-2299.
975 Cormier L. and Cuello G. (2013) Structural investigation of glasses along the MgSiO3-CaSiO3 join:
976 diffraction studies. Geochimica et Cosmochimica Acta 122 (2013) 498-510.
977 Cormier L. 2019 Neutron and X-Ray Diffraction of Glass. Hand Book of glass. 1045-1090
978 Coté, B., Massiot, D., Taulelle, F., Coutures, J.-P. (1992) 27Al NMR spectroscopy of aluminosilicate
979 melts and glasses. Chemical Geology, 96, 367-370.
980 Courtial P. (1993) Propriétés thermodynamiques des silicates fondus et des minéraux au voisinage de la
981 fusion. Thèse Université Paris 7
982 Courtial P. and Richet P. (1993) Heat capacity of magnesium aluminosilicate melts. Geochimie and
983 Cosmochimica Acta Vol. 57, pp. 1267-1275
984 Coutures, J.-P., Massiot, D., Bessada, C., Echegut, P., Rifflet, J.-C., and Taulelle, F. (1990) Etude par
985 RMN 27Al d'aluminates liquides dans le domaine 1600-2100°C. C.R. Acad. Sci. Paris, 310, 1041-
986 1045.
987 Davis R.O., and Jones G.O. (1953) Thermodynamic and kinetic properties of glasses. Adv. Phys., 2, 370
988 Davis M., Kaseman D., Parvani S., Sanders K., Grandinetti P., Massiot D., Florian P. (2010) Q(n) Species
989 Distribution in K2O· 2SiO2 Glass by 29Si Magic Angle Flipping NMR. J. Phys. Chem. A 2010, 114,
990 5503–5508
991 Day D. E. (1976) Mixed alkali glasses - Their properties and uses. J. Non-Cryst. Solids 21, 343–372.
992 Descamps M. (2017) États amorphe et vitreux des composés moléculaires et pharmaceutiques –
993 Propriétés générales. Techniques de l'Ingénieur., PHA2030 v1
994 Dingwell D.B. and S.L. Webb, (1990) Relaxation of silicate glass. Eur. J. Mineral., 2 427.
995 Doremus R.H. (1973) Glass science ; John Wiley and Sons N.Y. 349p
996 Doweidar H. (1999) Density-structure correlations in silicate glasses, J. Non-Cryst. Solids 249, 194–200
997 Doweidar, H., S. Feller, M. Affatigato, B. Tischendorf, C. Ma, E. Hammarsten: (1999) Density and molar
998 volume of extremely modified alkali silicate glasses, Phys. Chem. Glasses 40, 339–344
999 Drewitt J.W.E, L. Hennet, Zeidler A., Jahn S., P.S. Salmon, Neuville D.R. and Fischer H.E. (2012)
000 Structural transformations on vitrification in the fragile glass forming system CaAl2O4. Physical
001 Review Letters. 109 (23), 235501-235506.
002 Drewitt J.W.E, Barnes A.C., Jahn S., Kohn S.C., Walter M.J., Novikov A., Neuville D.R., Fischer H.E.

003 and Hennet L. (2017) Structure of liquid tri-calcium aluminate. Physical Review B. 95, 064203-
004 064214.
005 Drewitt J., Hennet L., Neuville D.R., (2021) The structure of glasses from short distance order to long
006 distance. In Neuville D.R., Henderson G.S, Dingwell D. B. (2021) "Magmas, melts, liquids and
007 glasses: Experimental insights " Review in Mineralogy and Geochemistry. in press – DOI :
008 Du J. and Cormack A.M. (2004) The medium range structure of sodium silicate glasses: a molecular
009 dynamics simulation. Journal of Non-Crystalline Solids 349, 66–79
010 Dulong, P.L., and Petit, A.T. (1819) Recherches sur quelques points importants de la théorie de la chaleur.
011 Annales de chimie et de physique, 10, 395–413.
012 Dupree R., D. Holland, D.S.Williams (1986) The structure of binary alkali silicate glasses, J. Non-Cryst.
013 Solids 81, 185–200, http://dx.doi.org/10.1016/0022-3093(86)90269-3.
014 Dupree, N. Ford, D. Holland, Examination of the/sup 29/Si environment in the PbO-SiO/sub 2/system
015 by magic angle spinning nuclear magnetic resonance. Pt. 1. Glasses. Phys. Chem. Glasses 28 (1987)
016 78-87.
017 Edén, M. (2012) NMR studies of oxide-based glasses. Annual Reports Section "C" (Physical Chemistry),
018 108, 177.
019 Emerson J.F., Stallworth P.E. and Bray P.J. (1989) HIGH-FIELD 29Si NMR STUDIES OF ALKALI
020 SILICATE GLASSES. Journal of Non-Crystalline Solids 113 (1989) 253-259
021 Emerson J.F., P.J. Bray, Nuclear magnetic resonance and transmission electron microscopy studies of
022 mixed-alkali silicate glasses, J. Non-Cryst. Solids 169 (1994) 87–95.
023 English S., 1923. The effect of composition on the viscosity of glass, Part II. J. Soc. Glass. Tech., 8, 205-
024 251.
025 Eppler R.A. (1966), Viscosity of Molten B2O3. Journal of the American Ceramic Society, 49, 679-680.
026 https://doi.org/10.1111/j.1151-2916.1966.tb13202.x
027 Fanderlik I. (1990) Silica Glass and Its Application. Elsevier, Amsterdam.
028 Farnan I., and Stebbins J.F. (1990) High-temperature 29Si NMR investigation of solid and molten
029 silicates. J. Amer. Chem. Soc., 112, 32
030 Farnan, I., and Stebbins, J.F. (1994) The nature of the glass-transition in a silica-rich oxide melt, Nature,
031 265, 1206-1209.
032 Fayon, F., Bessada, C., Massiot, D., Farnan, I., Coutures, J.P., 1998. 29Si and 207Pb NMR study of local
033 order in lead silicate glasses. J. Non-Cryst. Solids 232, 403–408.
034 Fayon, F., Landron, C., Sakurai, K., Bessada, C., Massiot, D., 1999. Pb2+ environment in lead silicate
035 glasses probed by Pb-LIII edge XAFS and 207Pb NMR. J. Non-Cryst. Solids 243, 39–44.
036 Feller, S., Lodden, G., Riley, A., Edwards, T., Croskrey, J., Schue, A., Liss, D., Stentz, D., Blair, S.,
037 Kelley, M., Smith, G., Singleton, S., Affatigato, M., Holland, D., Smith, M.E., Kamitsos, E.L.,
038 Varsamis, C.P.E., Loannou, E., 2010. A multispectroscopic structural study of lead silicate glasses
039 over an extended range of compositions. J. Non-Cryst. Solids 356, 304–313.

040 Fiske P.S and Stebbins J.F. (1994) The structural role of Mg in silicate liquids: A high-temperature 25Mg,
041 23Na, and 29Si NMR study. American Mineralogist, Volume 79, pages 848-861, 1994
042 Florian P., Massiot D., Poe B., Farnan I. and Couture J.P. (1995) A time resolved 27AL NMR study of
043 the cooling process of liquid alumina from 2450°C to crystallisation. Sol. Stat. Magnet. Reson., 5,
044 233-238.
045 Florian P., K.E. Vermillion, P.J. Grandinetti, I. Farnan, J.F. Stebbins, Cation distribution in mixed alkali
046 disilicate glasses, J. Am. Chem. Soc. 118 (1996) 3493–3497.
047 Florian, P., Sadiki, N., Massiot, D., and Coutures J.P (2007) 27Al NMR study of the Structure of
048 Lanthanum- and Yttrium-Based Aluminosilicate glasses and melts. Journal of Physical Chemistry B,
049 111, 9747-9757.
050 Florian P., Novikov A., Drewitt J.W.E, Hennet L., Sarou-Kanian V., Massiot D., Fischer H.E. and
051 Neuville D.R. (2018) Structure and Dynamics of High-Temperature Strontium Aluminosilicate Melts.
052 Physical Chemistry Chemical Physics. 20, 27865-27877
053 Fulcher G.S. (1925) Analysis of recent measurements of the viscosity of glasses. J. Am. Ceram. Soc., 8, 339
054 Fontana and Plummer (1966) A study of viscosity-temperature relation-ship in the GeO2 and SiO2
055 system. Phys Chem Glass, 7, 139.
056 Frantz J.D. and Mysen B.O., 1995. Raman spectra and structure of BaO-SiO2, SrO-SiO2 and CaO-SiO2
057 melts to 1600°C. Chem. Geol. 121, 155-176.
058 Frischat G.H., Poggemann J.F, Heide G. (2001) Nanostructure and atomic structure of glass seen by
059 atomic force microscopy. Journal of Non-Crystalline Solids 345&346, 197–202
060 Frischat G.H. and Sebastian K, (1985) Leach resistance of nitrogen-containing Na2O-CaO-SiO2 glasses.
061 J. Am. Ceram. Soc, 68, C305-C307.
062 Galeener F.L., Leadbetter A.J, Stringfellow M.W. (1983) Comparison of the neutron, Raman and infrared
063 vibrational spectra of vitreous SiO2, GeO2, BeF2. Physical Review B, 27, 1052-1079.
064 Gahay V.M.C., Tomozawa M. (1989) "The origine of phase separation in silicate melts and glasses." J.
065 Non-Cryst. Solids, 109, 27-34.
066 Gaskell P, , MC Eckersley, AC Barnes, P Chieux (1991) Medium-range order in the cation distribution
067 of a calcium silicate glass. Nature, 350, pages675–677
068 Georges A.M. and Stebbins J.F. (1998) Structure and dynamics of magnesium in silicate melts: A high-
069 temperature 25Mg NMR study American Mineralogist, Volume 83, pages 1022–1029, 1998
070 Gibbs J.H. and Dimarzio E.A. (1958) Nature of the glass transition and the glassy state. J. Chem. Phys.,
071 28, 373
072 Giordano D. and Russell J. K. (2018) Towards a structural model for the viscosity of geological melts.
073 Earth Planet. Sci. Lett. 501, 202–212.
074 Giordano D., Russell J. K. and Dingwell D. B. (2008) Viscosity of magmatic liquids: A model. Earth
075 Planet. Sci. Lett. 271, 123–134.
076 Giordano, D., Dingwell, D.B., (2003). Non-Arrhenian multicomponent melt viscosity: a model. Earth
077 Planet. Sci. Lett. 208, 337–349 Erratum Earth Planet. Sci. Lett. 221, 449.

078 Goldstein M. (1969) Viscous liquids and the glass transition: a potential energy barrier picture. J. Chem.
079 Phys., 51, 3728
080 Goldstein M. (1976) Viscous liquids and the glass transition. V. Sources of the excess specific heat of
081 the liquid. J. Chem. Phys., 64, 4767
082 Goldstein M. (2011) On the reality of the residual entropy of glasses and disordered crystals: The entropy
083 of mixing. *Journal of Non-Crystalline Solids* **357**, 463–465.
084 Greaves, G.N., Fontaine, A., Lagarde, P., Raoux, D., and Gurman, S.J. (1981) Local structure of silicate
085 glasses. Nature, 293, 611-616.
086 Greaves, G. N. Exafs and the structure of glass. J. Non-Cryst. Solids 71, 203–217 (1985).
087 Greig J.W (1927) Immiscibility in silicate melts. American Journal of Science. s5-13 (73) 1-44; DOI:
088 https://doi.org/10.2475/ajs.s5-13.73.1
089 Grest G.S. and Cohen M.H. (1980) Liquids, glasses, and the glass transition: a free-volume approach ; in
090 "Advances in Chemical Physics", 48, Prigogine I. and Rice S.A. eds John Wiley and Sons N.Y., 545
091 Gruener G. P. Odier, D. De Sousa Meneses, P. Florian, and P. Richet (2001) Bulk and local dynamics in
092 glass-forming liquids: A viscosity, electrical conductivity, and study of aluminosilicate melts. Phys.
093 Rev. B 64, 024206
094 Guignard, M. and Cormier, L. (2008) Environments of Mg and Al in MgO-Al2O3-SiO2 glasses: a study
095 coupling neutron and X-ray diffraction and Reverse Monte Carlo simulations. Chemical Geology.
096 256, 111–118
097 Hannon, A.C. and Parker, J.M. (2000) The structure of aluminate glasses by neutron diffraction. Journal
098 of Non-Crystalline Solids, 274, 102–109.
099 Hater W., W. Müller-Warmuth, M. Meier, G.H. Frischat, High-resolution solid-state NMR studies of
100 mixed-alkali silicate glasses, J. Non-Cryst. Solids 113 (1989) 210–212.
101 El Hayek R., Ferey F., Florian P., Pisch A. and Neuville D.R. (2017) Structure and properties of lime
102 alumino-borate glasses and melts. Chemical Geology, 461, 75-81.
103 Hehlen B., Courtens E., Yamanka A. and Inoue K., 2002. Nature of the Boson peak of silica glasses from
104 hyper-Raman scattering. J. Non-Cryst. Solids 307, 185-190.
105 Hehlen B. and Neuville D.R. (2015) Raman response of network modifier cations in alumino-silicate
106 glasses. The Journal of Physical Chemistry B. 119, 4093–4098.
107 Hehlen B. and Neuville D.R. (2020) Non-network-former cations in oxide glasses spotted by Raman
108 scattering. Physical Chemistry Chemical Physics., 22, 12724 – 12731. DOI: 10.1039/D0CP00630K.
109 Hench L.L., 1991. Bioceramics : from concept ot clinic. J. Am. Ceram. Soc. 74, 1487-1510.
110 Henderson G.S., Neuville D.R., Cormier L. (2007) An O K-edge XANES study of Calcium Aluminates.
111 Can. J. Chem., 85, 801-806.
112 Henderson G.S. (1995) A Si K-edge EXAFS/XANES study of sodium silicate glasses. Journal of Non-

113 Crystalline Solids, 183, 43-50.
114 Hennet L. Drewitt J.W.E., Neuville D.R., Cristiglio V., Kozaily J., Brassamin S., Zanghi D., Fischer H.E.
115 (2016) Neutron diffraction of calcium aluminosilicate glasses and melts. Journal of Non-Crystalline
116 Solids. 451, 89-93.
117 Herzog F. et Zakaznova-Herzog V.P. (2011) Quantitative Raman spectroscopy: Challenges, shortfalls,
118 and solutions—Application to calcium silicate glasses. *American Mineralogist, 96914–927*
119 Hetherington G. Jack, H, Kennedy J.C. (1964) The viscosity of vitreous silica. Physics and Chemistry of
120 Glass. 5, 130-137.
121 Hiet, J., Deschamps, M., Pellerin, N., Fayon, F., Massiot, D., (2009) Probing chemical disorder in glasses
122 using silicon-29 NMR spectral editing. Phys. Chem. Chem. Phys. 11, 6935. doi:10.1039/b906399d
123 Higby, P. L., Ginther, R.J., Aggarwal, I.D., Friebele, E.J., (1990) Glass formation and thermal properties
124 of low-silica calcium aluminosilicate glasses. J. Non-Cryst. Solids 126, 209-215.
125 Hill R. and Brauer D.S. (2011) Predicting the bioactivity of glasses using the network connectivity or
126 split network models. Journal of Non-Crystalline Solids 357, 3884–3887
127 Hosono H. Yamazaki K, and abe Y. (1985) Dopant-Free Ultraviolet-Sensitive Calcium Aluminate
128 Glasses. J. Am. Ceram. Soc., 68, C-304-C-305
129 Hudon P, Baker D.R. (2002a) The nature of phase separation in binary oxide melts and glasses. I. Silicate
130 systems. Journal of Non-Crystalline Solids 303, 299–345
131 Hudon P, Baker D.R. (2002b) The nature of phase separation in binary oxide melts and glasses. II.
132 Selective solution mechanism. Journal of Non-Crystalline Solids 303 (2002) 346–353
133 Hung I, Gan Z., Gor'kov P.L., Kaseman D.C., Sen S., LaComb M., Stebbins J.F. (2016) Detection of
134 “free” oxide ions in low-silica Ca/Mg silicate glasses: Results from 17O → 29Si HETCOR NMR.
135 Journal of Non-Crystalline Solids, 445–446, 1-6
136 Hui H. and Zhang Y. (2017) Toward a general viscosity equation for natural anhydrous and hydrous
137 silicate melts. Geochimica et Cosmochimica Acta 71 (2007) 403–416
138 Imaoka M. and Yamazaki T. (1963) Studies of the Glass-formation Range of Silicate
139 Systems.Investigations on the Glass-formation Range, 2. J. Ceram. Assoc. Japan , 79, 215-232.
140 Inaba S., Fujino S., Sakai K. (2010) Non-contact measurement of the viscosity of a soda–lime–silica melt
141 using electric field tweezers. Phys. Chem. Glasses: Eur. J. Glass Sci. Technol. B, 51, 304–308
142 Ispa S., Charpentier T., Mauri F. and Neuville D.R. (2010) Structural properties of Lithium and Sodium
143 tetrasilicate glasses: molecular dynamics simulations vs NMR experimental and first principles data.
144 Solid State Sciences, 12, 183-192.
145 Iuga D., Morais C., Gan Z., Neuville D.R., Cormier L., Massiot D. (2005) 27Al/17O NMR correlation
146 in crystalline and vitreous materials. J. Amer. Chem. Soc., 127, 11540-11542.
147 Jakse N., Bouhadja M., Kozaily J., Hennet L., Drewitt J.W.E., Neuville D.R., Fischer H. E., Cristiglio

V., Pasturel A. (2012) Interplay between non-bridging oxygen, triclusters, and fivefold Al coordination in low silica content calcium aluminosilicate melts. Applied Physics Letters, 101, 201903-201908.

Joly, Y. (2001) X-ray absorption near edge structure calculations beyond the muffin-tin approximation. Phys. Rev. B, 63, 125120.

Jones A.R., Winter R., Greaves G.N, and Smith I.H., 2001. MAS NMR study of soda-lime silicate glasses with variables degree of polymerisation. J. Non-Cryst. Solids 293-295, 87-92.

Kanehashi, K. and Stebbins J.F. (2007) In situ high temperature 27Al NMR study of structure and dynamics in a calcium aluminosilicate glass and melt. Journal of Non-Crystalline Solids 353, 4001–4010.

Kashio S., Iguchi y., Goto t., Nishina y., Fuwa t. (1980) Raman Spectroscopic Study on the Structure of Silicate Slag. Transactions of the Iron and Steel Institute of Japan, 20, 251-253 https://doi.org/10.2355/isijinternational1966.20.251

Kauzmann, W., 1948. The nature of the glassy state and the behavior of liquids at low temperatures. Chem. Rev. 43, 219-243.

Kim H-M, Miyaji F. And Kokubo T., 1995. Bioactivity of Na2O-CaO-SiO2 glasses. J. Amer. Ceram. Soc. 78, 2405-2411.

King W. and Shelby J. (1996) Strontium calcium aluminate glasses. Physics and chemistry of glasses, 37, 1-14.

Kim N. Bassiri R, Fejer M.M, Stebbins J.F. (2014) The structure of ion beamsputtered amorphous alumina films and effects of Zn doping: High-resolution 27Al NMR. Journal of Non-Crystalline Solids 405, 1–6.

Kohara S., Ohno, M., Takata T., Usuki L, Morita H., Suzuya S., Akola S., Pusztai L. (2010) Lead silicate glasses: Binary network-former glasses with large amounts of free volume. PHYSICAL REVIEW B 82, 134209

Koike A. and Tomozawa M., 2007, IR investigation of density changes of silica glass and soda-lime silicate glass caused by microhardness indentation. Journal of Non-Crystalline Solids, 353, 2318-2327

Koike A, Tomozawa M., Ito S., (2007), Sub-critical crack growth rate of soda-lime-silicate glass and less brittle glass as a function of fictive temperature. Journal of Non-Crystalline Solids, 353, 2675-2680

Kroecker, S. and Stebbins, J.F. (2000) Magnesium coordination environments in glasses and minerals: New insight from high-field magnesium-25 MAS NMR. American Mineralogist, 85, 1459–1464.

Kusabiraki K. and Shiraishi K.T.(1981) The infrared spectrum of vitreous fayalite. Journal of Non-Crystalline Solids. 44, 365-368.

Kusabiraki K. (1986) Infrared spectra of vitreous silica and sodium silicates containing titanium. Journal

182 of Non-Crystalline Solids, 79, 208-212
183 Lacy, E.D., 1963. Aluminium in glasses and melts. Phys. Chem. Glasses 4, 234-238.
184 Lange R. A. (1996) Temperature independent thermal expansivities of sodium aluminosilicate melts.
185 Geochim. Cosmochim. Acta 60, 4989-4996.
186 Lange R. A. (1997) A revised model for the density and thermal expansivity of K20-Na20-CaOMgO-
187 A1203-SiO 2 liquids from 700 to 1900 K: extension to crustal magmatic temperatures. Contrib.
188 Mineral. Petrol. 130, 1-11.
189 Lange R. A. and Carmichael I. S. E. (1987) Densities of Na2O-K2O-CaO-MgO-Fe2O3-Al2O3-TiO-
190 SiO2 liquids: New-measurements and derived partial molar properties. Geochim. Cosmochim. Acta
191 51,2931-2946.
192 Lange RA, Navrotsky A (1992) Heat capacities of Fe2O3-bearing silicate liquids. Contrib Mineral Petrol
193 110:311-320
194 Lee S.K., Park S.Y, Yi Y.S., and Moon J. (2010) Structure and Disorder in Amorphous Alumina Thin
195 Films: Insights from High-Resolution. J. Phys. Chem. C 2010, 114, 13890–13894
196 Leko BK (1979) Viscosity of vitreous silica. Fiz Khim Stekla 5 : 258-278
197 Larson C. Doerr, Affatigato M, Feller S, Holland D and Smith M E (2006), A 29Si MAS NMR study of
198 silicate glasses with a high-lithium content. J. Phys.: Condens. Matter 18, 11323–11331
199 doi:10.1088/0953-8984/18/49/023
200 Leko V. K., Gusakova N. K., Meshcheryakova E. V., and Prokhorova T. I. (1977) The effect of impurity
201 alkali oxides, hydroxyl groups, AI203, and Ga203 on the viscosity of vitreous silica. Soy. J. Glass
202 Phys. Chem. 3, 204-210.
203 Lee, S.K. and J.F. Stebbins, (2003) Nature of cationmixing and ordering in Na-Ca silicate glasses and
204 melts, J. Phys. Chem. B 107 3141–3148, http://dx.doi.org/10.1021/jp027489y.
205 Lee S.K., Stebbins J. (2009) Effects of the degree of polymerization on the structure of sodium silicate
206 and aluminosilicate glasses and melts: An 17O NMR study, Geochim. Cosmochim. Acta 73, 1109–
207 1119
208 Lee S. K. (2005) Structure and the extent of disorder in quaternary (Ca-Mg and Ca-Na) aluminosilicate
209 glasses and melts. Am. Mineral. 90, 1393–1401.
210 Lee S. K. and Stebbins J. F. (1999) The degree of aluminum avoidance in aluminosilicate glasses. Am.
211 Mineral. 84, 937–945.
212 Lee, S.K. and Stebbins, J.F. (2000) Al-O-Al and Si-O-Si sites in framework aluminosilicate glasses with
213 Si/Al=1: quantification of framework disorder. Journal of Non-Crystalline Solids, 270, 260-264.
214 Lee S.K. and Stebbins J.F. (2002) The extent of inter-mixing among framework units in silicate glasses
215 and melts. Geochimica et Cosmochimica Acta, 66, 303–309.

Lee S. K., Mysen B. O. and Cody G. D. (2003) Chemical order in mixed-cation silicate glasses and melts. Phys. Rev. B 68, 214206.

Lee S.K. and Kim E. J. (2015) Probing Metal-Bridging Oxygen and Configurational Disorder in Amorphous Lead Silicates: Insights from 17O Solid-State Nuclear Magnetic Resonance. The Journal of Physical Chemistry C, 119, 1, 748–756.

Lee S. K., Kim H.-I., Kim E. J., Mun K. Y. and Ryu S. (2016) Extent of Disorder in Magnesium Aluminosilicate Glasses: Insights from 27Al and 17O NMR. J. Phys. Chem. C 120, 737–749.

Léger, A., Rouan, D., Schneider, J., Barge, P., Fridlund, M., Samuel, B., Ollivier, M., Guenther, E., Deleuil, M., Deeg, H.J., Auvergne, M., Alonso, R., Aigrain, S., Alapini, A., Almenara, J.M., Baglin, A., Barbieri, M., Bruntt, H., Bordé, P., Bouchy, F., Cabrera, J., Catala, C., Carone, L., Carpano, S., Csizmadia, S., Dvorak, R., Erikson, A., Ferraz-Mello, S., Foing, B., Fressin, F., Gandolfi, D., Gillon, M., Gondoin, P., Grasset, O., Guillot, T., Hatzes, A., Hébrard, G., Jorda, L., Lammer, H., Llebaria, A., Loeillet, B., Mayor, M., Mazeh, T., Moutou, C., Pätzold, M., Pont, F., Queloz, D., Rauer, H., Renner, S., Samadi, R., Shporer, A., Sotin, C., Tingley, B., Wuchterl, G., Adda, M., Agogu, P., Appourchaux, T., Ballans, H., Baron, P., Beaufort, T., Bellenger, R., Berlin, R., Bernardi, P., Blouin, D., Baudin, F., Bodin, P., Boisnard, L., Boit, L., Bonneau, F., Borzeix, S., Briet, R., Buey, J.-T., Butler, B., Cailleau, D., Cautain, R., Chabaud, P.-Y., Chaintreuil, S., Chiavassa, F., Costes, V., Parrho, V.C., Fialho, F.D.O., Decaudin, M., Defise, J.-M., Djalal, S., Epstein, G., Exil, G.-E., Fauré, C., Fenouillet, T., Gaboriaud, A., Gallic, A., Gamet, P., Gavalda, P., Grolleau, E., Gruneisen, R., Gueguen, L., Guis, V., Guivarc'h, V., Guterman, P., Hallouard, D., Hasiba, J., Heuripeau, F., Huntzinger, G., Hustaix, H., Imad, C., Imbert, C., Johlander, B., Jouret, M., Journoud, P., Karioty, F., Kerjean, L., Lafaille, V., Lafond, L., Lam-Trong, T., Landiech, P., Lapeyrere, V., Larqué, T., Laudet, P., Lautier, N., Lecann, H., Lefevre, L., Leruyet, B., Levacher, P., Magnan, A., Mazy, E., Mertens, F., Mesnager, J.-M., Meunier, J.-C., Michel, J.-P., Monjoin, W., Naudet, D., Nguyen- Kim, K., Orcesi, J.-L., Ottacher, H., Perez, R., Peter, G., Plasson, P., Plesseria, J.-Y.,Pontet, B., Pradines, A., Quentin, C., Reynaud, J.-L., Rolland, G., Rollenhagen, F., Romagnan, R., Russ, N., Schmidt, R., Schwartz, N., Sebbag, I., Sedes, G., Smit, H., Steller, M.B., Sunter, W., Surace, C., Tello, M., Tiphène, D., Toulouse, P., Ulmer, B., Vandermarcq, O., Vergnault, E., Vuillemin, A., Zanatta, P., 2009. Transiting exoplanets from the CoRoT space mission - VIII. CoRoT-7b: the first super-Earth with measured radius. Astron. Astrophys. 506, 287–302. https://doi.org/10.1051/0004-6361/200911933

Levin EM., Robbins C.R. and Mc Murdie H.F. (1964) Phase diagram for ceramist, 2nd ed Amer Ceram Soc. Columbus, Ohio 601pp.

Losq C. and Neuville D.R. (2013) Effect of K/Na mixing on the structure and rheology of tectosilicate silica-rich melts. Chemical Geology, 346, 57-71.

Le Losq Ch., Neuville D.R., Florian P., G.S. Henderson and Massiot D. (2014) Role of Al3+ on rheology and nano-structural changes of sodium silicate and aluminosilicate glasses and melts. Geochimica Cosmochimica Acta, 126, 495-517.

Le Losq C, Neuville D.R., Florian P., Massiot D., Zhou Z., Chen W., Greaves N. (2017) Percolation channels: a universal idea to describe the atomic structure of glasses and melts. Scientific Reports, 7, Article number: 16490, doi:10.1038/s41598-017-16741-3

Le Losq Ch., Neuville D.R. (2017) Molecular structure, configurational entropy and viscosity of silicate melts: link through the Adam and Gibbs theory of viscous flow. Journal of Non-Crystalline Solids. 463, 175-188.

Le Losq C., Cicconi M.R., Greaves G.N. and Neuville D.R. (2019) Silicate glasses. Springer Hanbook of Glass. 441-488 – DOI 10.1007/978-3-319-93728-1

Le Losq C., Valentine A., Mysen B.O., Neuville D.R. (2021) Deep learning model to predict the structure and properties of aluminosilicate glasses and melts. Geochimica and Cosmochimica Acta. DOI: https://doi.org/10.1016/j.gca.2021.08.023

de Ligny and Westrum E.F. (1996) Entropy of calcium and magnesium aluminosilicate glasses. Chemical Geology 128 113-128

Licheron M., Montouillout V., Millot F., Neuville D.R. (2011) Raman and 27Al NMR structure investigations of aluminate glasses: (1-x)Al2O3- x MO, with M=Ca, Sr, Ba and 0.5<x<0.75). Journal of Non Crystalline Solids. 257, 2796-2801.

Lines, M. E., MacChesney, J. B., Lyons, K. B., Bruce, A. J., Miller, A. E., Nassau K., 1989. Calcium aluminate glasses as pontential ultralow-loss optical materials at 1.5–1.9 □m. J. Non-Cryst. Solids 107, 251-260.

Lockyer M.W.G., Holland D. and Dupree R., 1995. NMR investigation of the structure of some bioactive and related glasses. J. Non-Crystal. Sol. 188, 207-219.

Loewenstein, W., 1954. The distribution of aluminum in the tetrahedra of silicates and aluminates. Am. Mineral. 39, 92-96.

Macedo P.B and Litovitz P.B. (1965), On the relative roles of free volume and activation energy in the viscosity of liquids. J. Chem. Phys. 42, 24. https://doi.org/10.1063/1.1695683

McMillan, P., Piriou, B., 1983. Raman spectroscopy of calcium aluminate glasses and crystals. J. Non-Cryst. Solids 55, 221-242.

McMillan, P.F. and Kirkpatrick, R.J. (1992) Al coordination in magnesium aluminosilicate glasses. American Mineralogist 77, 898-900.

McMillan, P., Piriou, B., and Navrotsky, A. (1982) A Raman spectroscopic study of glasses along the joins silica-calcium aluminate, silica-sodium aluminate, and silica-potassium aluminate. Geochimica

and Cosmochimica Acta, 46, 2021-2037.
McMillan P. F. (1984) Structural studies of silicate glasses and melts - Applications and limitations of Raman spectroscopy. Am. Mineral. 69, 622–644.
Maekawa H., Maekawa T., Kawamura K. and Yokokawa T., 1991. The structural group of alkali silicate glasses determined from 29Si MAS-NMR. J. Non-Cryst. Solids 127, 53-64.
Magnien V., Neuville D.R., Cormier L., Mysen B.O. and Richet P. (2004) Kinetics of iron oxidation in silicate melts: A preliminary XANES study. Chem. Geol., 213, 253-263.
Magnien V, Neuville D.R., Cormier L., Roux J., Hazemann J-L., de Ligny D., Pascarelli S., Vickridge I., Pinet O. and Richet P. (2008) Kinetics and mechanisms of iron redox reactions in silicate melts: The effects of temperature and alkali cations. Geochim. Cosmochim. Acta., 72, 2157-2168.
Malfait W. J. (2009) Quantitative Raman spectroscopy: speciation of cesium silicate glasses. J. Raman Spectrosc. 40, 1895–1901.
Malfait W. J., Zakaznova-Herzog V. P. and Halter W. E. (2007) Quantitative Raman spectroscopy: high-temperature speciation of potassium silicate melts. J. Non-Cryst. Solids 353, 4029–4042.
Massiot D., Fayon F., Montouillout V., Pellerin N., Hiet J., Roiland C., Florian P., Coutures J-P. , Cormier L. and Neuville D.R. (2008) Structure and dynamics of oxide melts and glasses: a view from multinuclear and high temperature NMR. J. Non-Crystal Solids. 354, 249-254.
Mastelaro V, Zanotto E., Lequeux N., Cortes R. (2000) Relationship between short-range order and ease of nucleation in Na2Ca2Si3O9, CaSiO3 and PbSiO3 glasses. Journal of Non-Crystalline Solids 262, 191-199
Mauro J. (2011) Through a Glass, Darkly: Dispelling Three Common Misconceptions in Glass Science. International Journal of Applied Glass Science 2 [4] 245–261
Mauro J. , Y. Yue, A.J. Ellison, P.K. Gupta, D.C. Allan, (2009) Viscosity of glass-forming liquids, Proc. Natl. Acad. Sci. 106 (2009) 19780–19784.
Méducin F., Redfern S.A.T., Le Godec Y., Stone H.J., Tucker M.G., Dove M.T. and Marshall W.G. (2004) Study of cation order-disorder in MgAl2O4 spinel by in situ neutron diffraction up to 1600K and 3.2GPa. Americ Mineral., 89, 981-986.
Meiling G.S. and Uhlmann D.R., 1977. Crystallisation and melting kinetics of soda disilicate. Phys. Chem. Glas. 8, 62-68.
Merzbacher, C.I., Sheriff, B.L., Hartman, J.S., White, W.B., 1990. A high-resolution 29Si and 27Al NMR study of alkaline-earth aluminosilicate glasses. J. Non-Cryst. Solids 124, 194-206.
Merzbacher, C.I., McGrath, K.J., Highby, P.L., 1991. 29Si NMR and infrared reflectance spectroscopy of low-silica calcium aluminosilicate glasses. J. Non-Cryst. Solids 136, 249-259.
Merzbacher C. I. and White W. B. (1991) The structure of alkaline-earth aluminosilicate glasses as

318 determined by vibrational spectroscopy. J. Non-Cryst. Solids 130, 18–34.
319 Moore and Carey (1951) Limiting Compositions of Binary Glasses of the Type xR2O· SiO2 and of
320 Ternary Glasses of Types yR2O· yR2O3· SiO2 in Relation to Glass Structure. Trans. Soc. Glass
321 Technol.,
322 Morey G. W. and Bowen N.L.,1925. The melting relations of the soda-lime-silica glasses. J. Soc. Glass.
323 Tech. 9, 226-264.
324 Moretti R. (2005). Polymerisation, basicity, oxidation state and their role in ionic modelling of silicate
325 melts. Annals of Geophysics, 48, 4/5, 583-608.
326 Morey G. (1930) The devitrification of soda-lime-silica glasses. Journal of the American Ceramic
327 Society. 683-714.
328 Morikawa, H., Takagi, Y., Ohno, H., 1982. Structural analysis of 2PbO·SiO2 glass. J. Non-Cryst. Solids
329 53, 173–182.
330 Mossa S., La Nave E., Stanley H. E., Donati C., Sciortino F. and Tartaglia P. (2002) Dynamics and
331 Configurational Entropy in the LW Model for Supercooled Orthoterphenyl. Condensed Matter.
332 arXiv:cond-mat/0111519v2
333 Moulton B. and Henderson G.S. (2021) Glasses: Alkali and Alkaline-Earth Silicates.ed Encyclopedia of
334 Materials: Technical Ceramics and Glasses, vol. 2, pp. 462–482. Oxford: Elsevier.
335 http://dx.doi.org/10.1016/B978-0-12-818542-1.00050-3.
336 Moynihan C.T. Easteal A.J. Wilder J. (1974) Dependence of the glass transition temperature on heating
337 and cooling rate. The Journal of Physical Chemistry. 78, 2873-2879.
338 Moynihan C.T., Sasabe J. Tucker (1976) Kinetics of the Glass Transition in a Calcium-Potassium Nitrate
339 Melt. Proceedings of The Electrochemical Society, 6, 182-194
340 Moynihan C.T., Gupta P.K. (1978) The order parameter model for structural relaxation in glass. J. Non-
341 Cryst. Solids., 29, 143
342 Moynihan C.T., Easteal A.J., Tran D.C., Wilder J.A. and Donovan E.P. (1976a) Heat capacity and
343 structural relaxation of mixed-alkali glasses. J. Phys. Chem., 78, 2673
344 Moynihan C.T., Macedo P.B., Montrose C.J., Gupta P.K., De Bolt M.A., Dill J.F., Dom B.E., Drake
345 P.W., Easteal A.J., Elterman P.B., Moeller R.P., Sasabe M. and Wilder J.A. (1976b) Structural
346 relaxation in vitreous materials. Ann. New-York Acad. Sci., 279, 15
347 Musgraves J.D., J. Hu, L. Calvez (Eds.), Springer Handbook of Glass, Springer Handbooks,
348 https://doi.org/10.1007/978-3-319-93728-1_1
349 Murdoch, J.B., Stebbins, J.F., and Carmichael, I.S.E. (1985) High-resolution 29Si NMR study of silicate
350 and aluminosilicate glasses: the effect of network modifying cations. American Mineralogist, 70, 332-
351 343.

352 Mysen B.O. (1990) Role of Al in depolymerized, peralkaline aluminosilicate melts in the systems Li_2O-
353 Al_2O_3-SiO_2, Na_2O-Al_2O_3-SiO_2, and K_2O-Al_2O_3-SiO_2, Am. Mineral. 75,120–134.
354 Mysen, B.O. (1999). Structure and properties of magmatic liquids: From haplobasalt to haploandesite.
355 Geochimica and Cosmochimica Acta 63: 95-112.
356 Mysen B. O. (1995) Experimental, in situ, high-temperature studies of properties and structure of silicate
357 melts relevant to magmatic processes. Eur. J. Mineral. 7, 745–766.
358 Mysen B. O. (1990) Role of Al in depolymerized, peralkaline aluminosilicate melts in the systems Li_2O-
359 Al_2O_3-SiO_2, Na_2O-Al_2O_3-SiO_2, and K_2O-Al_2O_3-SiO_2. Am. Mineral. 75, 120–134.
360 Mysen B.O. J.D. Frantz (1993) Structure of silicatemelts at high temperature: in-situ measurements in
361 the system BaO-SiO2, Am. Mineral. 78, 699–709.
362 Mysen, B.O. J.D. Frantz, Structure of haplobasaltic liquids at magmatic temperatures: in situ, high-
363 temperature study ofmelts on the join Na2Si2O5-Na2(NaAl)2O5, Geochim. Cosmochim. Acta 58
364 (1994) 1711–1733.
365 Mysen B. O., Lucier A. and Cody G. D. (2003) The structural behavior of Al3+ in peralkaline melts and
366 glasses in the system Na_2O-Al_2O_3-SiO_2. Am. Mineral. 88, 1668–1678.
367 Mysen B. O., Virgo D. and Seifert F. A. (1982) The structure of silicate melts: Implications for chemical
368 and physical properties of natural magma. Rev. Geophys. 20, 353–383.
369 Mysen, B.O., Virgo, D., and Kushiro, I. (1981) The structural role of aluminum in silicate melts -A
370 Raman spectroscopic study at 1 atmosphere. American Mineralogist, 66, 678-701.
371 Nakamura K., Takahashi Y., Osada M. and Fujiwara T. (2013) Low-frequency Raman scattering in
372 binary silicate glass: Boson peak frequency and its general expression. J. Ceram. Soc. Japan 121,
373 1012–1014.
374 Napolitano A.n Macedo P.B. and Hawkins E.G. (1965). Viscosity and Density of Boron Trioxide. Journal
375 of the American Ceramic Society. https://doi.org/10.1111/j.1151-2916.1965.tb14690.x
376 Navrotsky, A., Perandeau, P., McMillan, P.F., and Coutures, J.P. (1982) A thermochemical study of
377 glasses and crystals along the joins silica-calcium aluminate and silica-sodium aluminate. Geochimica
378 and Cosmochimica Acta, 46, 2039-2049.
379 Navrotsky A., Geisinger K., P., Gibbs G.V. (1985) The tetrahedral framework in glasses and melts —
380 inferences from molecular orbital calculations and implications for structure, thermodynamics, and
381 physical properties. Physics and Chemistry of Minerals volume 11, pages284–298
382 Natrup F.V., Bracht H, Murugavel S. and Roling B. (2005) Cation diffusion and ionic conductivity in
383 soda-lime silicate glasses. Phys. Chem. Chem. Phys . 7 , 2 2 7 9 – 2 2 8 6
384 Nernst W. (1911) Theoretical Chemistry," London, 810p.
385 Nesbitt H.W, O'Shaughnessy C., Bancroft G.M., Henderson G.S., and Neuville D.R. (2018) Factors

affecting line shapes and intensities of Q3 and Q4 Raman bands of Cs silicate glasses. Chemical Geology. 10.1016/j.chemgeo.2018.12.009

Nesbitt, H.W., Henderson, G.S., Bancroft, G.M., Neuville D.R., (2021) Spectral resolution and Raman Q and Q cross sections. Chemical Geology. DOI : 10.1016/j.chemgeo.2020.120040

Neuville D.R. (1992) Etude des Propriétés Thermodynamiques et Rhéologiques des Silicates Fondus. Thèse de l'Université de Paris VII, spécialité Géochimie Fondamentale.

Neuville D.R., (2005) Structure and properties in (Sr, Na) silicate glasses and melts. Phys Chem Glasses, 46, 112-119.

Neuville D.R. (2006) Viscosity, structure and mixing in (Ca, Na) silicate melts. Chem. Geol., 229, 28-42. Neuville D.R. et Richet P. (1990) Viscosité et entropie des silicates fondus. Rivista del la Staz. Sper. Vetro, 6, 213-221.

Neuville D.R. and Richet P. (1991) Viscosity and mixing in molten (Ca,Mg) pyroxenes and garnets. Geochim. Cosmochim. Acta., 55, 1011-1021.

Neuville D.R. and Mysen B.O (1996) Role of aluminiun in the silicate network: in situ, high-temperature study of glasses and melts on the join SiO2-NaAlO2. Geochimica Cosmochimica Acta., 60, 1727-1737.

Neuville D.R., Cormier L, R., Flank A.M., Prado R.J. and Lagarde P. (2004) Na K-edge XANES spectra of minerals and glasses. Eur. J Mineral, 16, 809-816.

Neuville D.R., Cormier L, Flank A.M. and Lagarde P. Massiot D. (2004) Aluminum X-ray absorption near edges structure in minerals and glasses. Chem Geol., 213, 153-163.

Neuville D.R., Cormier L. and Massiot D. (2004) Role of aluminium in peraluminous region in the CAS system. Geochim. Cosmochim. Acta., 68, 5071-5079.

Neuville D.R., Cormier L, Flank A.M, Lagarde P. (2005) A XANES study at the Na and Al K-edge of soda-lime aluminosilicate glasses. Phys. Scripta., 115, 316-318.

Neuville D.R., Cormier L., Massiot D. (2006) Al speciation in calcium aluminosilicate glasses: A NMR and Raman spectrocospie. Chem Geol., 229, 173-185

Neuville D.R., Courtial P., Dingwell D.B. and Richet P. (1993) Thermodynamic and rheological properties of rhyolite and andesite melts.Contrib. Mineral. Petrol., 113, 571-581.

Neuville D.R. Cormier L., Montouillout V., Massiot D. (2007) Local environment of Al in aluminosilicate glasses: a NMR point of view. J. Non Crystal Solid, 353, 180-185.

Neuville D.R., Cormier L., Montouillout V., Florian P., Millot F., Rifflet J.C. and Massiot D. (2008a) Structure of Mg- and Mg/Ca aluminosilicate glasses: 27Al NMR and Raman spectroscopy investigations. American Mineralogist 83, 1721-1731.

Neuville D.R. Cormier L., Flank AM, de Ligny D., Roux J. and Lagarde P. (2008b) Environment around

Al, Si and Ca in aluminate and aluminosilicate melts by X-ray absorption spectroscopy at high temperature. American Mineralogist, 93, 228-234.

Neuville D.R., de Ligny D., Cormier L., Henderson G.S., Roux J., Flank AM, and Lagarde P. (2009) The crystal and melt structure of spinel and alumina at high temperature: an in-situ XANES study at the Al and Mg K-edge. Geochimica Cosmochimica Acta, 73, 3410-3422.

Neuville D.R., Henderson G.S., Cormier L., Massiot D. (2010) Structure of CaO-Al2O3 crystal, glasses and liquids, using X-ray absorption at Al L and K edges and NMR spectroscopy. American Mineralogist, 95, 1580-1589.

Neuville D.R., Henderson G.S and de Ligny D. (2014) Advances in Raman Spectroscopy Applied to Earth and Material Sciences. In Henderson G.S, Neuville D.R., Down B. (2014) "Spectroscopic methods in Mineralogy and Material Sciences" Review in Mineralogy and Geochemistry, Vol 78, 509-541.

Neuville D.R., Hennet L., Florian P., de Ligny D. (2014) In situ high temperature experiment. In Henderson G.S, Neuville D.R., Down B. (2014) "Spectroscopic methods in Mineralogy and Material Sciences" Review in Mineralogy and Geochemistry, Vol 78, 779-800.

Novikov A., Neuville D.R., Hennet L., Thiaudière D., Gueguen Y., Florian P. (2017) Al and Sr environment in tectosilicate glasses and melts: viscosity, Raman and NMR investigation. Chemical Geology, 461, 115-127.

Alexey Novikov (2017) Structure et propriétés des aluminosilicates de Sr, Ba et Zn, Université d'Orléans

Ohtani E., Taulelle F., Angell C.A. (1985) Al3+ coordination changes in aluminosilicates under pressure. Nature, 314, 78-82.

O'Shaughnessy C., Henderson G.S., Nesbitt H.W., Bancroft G.M., Neuville D.R. (2017) The structure of caesium silicate glasses and melts: implications for the interpretation of Raman spectra. Chemical Geology, 461, 82-95.

O'Shaughnessy C., Henderson G. S., Nesbitt H.W, Bancroft G.M., Neuville D.R. (2020) The behaviour of modifier cations in alkali silicate glasses. Journal of the American Ceramic Society. DOI: 10.1111/jace.17081

Parks G.S. and Huffman H.M. (1926) Glass as a fourth state of matter. Science, 64, 364 (1926).

Parks G.S. and Huffman H.M. (1927) Studies on glass. I. The transition between the glassy and liquid states in the case of some simple organic compound. J. Phys. Chem., 31, 1842

Pena R.B., Sampaio D.V., Lancelotti R.F., Cunha T.R., Zanotto E.D., Pizani P.S. (2020) In-situ Raman spectroscopy unveils metastable crystallization in lead metasilicate glass. Journal of Non-Crystalline Solids. Volume 546, 120254

Persikov E. S. (1991) The viscosity of magmatic liquids : experiment, generalized patterns. A model for

454 calculation and prediction. Applications. Adv. Phys. Geochem. 9, 1–40.
455 Petit A. T. and Dulong P. L. (1819) Recherches sur quelques points importants de la théorie de la chaleur,
456 dans Annales de chimie et de physique,10, 395–413
457 Poe B.T., Romano C., Zotov N.,Cinin G., Marcelli A. (2001) Compression mechanism in aluminosilicate
458 melts : Raman and XANES stpectrocopy of glasses quenched from pressures up to 10Gpa. Chem
459 Geol., 174, 21-31.
460 Poe, B.T., McMillan, P.F., Angell, C.A., and Sato, R.K. (1992) Al and Si coordination in SiO2-Al2O3
461 glasses and liquids: a study by NMR and IR spectroscopy and MD simulations. Chemical Geology,
462 96, 333-349.
463 Poole J.P., 1948. Viscosité à basse température des verres alcalino-silicatés. Verres Réfrac. 2, 222-230.
464 Popov A.I. (2018) What is glass? Journ. Non-Cryst. Solids **502**, 249–250.
465 Poulain M. and Lucas J. (1970) NEW TRANSITION METAL FLUOROZIRCONATES. Comptes
466 Rendus de Seances de l'Academie des Sciences. 281, 2345-2349.
467 Poulain M. (1983) Halide glasses. Journal of Non-Crystalline Solids, 56, 1-14
468 Putnis, A. (1992) An introduction to mineral sciences. Cambridge press, ISBN 0521 419220
469 Rankin G. A., (1915) The ternary system CaO-Al2O3-SiO2. Amer. J. Sci., 39, 1-79.
470 Rekhson S.M. (1989) Computer modeling of glass behavior. Congress on glass in Leningrad, U.S.S.R.
471 Rekhson S.M. (1975) Relaxation of Glass, Sov. J. Glass Phys. Chem., 1 (1975) 417.
472 Rekhson S.L. (1980) Viscosity and stress relaxation in commercial glasses in the glass transition region.
473 Journal of Non-Crystalline Solids, 38-39; 457-462
474 Richet P. (1984) Viscosity and configurational entropy of silicate melts. Geochim. Cosmochim. Acta 48,
475 471–483.
476 Richet, P. and Bottinga, Y. (1985) Heat capacity of aluminum-free liquid silicates. Geochimica et
477 Cosmochimica Acta, 49, 471–486.
478 Richet P. (1987) Heat capacity of silicate glasses. Chem. Geol. 62, 111–124.
479 Richet P. (2009) Residual and configurational entropy: Quantitative checks through applications of
480 Adam-Gibbs theory to the viscosity of silicate melts. *Journal of Non-Crystalline Solids* **355**, 628–635.
481 Richet P. and Bottinga Y. (1984) Glass transitions and thermodynamic properties of amorphous SiO2,
482 NaAlSinO2n+2 and KAlSi3O8. Geochim. Cosmochim. Acta 48, 453–470.
483 Richet P. and Neuville D.R. (1992) Thermodynamics of silicates melts: Configurational properties. Adv.
484 Phys. Geochim., 10, 132-161. https://doi.org/10.1007/978-1-4612-2842-4_5
485 Richet P., Robie R. A. and Hemingway B. S. (1986) Lowtemperature heat capacity of diopside glass
486 (CaMgSi2O6): a calorimetric test of the configurational entropy theory applied to the viscosity of
487 liquid silicates. Geochim. Cosmochim. Acta 50, 1521–1533.

Richet P., Nidaira A., Neuville D.R. and Atake T. (2009a) Aluminum speciation, vibrational entropy and short-range order in calcium aluminosilicate glasses Geochimica Cosmochimica Acta, 73, 3894-3904.

Richet P., Nidaira A., Neuville D.R., Atake T. (2009b) Low-temperature heat capacity and short-range order in alkaline-earth metasilicates. American Mineralogist, 94, 1591-1596.

Riebling E. F. (1966) Structure of sodium aluminosilicate melts containing at least 50 mol% SiO2 at 1500°C. J. Chem. Phys. 44, 2857–2865.

Risbud, S.H., Kirkpatrick, R.J., Taglialavore, A.P., Montez, B. (1987) Solid-sate NMR evidence of 4-, 5- and 6-fold aluminum site in roller-quenched SiO2-Al2O3 glasses. Journal of the American Ceramics Society, 70, C10-C12.

Ritland H.N. (1954) Density phenomena in the transformation range of a borosilicate crown glass. J. Am. Ceram. Soc., 37, 370

Robert G., Smith R. A. and Whittington A. G. (2019) Viscosity of melts in the NaAlSiO4-KAlSiO4-SiO2 system: Configurational entropy modelling. J. Non-Cryst. Solids 524, 119635.

Rosenhauer M., Scarfe C.M. and Virgo D. (1979) Pressure dependence of the glass transition temperature in glasses of diopside, albite, and sodium trisilicate composition. Carnegie Inst. Wash. Yearb., 78, 547

Robie R.A, Hemingway B.S. and Fisher J.R. (1979) Thermodynamic Properties of Mineral and related substance ar 298,15K and 1 bar Pressure and at higher temperature. USGS Bulletin 1432.

Roling, B., Ingram, M.D., 2000. Mixed alkaline-earth effects in ion conducting glasses. J. Non-Cryst. Solids 265, 113–119.

Roy, B.N. and Navrostsky, A. (1984) Thermochemistry of charge-coupled subsitution in silicate glasses: the system M1/nn+AlO2-SiO2 (M=Li, Na, K, Rb, Cs, Mg, Ca, Sr, Ba, Pb) Journal of the American Ceramic Society, 67, 606-610.

Russell, J.K. D. Giordano, (2005) A model for silicate melt viscosity in the system CaMgSi2O6-CaAl2Si2O8-NaAlSi3O8, Geochim. Cosmochim. Acta 69 5333–5349, http://dx.doi.org/10.1016/j.gca.2005.06.019.

Russell J. K. and Giordano D. (2017) Modelling configurational entropy of silicate melts. Chem. Geol. 461, 140–151.

Ryan M. and Blevins S., 1987. Viscosity of silicate melts and glasses. U.S.G.S. 1764. 1080pp

Sampaio D.V., Picinin A., Moulton B.J., Rino J.P., Pizani P.S., Zanotto E.D. (2018) Raman scattering and molecular dynamics investigation of lead metasilicate glass and supercooled liquid structures. Journal of Non-Crystalline Solids 499, 300–308

Sato, R. K., McMillan, P. F., Dennison, P., Dupree, R., 1991. High-resolution 27Al and 29Si MAS NMR investigation of SiO_2-Al_2O_3 glasses. J. Phys. Chem. 95, 4483-4489.

Schreiber, H.D. (1986) REDOX PROCESSES IN GLASS-FORMING MELTS. Journal of Non-Crystalline Solids 84, 129-141

Schmelzer J. and Tropin T. (2018) Glass Transition, Crystallization of Glass-Forming Melts, and Entropy. Entropy 20, 103.

Schmelzer J.W.P., Abyzov A.S and Fokin W.M. (2016) Thermodynamic Aspects of Pressure-Induced Crystallization: Kauzmann Pressure International Journal of Applied Glass Science, 7, 474-486.

Sakamaki and Ohtani (2021) High pressure melts. Review in Mineralogy and Geochemistry. (this issues)

Sasabe H., De Bolt M.A., Macedo P.B., Moynihan C.T. (1977) Structural relaxation in an alkali-lime-silicate glass. Proc. XIth International Congress on Glass, 1, 339

Sharma S.K., Virgo D. and Mysen B.O. (1978) Structural of glasses and melts of Na2O.xSiO2 (x = 1,2,3) composition from Raman spectroscopy. Carnegie Inst. Wash. Yearb., 77, 649

Sharma S.K., J.A. Philpotts, D.W. Matson (1985) Ring distributions in alkali- and alkaline-earth aluminosilicate framework glasses – A Raman spectroscopic study, J. Non-Cryst. Solids 71, 403–410

Shaw, H.R. (1972) Viscosities of magmatic silicate liquids: an empirical method of prediction, Am. J. Sci. 272 870–893.

Shi C., Alderman O., Berman D., Du J., Neuefeind J., Tamalonis A., Weber R., You J., Benmore C. (2019) The structure of amorphous and deeply supercooled liquid alumina. Front. Mater., 19 March 2019 | https://doi.org/10.3389/fmats.2019.00038

Schneider, V.R. Mastelaro, E.D. Zanotto, B.A. Shakhmatkin, N.M. Vedishcheva, A.C. Wright, H. Panepucci: (2003) Qn distribution in stoichiometric silicate glasses: thermodynamic calculations and 29Si high resolution NMR measurements, J. Non- Cryst. Solids 325, 164–178

Schuller S. (2017) Phase separation processes in glass in Neuville et al., 2017 EDP Sciences. 665pp. ISBN 978-2-7598-1783-2

Shevyakov A.M., Trofinenko A.V., Sizonznko A.P., Burkov V.P. and Zhuravlev G.I. (1978) Study of the structure and crystallisation of melts of the system Li2O-SiO2 by high temperature infrared spectroscopy. Zh. Priklad. Khim., 51, 2612

Schairer J. F. and Bowen N. L. (1956) The system Na_2O-Al_2O_3-SiO_2. Am. J. Sci. 254, 129–195.

Scherer G. W. (1984) Use of the Adam-Gibbs Equation in the Analysis of Structural Relaxation. J. Am. Ceram. Soc. 67, 504–511.

Seifert, F. A., Mysen, B. O., & Virgo, D. (1982). Three-dimensional network structure in the systems SiO2-NaAlO2, SiO2-CaAl2O2 and SiO2-MgAl2O2. Amer. Mineral., 67, 696-711.

Sen S., George A.M., Stebbins J.F. (1996) Ionic conduction and mixed cation effect in silicate glasses and liquids: 23Na and 7Li NMR spin-lattice relaxation and a multiple-barrier model of percolation. Journal of non-crystalline solids, 197, 53-59.

Sen S., R.E. Youngman, (2003) NMR study of Q-speciation and connectivity in K2O–SiO2 glasses with high silica content. Journal of Non-Crystalline Solids, 331, 100–107, http://dx.doi.org/10.1016/j.jnoncrysol.2003.08.071.

Sen S., Maekawa H. and G. Papatheodorou. (2009) Short-Range Structure of Invert Glasses along the Pseudo-Binary Join MgSiO3−Mg2SiO4: Results from 29Si and 25Mg MAS NMR Spectroscopy. J. Phys. Chem. B 2009, 113, 46,

Shan Z., Liu S., Tao H. and Yue Y. (2018) Mixed alkaline-earth effects on several mechanical and thermophysical properties of aluminate glasses and melts. Journal of the American Ceramic Society. 102, 1128–1136. DOI: 10.1111/jace.15975.

Shimoda, K., Tobu, Y., Shimoikeda, Y., Nemoto, T., and Saito K. (2007a) Multiple Ca2+ environments in silicate glasses by high-resolution 43Ca MQMAS NMR technique at high and ultra-high (21.8 T) magnetic fields. Journal of Magnetic Resonance, 186, 114–117.

Shimoda, K., Tobu, Y., Hatakeyma, M., Nemoto, T., and Saito K. (2007b) Structural investigation of Mg local environments in silicate glasses by ultra-high field 25Mg 3QMAS NMR spectroscopy. American Mineralogist, 92, 695-698.

Schirmacher W. and Ruocco G. (2020) Heterogeneous Elasticity: The tale of the boson peak. Condensed Matter. arXiv:2009.05970

Schirmacher W., Ruocco G. Mazzone V. (2015) Heterogeneous viscoelasticity: a combined theory of dynamic and elastic heterogeneity. Phys. Rev. Lett. 115, 015901

Simmons J.H., S.A. Mills and A. Napolitano, (1974) Viscous flow in glass during phase separation J. Am. Ceram. Soc. 57 109.

Simmons J.H., A. Napolitano and P.B. Macedo, (1970) Supercritical viscosity anomaly in oxide mixtures J. Chem. Phys. 53 1170.

Sipp A., Neuville D.R. and Richet P. (1997) Viscosity and configurational entropy of borosilicate melts. J. Non-Crystal. Solids., 211, 281-293.

Sossman, (1933) The “Physical Chemistry” of a System of Refractory Components. Journal of the American Ceramic Society. https://doi.org/10.1111/j.1151-2916.1933.tb17098.x

Sreenivasan H. Kinnunen P., Adesanya E., Patanen M., Kantola A., (2020) Field Strength of Network-Modifying Cation Dictates the Structure of (Na-Mg) Aluminosilicate Glasses. Frontier in Material. doi: 10.3389/fmats.2020.00267

Starodub K., Wu G., Yazhenskikh E., Müller M., Khvan A. and Kondratiev A. (2019) An Avramov-based viscosity model for the SiO2-Al2O3-Na2O-K2O system in a wide temperature range. Ceram. Int. 45, 12169–12181.

Stebbins, J. F., 1991. NMR evidence for five-coordinated silicon in silicate glass at atmospheric pressure. Nature 351, 638-639.

Stebbins, J.F. and Farnan, I. (1992) Effects of high temperature on silicate liquid structure: a multinuclear NMR study. Science, 255, 586-589.

592 Stebbins J.F., I. Farnan, X. Xue, (1992) The structure and dynamics of alkali silicate liquids: a view from
593 NMR spectroscopy, Chem. Geol. 96, 371–385, http://dx.doi.org/10.1016/0009-2541(92)90066-E.
594 Stebbins J. F., Carmichael I. S. E. and Moret L. K. (1984) Heat capacities and entropies of silicate liquids
595 and glasses. Contrib. Mineral. Petrol. 86, 131–148.
596 Stebbins J. F., Dubinsky E. V., Kanehashi K. and Kelsey K. E. (2008) Temperature effects on non-
597 bridging oxygen and aluminum coordination number in calcium aluminosilicate glasses and melts.
598 Geochim. Cosmochim. Acta 72, 910–925.
599 Stebbins J. F., Kroeker S., Lee S. K. and Kiczenski T. J. (2000) Quantification of five- and six-
600 coordinated aluminum ions in aluminosilicate and fluoride-containing glasses by high-field, high-
601 resolution 27Al NMR. J. Non-Cryst. Solids 275, 1–6.
602 Stebbins J. F., Lee S. K. and Oglesby J. V. (1999) Al-O-Al oxygen sites in crystalline aluminates and
603 aluminosilicate glasses; high-resolution oxygen-17 NMR results. Am. Mineral. 84, 983–986.
604 Stebbins J. F. and Xu Z. (1997) NMR evidence for excess non-bridging oxygen in an aluminosilicate
605 glass. Nature 390, 60–62.
606 Stebbins J.F. (2008) Temperature effects on the network structure of oxide melts and their consequences
607 for configurational heat capacity. Chemical Geology 256, 80–91
608 Strukelj, E. (2008) Propriété des verres d'aluminosilicate de lithium. M2, Université Paris 6
609 Sugawara T. Seto M., Kato M., Yoshida S., Matsuoka J., Miura Y. (2013) Na_2O activity and
610 thermodynamic mixing properties of SiO_2–Na_2O–CaO melt. Journal of Non-Crystalline Solids 371–
611 372 (2013) 58–65
612 Suzuki A., Ohtani E., Funakoshi K., Terasuki H., Kubo T. (2002) Viscosity of albite melt at High-
613 pressure and High-temperature. Phys. Chem. Mineral., 29, 159-165.
614 Takahashi S., Neuville D.R., Takebe H. (2015) Thermal Properties, Density and Structure of Percalcic
615 and Peraluminus CaO–Al2O3–SiO2 Glasses. Journal of Non-Crystalline Solids. 411, 5-12.
616 Tamman, G. 1925. States of Aggregation, Edited by: Mehl, R. New York: Van Nostrand.
617 Tammann G., and Hesse W. (1926) Die Abhängigkeit der Viskosität von der Temperatur bei unterkühlten
618 Flüssigkeiten. Z. Anorg. Allg. Chem., 156, 245
619 Tangemann, J and R.A. Lange, The effect of Al3+, Fe3+, and Ti4+ on the configurational heat capacities
620 of sodium silicate liquids, Phys. Chem. Miner. 26 (1998) 83–99.
621 Taylor T. D. and Rindone G. E. (1970) Properties of Soda Aluminosilicate Glasses: V, Low-Temperature
622 Viscosities. J. Am. Ceram. Soc. 53, 692–695.
623 Téqui C., Robie R.A., Hemingway B.S., Neuville D.R. and Richet P. (1991) Melting and thermodynamic
624 properties of pyrope (Mg3Al2Si3O12). Geochim. Cosmochim. Acta., 55, 1005-1011.
625 Thompson L. M. and Stebbins J. F. (2011) Non-bridging oxygen and high-coordinated aluminum in

626 metaluminous and peraluminous calcium and potassium aluminosilicate glasses: High-resolution 17O
627 and 27Al MAS NMR results. Am. Mineral. 96, 841–853.
628 Thompson L. M. and Stebbins J. F. (2012) Non-stoichiometric non-bridging oxygens and five-
629 coordinated aluminum in alkaline-earth aluminosilicate glasses: Effect of modifier cation size. J. Non-
630 Cryst. Solids 358, 1783–1789.
631 Thompson L. M. and Stebbins J. F. (2013) Interaction between composition and temperature effects on
632 non-bridging oxygen and high-coordinated aluminum in calcium aluminosilicate glasses. Am.
633 Mineral. 98, 1980–1987.
634 Tomozawa M. (1978) "Compositional changes as evidence for spinodal decomposition in glass." J. Am.
635 Ceram. Soc., 61, 444-447.
636 Tomozawa M. (1999) "A source of the immiscibility controversy of borate and borosilicate glass
637 systems." J. Am. Ceram. Soc., 82, 206-209.
638 Toplis M. and Dingwell D.B., (2004) Shear viscosities of CaO-Al2O3-SiO2 and MgO-Al2O3-
639 SiO2 liquids: Implications for the structural role of aluminium and the degree of polymerisation of
640 synthetic and natural aluminosilicate melts. Geochimica et Cosmochimica Acta, 68, 5169-5188
641 Tool A.Q., and Eichlin C.G. (1931) Variations caused in the heating curves of glass by heat treatment. J.
642 Amer. Ceram. Soc., 14, 276
643 Trcera N., Cabaret D., Rossano S., Farges F., Flank A-M, Lagarde P. (2009) Experimental and theoretical
644 study of the structural environment of magnesium in minerals and silicate glasses using X-ray
645 absorption near-edge structure. Phys Chem Minerals 36:241–257
646 Urbain G. (1972) Etude expérimentale de la viscosité de silicoalumineux liquides et essai d'interprétation
647 structurale. Thèse de Doctorat d'Etat es Sciences Physiques, Université Paris VI.
648 Urbain, G., Y. Bottinga, P. Richet, Viscosity of liquid silica, silicates and alumino-silicates, Geochim.
649 Cosmochim. Acta 46 (1982) 1061–1072.
650 Urbain, G. (1983) Viscosités de liquide du système CaO-Al2O3. Revue Internationale des Hautes
651 Températures et Réfractaires, 20, 135–139.
652 Villeneuve N, Neuville D.R. Boivin P., Bachelery P. and Richet P. (2008) Magma crystallization and
653 viscosity: A study of molten basalts from the Piton de la Fournaise volcano (La Réunion island)
654 Chemical Geology, 256, 242-251.
655 Vogel H (1921) Das Temperaturabhängigkeitsgesetz der Viskosität von Flüssigkeiten. Phys. Z., 22, 645
656 Voigt U. Lammert H., Eckert H, and Heuer A. (2005) Cation clustering in lithium silicate glasses:
657 Quantitative description by solid-state NMR and molecular dynamics simulations. PHYSICAL
658 REVIEW B 72, 064207
659 Wallenberger, F. T. , Hicks, R. J. , Bierhals, A. T. , 2004. Design of environmentally friendly fiberglass

compositions: ternary eutectic SiO2-Al2O3-CaO compositions, structures and properties, J. Non-Cryst. Solids 349, 377-387

Wang, T. Sakamaki, L.B. Skinner, Z. Jing, T. Yu, Y. Kono, C. Park, G. Shen, M.L. Rivers, S.R. Sutton, Atomistic insight into viscosity and density of silicate melts under pressure, Nat. Commun. 5 (2014)http://dx.doi.org/10.1038/ncomms4241.

Wang Y., Wei S., *Cicconi M.R.*, Tsuji Y., Shimizu M., Shimotsuma Y., Miura K., Peng G.D., Neuville D.R., Poumellec B. and Lancry M. (2020) Femtosecond laser direct writing in SiO2-Al2O3 binary glasses and thermal stability of Type II permanent modifications. Journal of the American Ceramic Society. DOI: 10.1111/jace.17164

Whittaker and Muntus (1970) Ionic radii for use in geochemistry. Geochimica et Cosmochimica Acta, 23, 945-956

Woelffel, W., Claireaux, C., Toplis, M.J., Burov, E., Barthel, É., Shukla, A., Biscaras, J., Chopinet, M.-H., and Gouillart, E. (2015) Analysis of soda-lime glasses using non-negative matrix factor deconvolution of Raman spectra. Journal of Non-Crystalline Solids, 428, 121–131.

Worrell C.A. and Henshall T. (1978) Vibrational spectroscopic studies of some lead silicate glasses. Journal of Non-Crystalline Solids 29, 283-299.

Wright A. (1990) Diffraction studies of glass structure. Journal of Non-Crystalline Solids 123 (1990) 129-148

Winter A. (1943) Tranformation region of the glass. J. Am. Ceram. Soc., 26, 189Wright 1990,

Wong J. and Angell A.C. (1976) Glass Structure. Marcel Dekker. New-York, 864pp.

Wu J. and Stebbins J.F., (2009) Effects of cation field strength on the structure of aluminoborosilicate glasses: high-resolution 11B, 27Al and 23Na MAS NMR. Journal of Non-Crystalline Solids, 556-562

Zakaznova-Herzog V. P., Malfait W. J., Herzog F. and Halter W. E. (2007) Quantitative Raman spectroscopy: Principles and application to potassium silicate glasses. J. Non-Cryst. Solids 353, 4015–4028.

Zanotto E. D. and Mauro J. C. (2017) The glassy state of matter: Its definition and ultimate fate. J. Non-Cryst. Solids **471**, 490–495.

Zachariasen W.H. (1932) The atomic arrangement in glass. J. Am. Chem. Soc. 54, 10, 3841–3851

Zhang, P.; Dunlap, C.; Florian, P.; Grandinetti, P. J.; Farnan, I.; Stebbins, J. F. (1996) Silicon site distributions in an alkali silicate glass derived by two-dimensional 29Si nuclear magnetic resonance. J. Non.-Cryst. Solids 204, 294-300.

Zhang P., Grandinetti P. and Stebbins J.F. (1997) Anionic Species Determination in CaSiO3 Glass Using Two-Dimensional 29Si NMR. J. Phys. Chem. B101, 4004-4008

694
695
696
697
698
699
700
701
702
703
704
705
706
707
708
709
710
711
712
713
714
715
716
717
718
719
720
721